ARGONNE NATIONAL LABORATORY
9700 South Cass Avenue
Argonne, Illinois 60439

REACTOR DEVELOPMENT PROGRAM
PROGRESS REPORT

November 1967

Robert B. Duffield, Laboratory Director
Stephen Lawroski, Associate Laboratory Director

Division	Director
Chemical Engineering	R. C. Vogel
Idaho	M. Novick
Metallurgy	M. V. Nevitt
Reactor Engineering	L. J. Kock
Reactor Physics	R. Avery
Remote Control	D. P. Mingesz (Acting)

Report coordinated by
C. L. Chernick and A. Glassner

Issued December 28, 1967

DISCLAIMER

This report was prepared as an account of work sponsored by an agency of the United States Government. Neither the United States Government nor any agency Thereof, nor any of their employees, makes any warranty, express or implied, or assumes any legal liability or responsibility for the accuracy, completeness, or usefulness of any information, apparatus, product, or process disclosed, or represents that its use would not infringe privately owned rights. Reference herein to any specific commercial product, process, or service by trade name, trademark, manufacturer, or otherwise does not necessarily constitute or imply its endorsement, recommendation, or favoring by the United States Government or any agency thereof. The views and opinions of authors expressed herein do not necessarily state or reflect those of the United States Government or any agency thereof.

DISCLAIMER

Portions of this document may be illegible in electronic image products. Images are produced from the best available original document.

FOREWORD

The Reactor Development Program Progress Report, issued
monthly, is intended to be a means of reporting those items
of significant technical progress which have occurred in
both the specific reactor projects and the general engineer-
ing research and development programs. The report is or-
ganized in accordance with budget activities in a way which,
it is hoped, gives the clearest, most logical overall view of
progress. Since the intent is to report only items of signifi-
cant progress, not all activities are reported each month. In
order to issue this report as soon as possible after the end of
the month editorial work must necessarily be limited. Also,
since this is an informal progress report, the results and
data presented should be understood to be preliminary and
subject to change unless otherwise stated.

The issuance of these reports is not intended to constitute
publication in any sense of the word. Final results either
will be submitted for publication in regular professional
journals or will be published in the form of ANL topical
reports.

The last six reports issued
in this series are:

May 1967	ANL-7342
June 1967	ANL-7349
July 1967	ANL-7357
August 1967	ANL-7371
September 1967	ANL-7382
October 1967	ANL-7391

REACTOR DEVELOPMENT PROGRAM

Highlights of Project Activities for November 1967

EBR-II

Reactor operation in Run 26B during November totaled 383 MWd(t). Four new experimental subassemblies were loaded in the reactor at the end of Run 26B, making a total of 22 experimental subassemblies in the reactor. These subassemblies have a total of 349 capsules containing fuel, structural, graphite, and thermocouple specimens.

Measurements during Run 26B of power-reactivity decrement from 0 to 45 MWt showed essentially the same values as for Runs 25 and 26A (~40 Ih), with continuation of a near-zero power coefficient between 15 and 25 MWt. Analysis of rod-drop data taken at 25 MWt in Run 26A shows a strong, prompt, negative reactivity component, followed by a strong, delayed, positive component, with the net feedback remaining uniformly negative.

EBR-II driver fuel was fabricated on a reduced schedule in the FCF hot line, and surveillance was carried out on 25 irradiated subassemblies from Run 25. With the start of routine operations in the cold line, a total of 12 subassemblies were fabricated in the cold and hot lines.

ZPR-3

Analysis of experimental data from Assembly 50 yielded central reactivity worths for $^{239+240}$Pu, ^{235}U, ^{238}U, B, and Ta. Modifications of ZPR-3 for the FFTF Phase-B critical program were completed, and fuel is being loaded for the approach to critical for Assembly 51, the simple, nonsplit, cylindrical core of the FFTF series.

ZPPR

With many items in the construction contract nearing completion, the facility is expected to be ready for occupancy by about mid-January. The two sections of the reactor bed were lowered part way to their final position within the reactor pit, and the leveling jacks were positioned and grouted into place. A contractor was selected for installation of the reactor assembly and associated equipment, and the contract was submitted to the AEC for approval.

AARR

A preliminary survey has been completed of computer codes having possible use in loss-of-coolant accident analyses. The FLASH or FLASH-2 code will be used for coolant-blowdown studies.

Lightning that damaged the power controls for the transient-heat-transfer apparatus caused the destruction of two test sections; repairs and modifications were made to prevent a recurrence.

Static leaktests of the gas-rabbit blowers and blower pressure-vessel assembly has been completed.

The design of a reference rabbit sample and sample carrier has been established and described.

TABLE OF CONTENTS

TABLE OF CONTENTS

TABLE OF CONTENTS

I. LIQUID-METAL FAST BREEDER REACTORS--CIVILIAN

A. Fuel Development--LMFBR

1. Metallic

a. **Fuel-element Performance** (W. F. Murphy*)

Last Reported: ANL-7391, pp. 2-3 (Oct 1967).

(i) **U-Pu Alloy Fuel Performance.** Several of the elements irradiated in subassembly XA07 have been sectioned for metallographic examination. Fuel element ND-28 has been sectioned and examined in detail. This fuel element, with a calculated maximum burnup of 4.6 a/o, appeared to be in excellent condition after irradiation. The fuel in this element was U-15 w/o Pu-9 w/o Zr and the jacket was Type 304 stainless steel. The photomacrograph in Fig. I.A.1(a) shows a transverse section of the fuel and jacket. The concentric bands in the fuel are believed to represent the distribution of phases as they existed during irradiation. Calculated irradiation temperatures provide qualitative agreement for this concept. The alpha-autoradiograph obtained from this section, see Fig. I.A.1(b), showed slight differences in the alpha activity of three zones. However, the relative porosities of the zones may be responsible for the differences.

In Fig. I.A.1(c), a beta-gamma autoradiograph of the same section, the middle zone shows a relatively low degree of radio-activity as compared with the highly active center zone and the moderately less radioactive outer zone of fuel. The black areas in the beta-gamma autoradiograph are believed to be at least partially related to voids, which provide more exposed surface, hence yielding an apparent increase in radioactivity.

Samples taken from each of the three zones of another transverse section from ND-28 were analyzed with the results shown in Table I.A.1. These data require confirmation, but they do indicate, at least qualitatively, that technetium and zirconium, and perhaps other fission products, have migrated from the middle annular zone. These data are in agreement with the beta-gamma radiograph.

Autoradiographs of sections from ND-30 and ND-43 have been made and confirm the results from ND-28.

Transverse and longitudinal metallographic sections from fuel elements ND-28, ND-30, and ND-43 have been examined. The fuel alloy in ND-28 and ND-43 was U-15 w/o Pu-9 w/o Zr, jacketed, respectively,

---

* The work on the fuel/cladding reaction was performed by D. E. Walker and D. R. O'Boyle.
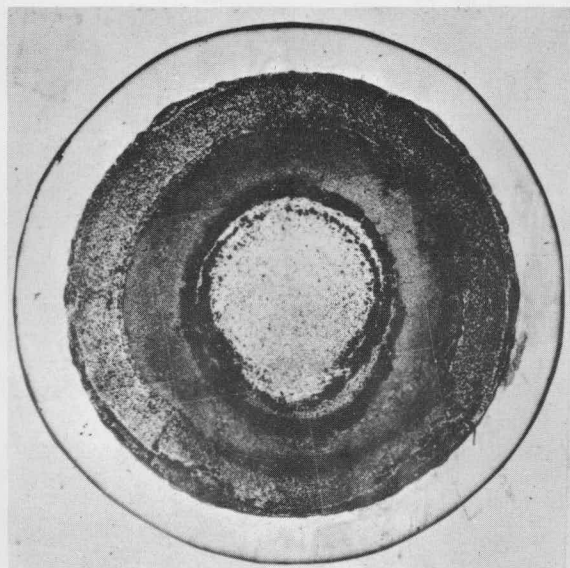
15X	15X	15X
(a) Metallographic Section	(b) Alpha Autoradiograph	(c) Beta-Gamma Autoradiograph
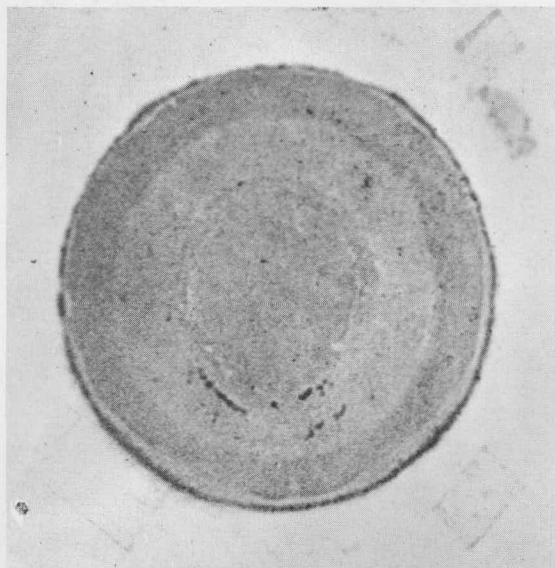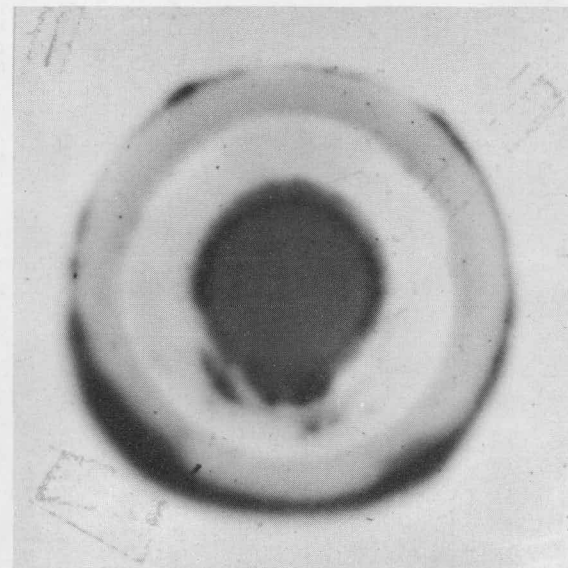
Fig. I.A.1. Transverse Section of U-15 w/o Pu-9 w/o Zr Alloy Fuel Element Irradiated in EBR-II to 4.6 a/o Burnup

TABLE I.A.1. Postirradiation Analyses of a U-15 w/o Pu-9 w/o Zr
Alloy Specimen from Fuel Element ND-28

Specimen Location	Atomic Ratio Tc/U+Pu, x 10^{-3}		Weight Percent			
	(1)	(2)	U (3)	Pu (3)	Zr (4)	Zr (5)
Center	2.0	2.5	55	18	27	22
Middle Ring	1.1	1.1	82	12	6	3
Outer Ring	2.8	3.8	53	13	34	10

(1) Based on original composition; accuracy, ±5%.
(2) Based on postirradiation analyses; accuracy, ±5%.
(3) Method of analysis; isotopic dilution--mass spectrometry.
(4) By difference from (3).
(5) Spectrochemical analyses; estimated accuracy, ±20%.

in Type 304 stainless steel and Hastelloy-X. Element ND-30 contained U-14 w/o Pu-12 w/o Zr alloy jacketed in Type 316 stainless steel. The concentric bands in the fuel shown in Fig. I.A.1(a) are typical for the three elements.

Evidence of a structural change was observed on the inside of each of the three jacket materials. Figure I.A.2 shows a typical section. A band on the inside of the Type 304 stainless steel ranged from 0 to 140 μ in thickness. The band does not penetrate along the grain boundaries, but affects the matrix material rather uniformly.

An electron microprobe analysis made of the Type 304 stainless steel shown in Fig. I.A.2 revealed no uranium, plutonium, or zirconium in either the reaction zone or the unreacted inner surface of the jacket. In the reaction zone, the concentrations of iron (71 w/o) and chromium (20 w/o) were higher than in the unreacted zone (67 and 19 w/o, respectively). The concentrations of nickel (1.2 w/o) and silicon (0.5 w/o) in the reaction zone were lower than in nominal Type 304 stainless steel (10 and 1 w/o, respectively), whereas the concentration of manganese was unchanged (2 w/o maximum). No change in concentration of Fe, Cr, Ni, Si, and Mn occurred in the unreacted zone of the jacket wall.

800X

Fig. I.A.2. Typical Appearance of Type 304 Stainless Steel Inner Jacket Surface. Etch, 2.0% nital, electrolytic.

The X-ray spectral profiles showed the following elements to be present in the reaction zone: lanthanum, cerium, praseodymium, neodymium, samarium, and possibly promethium. Promethium cannot be identified positively since the wavelengths of its principal X-ray lines overlap the wavelengths of other elements present. Concentrations of these elements in this zone were estimated as 3 w/o Ce, 2.5 w/o Nd, 1.6 w/o La, 1.4 w/o Pr, and 0.6 w/o Sm, based on an earlier measurement with a gadolinium standard (they should be considered as approximations). The observed concentrations of the rare-earth elements decreased in about the same order as their weight percent of the total fission products: Nd, 9.9%; Ce, 9.2%; La, 3.5%; Pr, 2.4%; and Sm, 1.8%. None of these elements was detected in the unreacted areas of the jacket. In the reaction zone, the cerium concentration was highest at the edge of the jacket and decreased to zero at the interface between the reaction zone and the unreacted stainless steel.

The Type 316 stainless steel jacket had only a thin band (maximum 20 μ) on its inner surface. The zone on the inner surface of Hastelloy-X was irregular in width and was about 100 μ wide at its maximum. No cracks were associated with these bands in either the Type 304 stainless steel, Type 316 stainless steel, or Hastelloy-X.

Two fuel elements in subassembly XG05 (see Table I.A.2) have accumulated about 80% of their target burnup of 7.5 a/o.

TABLE I.A.2. Status of Irradiations of Metal Fuels (Clad in V-20 w/o Ti) in Progress--Fast Reactor Development

		Design Parameters					Operating Conditions			
S/A No.	Spec No.	Fuel Composition (w/o)	Effective Density (%)	Cladding OD (in.)	Cladding Thickness (in.)	Max kW/ft	Max Cladding Temp (°C)	Burnup to Date		
								a/o	fiss/cc x 10^{-20}[a]	
XG05	ND-24	U-15 Pu-10 Zr	63.6	0.208	0.015	10.0	535	6.0	13.6	
XG05	NC-17	U-15 Pu-10 Ti	66.7	0.204	0.016	10.0	540	6.1	14.2	

[a]Based on effective density.

Fifteen U-15 w/o Pu-10 w/o Zr fuel elements (Group M-3) (see Table II.D.3, p. 75, of Progress Report for September 1967, ANL-7382) have been loaded into subassembly XO28, which is scheduled for insertion in position 4E3 of the EBR-II core during the midrun shutdown of Run No. 26.

Injection-cast fuel pins for Group M-4, with a nominal composition of U-15 w/o Pu-12 w/o Zr with 93% enriched uranium, have been made. The fuel columns are 14.22 in. long and 0.163 in. in diameter. About two-thirds of the required 40 pins have passed inspection for density, dimensions, and composition. Additional fuel pins will be cast to complete the number required.

Jackets are being fabricated from stainless steel Types 304, 316, and 318, Inconel 625 and Hastelloy-X, and V-15 w/o Ti-7.5 w/o Cr and V-15 w/o Cr-5 w/o Ti. The tubes have a 0.220-in. OD and a 0.188-in. ID. Procedures for welding the end plugs on the vanadium alloy jackets are being worked out.

Burnups at 10 a/o at linear heat ratings of 14 kW/ft are expected from this group of fuel elements.

2. Carbide--Fabrication and Evaluation

a. Fuel-element Performance (F. L. Brown)

Last Reported: ANL-7391, pp. 6-7 (Oct 1967).

Tables I.A.3 and I.A.4 list the status of elements undergoing irradiation and postirradiation examination, respectively. The effect of irradiation on the microstructure of the elements listed in Table I.A.4 is being evaluated. The three elements include one rod each of pressed-and-sintered solid-solution pellets, vibratorily compacted solid-solution particles, and vibratorily compacted physically mixed particles.

TABLE I.A.3. Status of Mixed-carbide Fuel Irradiations in Progress in EBR-II

S/A No.	Specimen Number	Fuel Composition (w/o)	Fuel Form[a]	Effective Density (%)	Cladding Composition (w/o)	Cladding OD (in.)	Cladding Thickness (in.)	Max kW/ft	Max Cladding Temp (°C)	Burnup to Date a/o	Burnup to Date fiss/cc x 10^{-20}[b]
XG05	SMV-2	UC-20 PuC	VIPAC	83.8	304 SS	0.296	0.021	24.0	675	6.6	18.1
XG05	HMV-5	UC-20 PuC	VIPAC	80.0	Hastelloy-X	0.295	0.015	26.6	685	6.8	17.9
XG05	NMV-11	$(U_{0.8}Pu_{0.2})C$	VIPAC	82.9	Nb-1 Zr	0.281	0.012	25.5	635	6.8	18.6
X008	NMP-2	$(U_{0.8}Pu_{0.2})C$	PELLET	81.6	Nb-1 Zr	0.284	0.013	17.4	545	4.2	11.2
X008	NMV-4	UC-20 PuC	VIPAC	80.0	Nb-1 Zr	0.283	0.013	27.0	645	6.3	16.6
X008	NMV-7	UC-20 PuC	VIPAC	80.0	Nb-1 Zr	0.283	0.013	26.0	630	6.2	16.3
X008	NMV-12	$(U_{0.8}Pu_{0.2})C$	VIPAC	85.5	Nb-1 Zr	0.284	0.014	26.7	645	6.2	17.5
X008	HMV-1	UC-20 PuC	VIPAC	80.0	Hastelloy-X	0.295	0.015	25.2	660	5.7	15.0
X008	HMV-4	UC-20 PuC	VIPAC	80.0	Hastelloy-X	0.295	0.016	27.2	690	6.1	16.2
X008	HWMP-1	$(U_{0.8}Pu_{0.2})C$	PELLET	81.4	Hastelloy-X + W	0.296	0.020	16.9	565	4.2	11.2
X008	HWMV-1	$(U_{0.8}Pu_{0.2})C$	VIPAC	82.9	Hastelloy-X + W	0.295	0.018	26.4	685	6.2	16.8
X015	NMP-1	$(U_{0.8}Pu_{0.2})C$	PELLET	81.6	Nb-1 Zr	0.284	0.013	16.5	535	1.5	4.0
X015	NMV-3	UC-20 PuC	VIPAC	80.0	Nb-1 Zr	0.284	0.013	26.0	635	2.2	5.9
X015	HMV-2	UC-20 PuC	VIPAC	80.0	Hastelloy-X	0.295	0.015	27.0	685	2.2	5.8
X015	TVMV-1	$(U_{0.8}Pu_{0.2})C$	VIPAC	83.7	V-20 Ti	0.298	0.021	23.4	640	2.0	5.6

[a]VIPAC = Vibratorily compacted into cladding; PELLET = Pressed and sintered pellets.
[b]Based on effective density.

TABLE I.A.4. Design Parameters, Operating Conditions, and Postirradiation
Measurements for Carbide Elements Irradiated in EBR-II

	Element Number		
	SMP-1	VMV-1	SMV-1
Fuel Composition	$(U_{0.8}Pu_{0.2})C$	$(U_{0.8}Pu_{0.2})C$	UC-20 w/o PuC
Fuel Synthesis	Arc Melted	Arc Melted	Arc Melted
Fuel Form	Pellets	Vibratorily Compacted	Vibratorily Compacted
Fuel Diameter, in.	0.253	0.253	0.257
Fuel Length, in.	13.4	14.0	14.0
Effective Density, %	81.4	85.9	80.0
Cladding Material	Type 316 SS	Vanadium	Type 316 SS
Cladding OD, in.	0.306	0.301	0.306
Cladding Wall, in.	0.024	0.024	0.025
Max Heat Rating, kW/ft	15.9	25.8	21.3
Max Cladding Temp, °C	565	645	630
Max Burnup, a/o	1.91	3.02	2.59
Element Length Change, %	0	+0.31	0
Element Diameter Change, %	0	+0.83	0
Element Density Change, %	-0.32	-1.46	-0.29
Gas Release, % of Theoretical	4.3	8.5	13.4

The stoichiometry of solid-solution fuel persisted after
irradiation, as shown in the microstructures of stoichiometric and hyper-
stoichiometric pellets, and hyperstoichiometric vibratorily compacted
material. Stoichiometric pellet structures exhibited little or no change
after 1.91 a/o burnup. Hyperstoichiometric structures--both pellet and
vibratorily compacted--were considerably altered after 1.91 and 3.02 a/o
burnup, respectively. The disappearance of the dicarbide phase from the
hyperstoichiometric pellet structures was accompanied by the appearance
of an equiaxed phase, located primarily in the monocarbide grains, tenta-
tively identified as the sesquicarbide. A large reduction in the amount of
sesquicarbide phase occurred in the sintered area of the vibratorily com-
pacted solid-solution fuel. A third phase, not present in preirradiation
structures, appeared in both the pellet and the vibratorily compacted
materials.

Fine porosity was observed in monocarbide grains and sesqui-
carbide particles of the pellet fuel, and in grains of the sintered central
zone of the solid-solution vibratorily compacted fuel. The vibratorily
compacted fuel, irradiated at higher central temperature than the pellet
fuel, exhibited migration of grain boundaries toward the hot center of the
element. Fine porosity was swept up by the advancing grain boundaries.
leaving relatively void-free areas in the grains on the cold side of the
boundaries. The size and shape of the regions of coarse porosity were
about the same in both solid-solution pellet and vibratorily compacted
fuels. These coarse pores were uniformly distributed throughout the
pellet cross section, but were clustered in areas previously (before irra-
diation) occupied by the unsintered fine particles in the structure of the
vibratorily compacted fuel.

The macrostructure of the physically mixed, vibratorily com-
pacted fuel was unchanged after irradiation. Examination at higher magni-
fication, after etching, disclosed limited solid-solution formation between
coarse UC particles and fine PuC particles. The sintered PuC formed a
continuous network between the large UC particles and even penetrated
the grain boundaries of the UC. Fine porosity was observed in the coarse
UC grains, but the presence of coarse porosity was sparse. The sintered
PuC near the center of the element was characterized by coarse pores,
larger than in either solid-solution pellet or vibratorily compacted fuel.

b. Compatibility of (U,Pu) Carbides with Potential Jacketing
Materials (T. W. Latimer)

Last Reported: ANL-7391, pp. 7-8 (Oct 1967).

(i) Vanadium-base Alloy. Two vanadium-base alloys obtained
from Westinghouse Advanced Reactor Division are identified as HSV-207
and HSV-208. Compatibility-test disks cut from 50-mil sheet were examined
after contact for 1000 hr at 800°C with hyperstoichiometric $(U_{0.8}Pu_{0.2})C$
containing approximately 20 v/o $(U,Pu)_2C_3$. The chemical compositions of
these alloys are listed in Table I.A.5. The compositions are the same on
an atomic basis except for the substitution of 3 a/o Ta in HSV-208 for the
3 a/o Fe in HSV-207.

TABLE I.A.5. Composition of Westinghouse Vanadium Alloys

Element	HSV-207		HSV-208	
	w/o	a/o	w/o	a/o
V	86.22	87.0	80.37	87.0
Cr	9.1	9.0	8.49	9.0
Fe	3.3	3.0	-	-
Ta	-	-	9.85	3.0
Zr	1.33	0.75	1.24	0.75
C	0.054	0.25	0.05	0.25

HSV-208 was unaffected after the test, and so was completely
compatible with hyperstoichiometric (U,Pu)C. A similar 4000-hr test is
planned. Grain-boundary precipitation 125 μ deep occurred in the HSV-207
alloy. This type of affect was also observed for an ANL-prepared alloy at
V-10 w/o Cr.* ANL alloy V-15 w/o Cr-5 w/o Ti has previously been found
to be unaffected by these testing conditions.

(ii) Compatibility of Uranium Phosphide with Selected Jacketing
Materials. To compare the interaction of various jacketing alloys with
ceramic fuel materials other than (U,Pu) carbides, certain alloys previously

*Reactor Development Program Progress Report for October 1967, ANL-7391, p. 8.

tested with stoichiometric and hyperstoichiometric (U,Pu)C were heat-treated at 800°C for 1000 hr with uranium monophosphide. Couples containing UP in contact with Type 304 stainless steel and Hastelloy-X have been examined by means of metallography and an electron-microprobe analyzer. In both cases, diffusion of iron and nickel from the jacket into the UP had occurred, resulting in well-defined zones of reasonably constant composition on each side of the fuel-jacket interfaces. The depths of these zones are listed in Table I.A.6. (The values given for the Hastelloy-X couple have been revised from those reported in the October Report, ANL-7391, p. 8, since microprobe analysis has more clearly defined the position of the original interface. This interface broke during cooling of the couple, and the resulting edges became slightly rounded during polishing.)

TABLE I.A.6. Extent of Interaction between UP and Two Potential
Jacketing Alloys after 1000 hr at 800°C

Direction of Affected Zone	Type 304 SS		Hastelloy-X	
	Avg (μ)	Max (μ)	Avg (μ)	Max (μ)
Fuel	18	21	50	55
Jacket	22	25	20	26

The average composition of these zones, estimated from microprobe analyses, is given in Tables I.A.7 and I.A.8. In both cases, the U to P atomic ratio remained at 1:1 in the affected zone in the fuel. The combined nickel-plus-iron atomic percentage was found to be between 35 and 40 a/o in these zones.

TABLE I.A.7. Composition of Interaction Zones
for UP vs. Type 304 Stainless Steel at 800°C

Element (w/o)	UP	Affected Zone in Fuel	Affected Zone in Jacketing	Type 304 SS
U	88.5	70.9	-	-
P	11.5	9.6	-	-
Fe	-	7.1	71.6	71.0
Ni	-	12.4	1.2	8.8
Cr	-	-	23.4	18.6

TABLE I.A.8. Composition of Interaction Zones
for UP vs. Hastelloy-X at 800°C

Element (w/o)	UP	Affected Zone in Fuel	Affected Zone in Jacketing	Hastelloy-X
U	88.5	68.9	-	-
P	11.5	8.8	-	-
Fe	-	0.3	24.4	18.2
Ni	-	22.0	12.9	48.2
Cr	-	-	41.8	21.2
Mo	-	-	17.0	8.7

In previous 800°C compatibility tests involving (U,Pu)C and US, no depletion of nickel from Type 304 stainless steel was observed and that from Hastelloy-X was less than for UP.

3. Carbide--Synthesis (P. A. Nelson)

a. Preparation of Carbide Fast Reactor Fuels for Testing

Last Reported: ANL-7308, pp. 31-32 (Feb 1967).

High-purity UC and (U,Pu)C powder of known stoichiometry is being prepared by the fluidized-bed technique. Powder so prepared is then pressed and sintered into pellets (see Progress Report for September 1967, ANL-7382, pp. 78-80) for irradiation tests by the Metallurgy Division. Powder is also supplied for other carbide fabrication programs.

The carbide powder is prepared by a process in which hydrided metal or alloy is reacted at 800°C with a methane-hydrogen fluidizing gas. In three recent runs, (U, 15 w/o Pu)C containing fully enriched uranium (93% ^{235}U) was prepared. In each run, a charge of 400 g of alloy was hydrided and dehydrided twice before initiation of the reaction with 6.2 v/o CH$_4$-93.8 v/o H$_2$ at 800°C and 2 atm pressure. The methane consumption, as determined from the inlet and outlet gas analysis (infrared continuous analyzer) and the gas flow rate, was slightly different for one of these experiments; there is as yet no apparent explanation.

In all recent experiments, the methane uptake became very slow when the stoichiometric monocarbide carbon content of 4.8 w/o was reached. (In several previous experiments to produce hyperstoichiometric (U,Pu)C, for example, carbiding times of up to 14 hr were required to attain a carbon content of only 4.9 to 5.0 w/o.) Small amounts of excess carbon were easily removed by reacting the powder with pure hydrogen. In order to establish that the excess carbon was not absorbed methane, the carbide powder of Run 24 was fluidized with helium at 800°C after the carbiding had been completed. The infrared analyzer gave no indication of the presence of methane in the offgas. However, when the helium treatment was followed by a hydrogen treatment, there was an immediate indication of the presence of methane in the offgas, thus confirming that the excess carbon was present as a higher carbide.

The extent of carbiding for the carbides produced in these experiments was determined (1) during the run by calculating the methane uptake, (2) immediately after the run from the increase in weight of the product over that of the charge, and (3) by chemical analysis of the product. This last technique is, of course, the most accurate; however, in the recent experiments, all three methods of determining the extent of carbiding have given results that agree to within about 2%.

b. Characterization of Fuel Materials

Last Reported: ANL-7342, pp. 73-75 (May 1967).

The powdered product of the fluidized-bed preparations reported above is being characterized by thermodynamic, chemical, and physical measurement techniques to aid in interpretation of irradiation test results.

Although oxygen and nitrogen analyses have not as yet been obtained for the runs reported above, past results with this preparation method (see Progress Report for February 1967, ANL-7308, pp. 31-32) have indicated the oxygen content to be commonly about 300 to 500 ppm, and the nitrogen content to be less than 200 ppm. The carbon content, sieve analysis, bulk density, and tap density of recently prepared (U, 15 w/o Pu)C are given in Table I.A.9. The bulk density of the powders was measured by the ASTM method as modified for our glovebox conditions.

TABLE I.A.9. Characteristics of (U, 15 w/o Pu)C Powder Prepared by the Fluidized-bed Technique

Conditions of Preparation:

Temperature:	800°C
Pressure:	2 atm
Gas Composition:	6.2 v/o CH_4-93.8 v/o H_2
Gas Velocity:	12 cm/sec

	Run Number			
	21[a]	22	23	24
Carbon Analysis of the Product, w/o	5.00[b]	4.93[c]	4.77	4.75
Bulk Density, g/cc	-	3.6	4.2	4.2
Tap Density, g/cc	-	4.4	4.5	5.0

Screen Opening (μ)	% Retained on Screen			
833	0.0	0.0	5.2	9.2
149	1.6	9.7	10.0	18.3
77	11.4	7.4	9.5	12.6
44	14.0	10.7	13.4	13.0
20	51.8	29.1	32.9	27.7
Pan	21.2	43.0	29.0	19.3

[a]In Run 21, the starting alloy contained normal uranium, whereas in Runs 22-24 the starting alloy contained fully enriched uranium.
[b]The carbide product in Run 21 was not treated with hydrogen at the end of the carbiding period, thus accounting for the high carbon content.
[c]The other measures of carbon content, noted in the text, have given lower values. The carbon content will be redetermined.

The screen analyses were determined with 3-in.-dia sieves vibrated on a Syntron jogger for 10 min. Apparently, a small amount of sintering of the powder took place in Runs 23 and 24, as evidenced by the material on the 833-micron screens.

The sieve fractions from Run 21 were separated and carbon analyses run on each fraction. The variation in the carbon content analysis between the various particle size fractions (see Table I.A.10) is not considered to be statistically significant. The uniformity of carbon content with size distribution is a strong indication that the extent of carbiding in the fluidized-bed method is self-limiting at a carbon content slightly above the stoichiometric value of 4.80 w/o.

TABLE I.A.10. Carbon Content of (U, 15 w/o Pu)C as a Function of Particle Size for Run 21

Material Retained on Screen Size (μ)	Analyzed w/o C
149	4.97
77	5.05
44	5.02
20	5.04
Pan	5.01
Composite Sample	5.00

4. Fuel Cladding and Structure--Jacket Alloys

    a. Mechanical Properties of Fuel-jacket Alloys (F. L. Yaggee)

        (i) Effect of Alloy Composition, Annealing Temperature, and Testing Temperature on the Short-term Tensile Properties of Vanadium-base Alloys

Last Reported: ANL-7391, pp. 9-10 (Oct 1967).

The effects of annealing temperature and test temperature on the short-term engineering properties of unalloyed vanadium and V-10 w/o Ti are illustrated in Tables I.A.11 and I.A.12. Similar values were previously reported for V-20 w/o Ti and V-40 w/o Ti (see ANL-7391, p. 10). The engineering uniform strain is usually taken as the value of engineering strain at the point of maximum load, but this convention is not always true. In alloys, such as these, that show strain aging (between 400 and 600°C), uniform strain can extend beyond the value of strain at maximum load. For this reason the strain-hardening exponent is a more realistic index of uniform strain.

TABLE I.A.11. Short-term Tensile Properties of Unalloyed Vanadium

Test Temp. (°C)	1000 psi			Percent Strain	
	UTS	0.2% Y.S.	Fracture Stress	Fracture	Engineering Uniform Strain
			Vacuum-annealed 1 hr at 1250°C		
R.T.	53.8	39.5	Zero	27.4	14.8
200	45.6	25.0	Zero	10.2	7.8
400	56.2	25.8	43.4	21.1	14.0
600	22.6	15.2	2.9	45.3	7.0
600	22.0	12.5	19.1	-	8.6
800	7.3	5.7	Zero	52.3	9.5

TABLE I.A.12. Short-term Tensile Properties of V-10 w/o Ti

Test Temp (°C)	1000 psi			Percent Strain	
	UTS	0.2% Y.S.	Fracture Stress	Fracture	Engineering Uniform Strain
			Vacuum-annealed 1 hr at 1000°C		
R.T.	68.8	60.2	44.3	32.8	20.1
200	60.4	42.6	40.3	26.7	21.4
400	63.8	39.3	48.8	12.8	10.9
600	70.2	39.8	70.2	12.5	12.5
800	43.3	30.4	0.9	29.2	8.7
			Vacuum-annealed 1 hr at 1250°C		
R.T.	72.9	57.1	52.1	35.2	20.1
200	59.2	40.1	45.7	25.8	14.7
400	61.7	36.3	51.7	17.8	12.8
600	68.7	35.4	59.4	13.3	12.2
800	49.4	36.6	33.3	28.9	8.5

(ii) Flash-annealing Studies on Vanadium-base Alloys. Rod specimens (of 0.51-cm OD by 0.95 cm long) of vanadium, V-10 w/o Ti, V-20 w/o Ti, V-40 w/o Ti, V-15 w/o Ti-7.5 w/o Cr and V-15 w/o Cr-5 w/o Ti have been annealed at 1650°C for 5 and 15 min in an apparatus provided with close inductive coupling. The unalloyed vanadium and the V-Ti binary alloys were annealed in vacuum (2×10^{-6} mm of Hg or better), whereas the V-Ti-Cr ternary alloys were annealed in an atmosphere of high-purity argon because of the excessive vapor pressure of chromium at 1650°C. All specimens were brought to 1650°C in about 6 sec.

The 15-min anneal at 1650°C produced a very large grain size in all of the specimens, clearly visible to the unaided eye (grain diameter greater than about 0.4 mm). The heat-treated specimens are being prepared for quantitative metallographic analysis.

b. <u>Irradiation Studies</u> (R. Carlander)

Last Reported: ANL-7391, p. 12 (Oct 1967).

Stressed and unstressed sections from specimens of irradiated Type 304 stainless steel that were tensile-tested at 25, 400, 550, and 650°C were metallographically examined. Extensive carbide precipitation occurred along slip planes and within the grains in irradiated specimens, and also in unirradiated specimens that had been annealed for 30 days at 550°C to simulate anticipated in-reactor thermal conditions. This is characteristic of material that has been solution-annealed, quenched, cold-worked, and reheated to intermediate temperatures. The occurrence of this precipitation indicates that the unirradiated alloy as received from the manufacturer was not in the fully annealed condition.

The existence of cold-work in the unirradiated specimens accounts for the increase in ductility of the unirradiated alloy (65 to 84% total elongation at room temperature and 30 to 34% total elongation at 650°C) due to annealing for 30 days at 550°C (see Progress Report for June 1967, ANL-7349, p. 84).

The tangential rupture strength of V-15 w/o Ti-7.5 w/o Cr alloy, which was irradiated in EBR-II subassembly XO13, is given in Figs. I.A.3 and I.A.4 as a function of fluence and test temperature, the data being
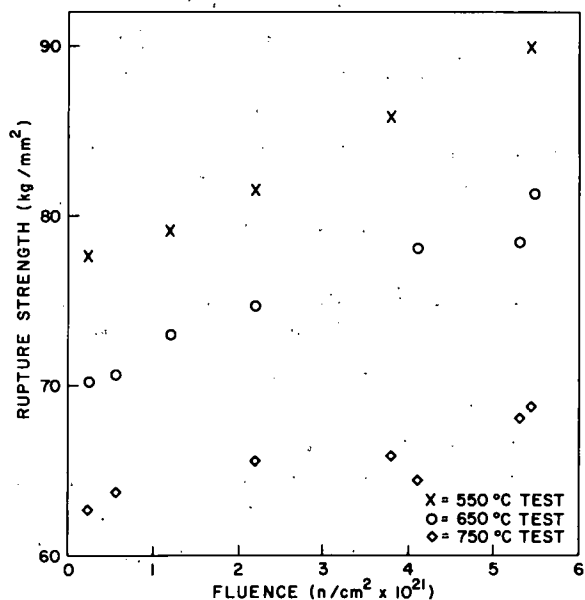
Fig. I.A.3. Effect of Fluence and Test Temperature on the Tangential Rupture Strength of Irradiated V-15 w/o Ti-7.5 w/o Cr Alloy
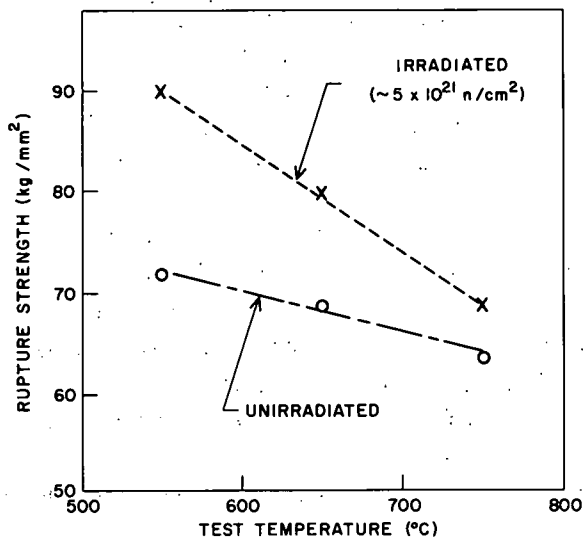
Fig. I.A.4. Effect of Test Temperature on the Tangential Rupture Strength of V-15 w/o Ti-7.5 w/o Cr Alloy

taken from the Progress Report for April 1967, ANL-7329, p. 48. The specimens were irradiated to a nominal fluence of 5×10^{21} at $600 \pm 100°C$ (previously given as 510 to 704°C).

The tangential rupture strength increased with fluence at all test temperatures (see Fig. I.A.3). The effect of fluence on the rupture strength was less pronounced at 750°C than at test temperatures of 550 and 650°C. The rupture strength of the irradiated alloy approached that of the unirradiated alloy with increasing test temperature (see Fig. I.A.4), indicating that the irradiation-induced defects are being annealed out at higher test temperatures.

c. Sodium Corrosion of Fuel-jacket Alloys (W. E. Ruther and D. Dorman)

(i) Development of Refractory-metal Alloys for Service in Oxygen-contaminated Sodium

Last Reported: ANL-7391, pp. 12-13 (Oct 1967).

Samples of vanadium alloys have been exposed to flowing sodium (6.1 m/s) at 600°C for 21 days in a continuing test. The cold trap on the system is operating at 110°C. Weight changes are small ($<0.2 \, mg/cm^2$), and the samples have acquired only a thin, superficial film. This behavior is as expected from previous runs at other temperatures, but is in sharp contrast to the results of Champeix et al.* at 600°C in which significant weight changes ($>2 \, mg/cm^2$) were reported. The discrepancy is attributable to the small differences in levels of sodium impurity in systems operating with cold traps at the same nominal temperature. For example, in our static refreshed system at 600°C (cold trap at a nominal 110°C), weight losses of the magnitude reported by Champeix et al. are noted.

Carbon is believed to be the significant sodium impurity when the oxygen level of the sodium has been reduced below 5 ppm by wt, the concentration required to form a vanadium oxide phase. The dynamic testing system is constructed largely of stabilized stainless steel. The refractory-metal stabilizers in the stainless steel inhibit the movement of carbon from the test loop walls to the vanadium-alloy specimens through the sodium. Our refreshed static system is constructed of unstabilized stainless steel, which presumably contributes carbon to the vanadium alloys.

---

*Champeix, L., Dorras, R., and Sannier, J., Corrosion of V and Its Alloys in Liquid Sodium, Alkali Metal Coolants, Vienna, 1967.

B. Physics Development--LMFBR

1. Theoretical Reactor Physics--General Fast Reactor Physics

  a. Dynamics Studies (H. H. Hummel)

  Two major revisions of the QX1[†] spatial kinetics code have been completed and checked out. The first revision was directed toward increasing the running speed. One major element affecting the run time is the computation of reactivity at each normal time step. Previously this was computed from the expression

$$\rho = \left\langle \psi^* \left[\delta M + \frac{1}{k_0} \delta F \right] \psi \right\rangle \tag{1}$$

where ψ^* is the static adjoint function, δM and δF are, respectively, the changes in the diffusion-plus-absorption-plus-transfer operator and the fission-source operator from zero time, ψ is the current shape function, and the $\langle \rangle$ brackets indicate integration over space and energy. This equation for the reactivity requires formation of δM and δF at each step, while the current operators $M(t)$ and $F(t)$ are available at all times. Since the system is exactly critical at zero time,

$$\left\langle \psi^* \left[M(o) + \frac{1}{k_0} F(o) \right] \psi \right\rangle \equiv \left\langle \psi, \left[M(o) + \frac{1}{k_0} F(o) \right]^T \psi^* \right\rangle = 0. \tag{2}$$

The term in brackets in the second inner product is the transpose of the solution operator at time zero. Thus the inner products are zero by definition of the static adjoint function at this time. Since the first inner product is identically zero, the reactivity may also be found from

$$\rho = \left\langle \psi^* \left[M(t) + \frac{1}{k_0} F(t) \right] \psi \right\rangle, \tag{3}$$

where

  M(t) = M(o) + δM and F(t) = F(o) + δF.

Equation (3) is now being used to compute reactivities; significant time savings have resulted.

  The second major revision was inclusion of a new version of the time-step sequencing logic. This is the portion of the code which fixes the time-step lengths for normal time steps and performs tests which determine whether or not a new flux-shape function is required at the end of each time step.

[†]Reactor Development Program Progress Report, ANL-7286, pp. 75-76 (Dec 1966); Ott, K., Meneley, D. A., and Wiener, E. S., "Quasistatic Treatment of Space Dependent Reactor Transients," Reactor Physics Division Annual Report, July 1, 1965 to June 30, 1966, ANL-7210 (Dec 1966).

2. <u>Theoretical Reactor Physics--Fast Critical Experiments--Theoretical Support</u>

Last Reported: ANL-7391, p. 21 (Oct 1967).

A study of possible drawer arrangements for Core 1 of ZPPR has resulted in the following proposal:

This possible core would consist of a 1500-liter simulated oxide core with a length-to-diameter ratio (L/D) of 0.33; the estimated homogeneous critical mass is 750 kg Pu. The core would have two-drawer cells with three fuel plates per cell. An interesting point that came out of the study was the very good agreement (to 1 percent) of critical-size calculations between simulated two-dimensional calculations (consistent buckling method) and two-dimensional diffusion-theory calculations. The agreement was constant over a range of L/D from 0.35 to 1.0.

The RABBLE code is being modified for better applicability to fast critical experiments. Periodic boundary conditions and an intermediate group-dependent potential scattering are being added.

Postanalysis of ZPR-3 Assemblies 48 and 49 and preanalysis of ZPPR Cores 1 and 2 continue.

3. <u>Experimental Reactor Physics--Fast Critical Experiments--Experimental Support</u>

Last Reported: ANL-7391, pp. 21-23 (Oct 1967).

a. <u>Neutron Spectrometry</u> (W. G. Davey)

The current work has centered on (a) the analysis of the proton-recoil measurements made in Assemblies 49 and 50 of ZPR-3, and (b) the continued development of the spectrometer based upon the use of a small digital data-acquisition system as a multiparameter analyzer.

The Assembly 49 and 50 data-reduction analysis revealed that the quality of the experimental data was unsatisfactory, leading to distortion of the derived neutron spectra. The primary cause of the distortion is believed to be space-charge saturation in the proportional counters, but count-rate effects could have contributed to the problem. Tests are planned to ascertain the origin of the unsatisfactory data. The importance of the simple systems of Assemblies 49 and 50 will probably require the brief reconstruction of these systems in ZPR-3 at some future date in order that the spectra can be measured precisely.

This work has revealed the penalty that may be paid when immediate data reduction is not practicable and has further emphasized the importance of the small computer-based equipment that is being developed. This equipment will make possible the immediate subtraction of the γ-ray background, and possibly also the direct reduction and prompt display of neutron spectra. Dubious experimental data will thus be more clearly identified in the course of the experiment, and new data will be obtained, if necessary, with negligible penalty in reactor utilization.

Development of the new equipment is proceeding very satisfactorily. Noise in the fast channel of the spectrometer has been identified as originating in the computer "clock," and the simple expedient of moving the central processor 65 ft from the preamplifier reduced the noise to an acceptable level. The experience gained with this separation of equipment is very valuable for ZPPR since much equipment will be located 150 to 200 ft from the ZPPR reactor.

The hardware of the live-time clock has been completed and the specifications for the necessary software has been written in part. After completion of the software and satisfactory tests of the equipment, test spectra can be measured with the new equipment.

b. <u>Heterogeneity Studies</u> (W. G. Davey)

Current work in this activity is centered on development of suitable foil-counting techniques for heterogeneity studies in large, fast, power reactors.

The initial work in technique development has been in activation analysis, using lithium-drifted germanium detectors. Two exposures of ^{235}U foils in the Argonne Fast Source Reactor (AFSR) in fast-neutron spectra have been made, and analysis of these is nearly complete. The first consideration is a search for several fission products that might be useful as reliable indicators in all fissionable isotopes. The desirable properties for these indicators are (a) large and well-known yield, (b) convenient half-life, and (c) distinct and easily resolvable gamma-ray lines.

Gamma-ray analysis of the two exposures covered the range from less than 100 keV to about 1900 keV, with approximately 4-keV resolution. All the major features of the spectrum have been identified as functions of time and energy. The major lines in a number of mass chains appear to meet the intensity and distinctness criteria. The major lines in the 131, 132, 133, 135, 138, and 140 mass chains stand out clearly among the heavy-fragment yields. Among the light fragments, only ^{91}Sr and ^{92}SR give gamma rays that appear to be very useful, in ^{235}U fission, at least. (The gammas from 95, 97, and 99 mass chains are mostly obscured by the natural activity of ^{235}U, the activity of other fission products, or bremsstrahlung and Compton activity.)

From the data it was possible to construct relative efficiency curves for the systems, and eventually it should be possible to obtain relative yields of the different isotopes. The preliminary estimates of relative yields are very encouraging. The analysis is now being concentrated on the detection and identification of small interferences.

Following this essential initial study the specification of equipment design for the ZPPR measurements can be made.

c. Computer Applications (W. G. Davey)

The basic design of a computer system for on-line assistance to experimental operations at ZPPR has been completed. Requirements of the computer mainframe and the peripheral equipment in the system have been defined from an evaluation of the experimental applications. Specifications for the system items which are intended for outside procurement have been drawn up. This Idaho Division system and a Reactor Physics Division system at the Illinois site will have a maximum of intersystem compatibility.

It is hoped that a firm order for the ZPPR computer and associated equipment can be placed in early calendar year 1968 (i.e., procured in FY 1968). This time scale must be met in order to utilize the computer at an early stage in the ZPPR program.

In the proposed ZPPR computer system the mainframe will probably contain a 24-bit work-length processor and a core memory of 16k words. An acceptable alternate will be a 32- or 36-bit processor with 12k of memory. These and other specified hardware features are designed to enable few-stage, time-sharing operations for real-time applications. Auxiliary memory storage for the system will be provided by a 350k-word magnetic disc and a magnetic tape unit. These will serve for rapid access to the numerous experimental programs and for permanent recording of experimental and reactor operational data.

The standard read-in and read-out peripheral equipment in the system will include a high-speed paper-tape reader, a high-speed paper-tape punch, a Hollerith card reader, a fast line printer, and a digital plotter. These items will be stationed in the ZPPR computer room to provide for programming operations, for generation of data or programs in formats for further processing, and for preparation of experimental results in forms immediately acceptable for publication. One typewriter unit will be located in the computer room, with one or more units also attached at remote data-link stations.

In the overall endeavors of the ZPPR programs, experiments will be conducted at a number of areas of the facility, including the AFSR and the counting room. The data-acquisition system of the central computer

will thus consist of a number of remote, data-link stations. As presently envisioned, the computer and basic peripherals will be housed in a separate basement room in the ZPPR support wing. Data links then will be constructed to several stations: the ZPPR control room, the reactor cell, the reactor loading room, the AFSR cell, the counting room, and the electronics shop. At each station, electronic equipment will be provided for selective routing of data buses, interrupt lines, control lines, and sense lines of the computer I/O system to and from the various experimental devices. A special buffering technique will be employed whereby data from experimental readouts will be transferred to computer I/O buses, and computer-generated external control data will be transferred to experimental equipment, via general-purpose buffer registers. The concept employed is to provide changeable, versatile interfacings which can be adapted to a variety of experimental setups.

The essential design objectives for the ZPPR computer system are to automate the data acquisition from experiments as much as possible, to control experiments wherever practical, and to provide real-time data reduction and evaluation. The on-line processing of data will permit quick evaluation of the propriety of the results obtained or of the experimental technique. Thus, reactor operating time per experiment will be minimized and loss of time on faulty experiments can be avoided. The communications between the experimenters at the data-link stations and the computer will be handled by teletypes and by cathode-ray tube display devices at the stations.

d. Integral Studies of Cross Sections (W. G. Davey)

The objective of this activity is the study in integral experiments of basic cross sections used in fast breeder reactor design.

An important preliminary to such experiments is the examination of basic microscopic (differential) data to determine regions of ambiguity that could be studied with integral experiments. As part of this work an examination of the measured captive cross section of ^{238}U has been initiated. In part this study is necessary as a portion of an invited paper to be presented at the 1968 Washington Conference on Neutron Cross Sections. The initial work confirms that wide discrepancies exist among the various measured data. A selective process plus renormalization may reduce the spread of values.

Comparison of calculated and measured ratios of ^{238}U(n,γ), and ^{235}U(n,f) cross sections in the many ZPR-3 assemblies in which this ratio has been determined may indicate the precision of the selected ^{238}U capture data.

e.   <u>On-line Computer Applications</u>   (R. Gold)

Last Reported: ANL-7349, p. 92 (June 1967)

(i)   "ENCODE/DECODE" Facility for FORTRAN-IV. The FORTRAN-IV formatted READ and WRITE statements cause transfer of alpha-numeric data to or from the external input or output device selected by the unit number. However, for some applications it is convenient if such data can be transferred, instead, to or from an area in the memory, so that further operations can be performed on it. These are the functions performed by the ENCODE and DECODE statements in Control Data FORTRAN.*

Such facilities can be added to a FORTRAN-IV system by adding a suitable subroutine to the library by appropriation of a unit number that is not otherwise used. The subroutine is written to transfer the data to or from an array. Such a routine has been written for the FORTRAN-IV system on our DDP-24 computer.

The array is designated by the statement

CALL BUFDEF(M,N),

where M is the name of the integer array that receives or supplies the alpha-numeric data and N is an integer constant or variable indicating the number of data words transferred. It must not be larger than the length of the array M and must never be greater than the length of the buffer area used by the I/O conversion routines. These assignments apply to all subsequent operations until altered by another CALL BUFDEF statement. The number of characters per word (four for the DDP-24) depends on the computer word length.

The unit number 8 was selected for this use. The statement

READ(8,n) list

takes N words of alpha-numeric data from the array M and converts them according to FORMAT statement n to fulfill the list. In the process, the input-output buffer area is loaded with N words of data from M. If N is less than the buffer length, the remainder of the buffer area is filled with space codes. The contents of M are not altered. (If the list and FORMAT statement are such as to call for multiline input, the contents of M are transmitted repeatedly.)

Going in the other direction, the statement

WRITE(8,n) list

---

*Control Data Corp., <u>3400/3600/3800 FORTRAN Reference Manual</u>, Publication No. 60132900A (Jan 1967), pp. 10-13.

converts the list according to FORMAT statement n and stores the first N words of the result in the array M. (If the list and FORMAT statement produce multiline output, the output from later lines will overwrite that from earlier lines.)

Example:

An example of the usage of this facility is as follows: Suppose an input deck contains eight different types of data cards, randomly intermixed. Each type must be read with a different list and FORMAT statement. The types are distinguished by an index digit, from 1 through 8, punched in Column 1. A card with 9 in Column 1 indicates the end of the deck.

The deck may be read by the following coding, which assumes four characters per word, and 3 as the card-reader unit number:

```
        DIMENSIØN MBUF(20),. . . .

        . . . .

10      READ(3,20)(MBUF(I),I=1,20

20      FØRMAT(20A4)

30      READ(8,31)INDEX

31      FØRMAT(11)

        GØ TØ(11,12,13,14,15,16,17,18,19),INDEX

11      READ(8,21)list 1

21      FØRMAT(1X, . . .)

        . . .

        GØ TØ 10

12      READ(8,22)list 2

22      FØRMAT(1X, . . .)

        . . .

        GØ TØ 10

        . . .

        . . .

19      . . .
```

Here, statement 10 reads the information on a card into the array MBUF in alpha-numeric form. Statement 30 then decodes the first column to obtain the index digit. A computed GØ TØ branches to the appropriate READ statement (11 through 18) for the particular card. The information in MBUF is then decoded according to the appropriate format (with the first column now ignored in each case) and loaded into the appropriate list. After the information is processed, return is made to statement 10 to read another card. When a card having an index digit of 9 is read, control passes to the remainder of the program, starting with statement 19.

4. <u>ZPR-3 Operations and Analysis</u> (W. G. Davey and R. L. McVean)

Last Reported: ANL-7391, pp. 23-26 (Oct 1967).

a. <u>Basic Studies of Plutonium Systems</u>. An analysis is being made of the data obtained with Assembly 50.

(i) <u>Assembly-50 Central Reactivity Coefficients</u>. The reactivity worths of several materials were measured at the center of the Assembly 50 core, inside a 2- by 2- by 2-in. cavity at the front of the fixed-half central drawer (Location 1-P-16). Two types of measurements were made: small-sample perturbation measurements and drawer-oscillation measurements. These two measurements will be considered separately and some of the results will then be discussed.

(a) <u>Small-sample Perturbation Measurements</u>. Most of the worth measurements were small-sample perturbation measurements, which involved alternately transferring a sample and its dummy into the measurement cavity while maintaining a constant power with a calibrated autorod, and, when required by a large sample worth, Rod No. 6. The sample and dummy were oscillated inside a 1/2-in.-dia radial through-tube so that when in the core they were centered in the cavity with their axes parallel to the matrix face. The samples consisted of 2-in.-long cylinders or annuli of different radii and thickness, as described in Table I.B.1.

The worths given are the measured sample worths relative to those of their dummies, after corrections where necessary for sample-dummy differences in stainless steel mass, for reactivity worth of the empty carriers, and for hydrogen content of the samples. The corrected worths were divided by the sample masses to obtain the specific worths listed. The uncorrected sample-dummy relative worths were obtained from the positions of the autorod and Rod No. 6 while maintaining level power with the two positions of the sample oscillator. The reactivity worth of the empty sample carriers was measured to be +0.0605 Ih. The corrections for the stainless steel mass differences, using the measured stainless steel worth, were no more than 0.012 Ih (less than 1 percent of the sample worths). Some of the powder samples contained hydrogen, whose worth was obtained

TABLE I.B.1. Central Perturbation Measurements in Assembly 50

Material	Sample Size (in.)	Sample Mass (g) Material	Sample Mass (g) Stainless Steel	Material Worth (Ih/kg)
Pu[a]	0.020-thick annulus	9.090	6.009	439 ± 10[h]
	0.010-thick annulus	4.673	6.213	447.2 ± 7.4
	0.006-thick annulus	2.400	6.261	439.0 ± 8.8
Pu[b]	0.020-thick annulus	9.315	6.498	522 ± 13[h]
	0.010-thick annulus	4.801	6.487	534.2 ± 8.5
	0.007-thick annulus	2.761	6.597	533 ± 13
U[c]	0.0106-thick annulus	7.128	1.794	422.8 ± 6.7
U[d]	0.0052-thick annulus	3.638	1.898	427.4 ± 7.6
	0.0034-thick annulus	2.327	1.826	431.1 ± 8.9
U[e]	1.995 x 1.995 x 1.988	2450	-	-31.15 ± 0.73
	0.420-dia cylinder	85.76	-	-33.83 ± 0.53
	0.200-dia cylinder	19.63	-	-36.79 ± 0.85
	0.100-dia cylinder	4.908	-	-40.7 ± 2.8
B[f]	0.040-thick annulus	1.370	10.152	$-(1.215 \pm 0.032) \times 10^4$[h]
	0.040-thick annulus	1.480	10.090	$-(1.187 \pm 0.029) \times 10^4$[h]
	0.020-thick annulus	0.801	11.464	$-(1.289 \pm 0.033) \times 10^4$[h]
	0.010-thick annulus	0.448	10.565	$-(1.352 \pm 0.037) \times 10^4$[h]
	0.200-dia cylinder	1.011	3.096	$-(1.124 \pm 0.026) \times 10^4$[h]
	0.100-dia cylinder	0.244	1.558	$-(1.300 \pm 0.028) \times 10^4$[h]
	0.060-dia cylinder	0.088	0.977	$-(1.443 \pm 0.025) \times 10^4$
Ta	0.0153-thick annulus	9.670	1.774	-290.7 ± 7.0[h]
	0.0106-thick annulus	6.701	1.836	-307.0 ± 4.7
	0.0053-thick annulus	3.300	1.815	-335.7 ± 6.2
	0.200 -dia cylinder	17.13	-	-215.2 ± 5.8[h]
	0.1005-dia cylinder	4.362	-	-259.8 ± 4.7
	0.0615-dia cylinder	1.596	-	-286.7 ± 8.7
SS-304	0.42-dia cylinder	35.90	-	-16.33 ± 0.42
Fe	0.42-dia cylinder	35.50	-	-13.17 ± 0.51
Fe₂O₃	0.42-dia cylinder	11.32	6.351	(i)
Ni	0.42-dia cylinder	40.30	-	-21.61 ± 0.45
Mn	0.42-dia cylinder	15.70	6.386	(i)
Cr	0.42-dia cylinder	15.36	6.412	(i)
Polyethylene	0.42-dia cylinder	4.072	-	2230 ± 58[h]
Na	2 x 2 x 2	(g)	(g)	-11.3 ± 0.9

[a] 98.78 w/o Pu, 1.09 w/o Al, 0.13 w/o other; 72.24 w/o ^{239}Pu, 22.28 w/o ^{240}Pu, 4.63 w/o ^{241}Pu, 0.79 w/o ^{242}Pu.

[b] 98.62 w/o Pu, 1.22 w/o Al, 0.16 w/o other; 95.05 w/o ^{239}Pu, 4.50 w/o ^{240}Pu, 0.45 w/o ^{241}Pu.

[c] 93.20 w/o ^{235}U.

[d] 93.10 w/o ^{235}U.

[e] 0.21 w/o ^{235}U.

[f] 92.8 w/o B; 92.1 w/o ^{10}B.

[g] The sodium worth is the average of two measurements, with samples of 110.2 and 111.5 g Na and 53.47 and 53.99 g stainless steel.

[h] Rod No. 6 was used for the measurement.

[i] The analysis of the worth has not been completed. The correction for the hydrogen content is awaiting completion of chemical analysis of the samples.

from the measured polyethylene worth. Although no carbon sample was measured in Assembly 50, the worth was estimated by reference to its calculated perturbation cross section (+2.13 b) and that of ^{238}U (-211 b), compared to the measured worth of ^{238}U. The results showed that the carbon contribution to the polyethylene worth is negligible (9 Ih/kg of carbon versus 2230 ± 58 Ih/kg of polyethylene). The hydrogen worth worth used for the correction was +(1.55 ± 0.004) x 10^4 Ih/kg. The hydrogen content of the boron samples was obtained by chemical analysis of the powder used in making the samples. The correction was trivial (+21.6 ± 0.5 Ih/kg of boron powder). The remaining powder samples, Cr, Mn, and Fe_2O_3, are being analyzed to determine the hydrogen content.

The uncertainties given in Table I.B.1 for the perturbation measurements are the sums of the uncertainties of the components of the corrected reactivities. The major source of uncertainty is the rod calibrations. The uncertainties in the relative and absolute worths of the autorod are $\pm 1\frac{1}{2}$ and $\pm 2\frac{1}{2}$ percent, respectively, while the uncertainty in the absolute worth of Rod No. 6 is $\pm 2\frac{1}{2}$ percent. Thus, the $1\frac{1}{2}$-percent uncertainty was used when comparing autorod-only measurements, but the $2\frac{1}{2}$-percent uncertainty was used for the autorod when the comparisons included Rod No. 6 measurements. The uncertainties given in Table I.B.1 for the perturbation measurements are the sums of the uncertainties of the components of the corrected reactivities. The major source of uncertainty is the rod calibrations. The uncertainties in the relative and absolute worths of the autorod are $\pm 1\frac{1}{2}$ and $\pm 2\frac{1}{2}$ percent, respectively, while the uncertainty in the absolute worth of Rod No. 6 is $\pm 2\frac{1}{2}$ percent. Thus, the $1\frac{1}{2}$-percent uncertainty was used when comparing autorod-only measurements, but the $2\frac{1}{2}$-percent uncertainty was used for the autorod when the comparisons included Rod No. 6 measurements. The uncertainties given in Table I.B.1 for autorod-only measurements should be increased by 0.02ρ when making a direct comparison with the measurements that included Rod No. 6, 0.02ρ being the square root of the difference between $(0.025 \rho)^2$ and $(0.015 \rho)^2$, where ρ is the corrected sample worth. Use of the corrected sample worth here instead of the uncorrected reactivities of the autorod positions introduces little error because the corrections are small.

The second most important source of uncertainty is reactor noise, which contributed from ±0.0086 to ±0.0149 IH per measurement. These values are those expected from consideration of the power level, length of the measurement, and dispersion of ν. The root-mean-square deviations of the individual reactivity values during a measurement agreed with the expected deviations, so there was no significant cause of the deviations other than reactor noise. The uncertainty in the empty carrier correction was ±0.0086 Ih. The uncertainty in the hydrogen corrections, derived as described above, was about 3 percent of the correction.

(b) <u>Drawer-oscillation Measurements</u>. These measurements were made with the use of a special drawer in location 1-P-16 which

had a partition making a 2- by 2- by 2-in. compartment at its front, and which was connected to a drive mechanism. The drawer was driven into position in the matrix to place various samples in the cavity, and the worths were measured by determining the positions of autorod and Rod No. 6 required to reproduce a standard flux level. The rod positions were also determined with a reference sample in the cavity before and after the measurement with a test sample, to permit correction for reactor temperature drift.

These measurements have a larger uncertainty than the perturbation measurements because of the moving of the core drawer. Its withdrawal from the matrix causes it and the material adjacent to the empty channel to cool significantly below the temperature of the remainder of the core. When the drawer is reinserted there is a fairly rapid heating of the central core, giving a short-term reactivity loss superimposed on the smaller change from the temperature drift of the entire core. This short-term effect introduces additional uncertainty in the worths.

One set of samples measured by this method was made of 2- by 2- by 1/8-in. plates of core materials in an open-topped stainless steel box. One sample had the same composition as the contents of the core drawers, while two others were variations of this with one of the fuel plates removed. These samples are described in Tables I.B.2 and I.B.3. A fourth sample of the set consisted of Pu-Al alloy plate No. 25-1342 (described in Table I.B.3), centered in the box in the same orientation as the core plates. The reference for the set of samples was an empty measurement cavity. The worths of the samples are given in Table I.B.4. The worths of the boxes have been subtracted from the measured worths to get the values in the table. The uncertainties include a $2\frac{1}{2}$-percent uncertainty in the calibration of Rod No. 6 and an uncertainty of ±0.15 Ih from the short-term temperature drift.

TABLE I.B.2. Specification of Core Material Samples for Assembly 50

Normal Loading		Pu-U-Mo Removed		Pu-Al Removed	
Material	Mass (g)	Material	Mass (g)	Material	Mass (g)
C(3 pieces)	39.39	C(3 pieces)	39.39	C(3 pieces)	39.39
Depleted U	148.30	Depleted U	148.17	Depleted U	148.301
Pu-Al	#2U-1454[a]	Pu-Al	#2S-1342[a]	SS can	17.347
Depleted U	148.961	Depleted U	148.17	Depleted U	148.961
C(5 pieces)	65.65	C(5 pieces)	65.65	C(5 pieces)	65.65
Pu-U-Mo	#2-049[a]	SS can	17.3	Pu-U-Mo	#2-049[a]
Pu-U-Mo	#2-224[a]	SS can	17.3	Pu-U-Mo	#2-224[a]
C(3 pieces)	39.39	C(3 pieces)	39.39	C(3 pieces)	39.39
2 x 2-in. box	39.438	2 x 2-in. box	39.001	2 x 2-in. box	39.438

Each sample consisted of sixteen 2- by 2- by 1/8-in. plates inside a stainless steel box.
[a]See Table I.B.3.

TABLE I.B.3. Specifications of Plutonium Plates Used in
Worth Measurements[a] in Assembly 50

Plate Number	Total Mass (g)	Core Mass (g)	Core Composition (w/o)		Pu Composition (w/o)		
			Al	Pu	^{239}Pu	^{240}Pu	^{241}Pu
Pu-1 w/o Al							
2U-1454	86.405	69.582	1.08	98.93	94.97	4.60	0.42
2S-1342	86.295	69.492	1.10	98.89	95.09	4.52	0.39

Plate Number	Total Mass (g)	Mo	^{238}U	^{235}U	$^{239+241}$Pu	^{240}Pu	Stainless Steel
Pu-U-Mo							
2-224	94.850	2.00	62.17	0.14	14.31	1.35	14.77
2-049	94.603	2.00	62.09	0.14	14.28	1.34	14.68

[a]The values of total mass are from weighings after the measurements. The remaining information is from the information supplied by Dow Chemical (Pu-1 w/o Al) and Numec (Pu-U-Mo). The w/o compositions do not add up to 100 w/o, but are as reported by these suppliers.

TABLE I.B.4. Worths of 2-in. Cube Sections of Core Materials
in Assembly 50

Sample	Worth (Ih)
Normal loading	41.2 ± 1.0
Plutonium-metal plate replaced with dummy can	1.44 ± 0.15
Pu-^{238}U-Mo plate replaced with dummy can	31.45 ± 0.76
Plutonium-metal plate at center of 2-in. cube cavity	38.10 ± 0.99

The worth of sodium was measured by cycling 2- by 2- by 2-in. stainless steel cans--two empty and two filled with sodium. It was assumed that the long-term reactor drift due to temperature was constant so that the successive values of the measured worths formed two parallel straight lines. It was estimated that each line was uncertain by ±0.06 Ih because of the short-term drift. The worth given in Table I.B.1 is the difference between the lines. The uncertainty in the autorod calibration is negligible compared to that of the drift correction.

The last worth measurement by this method was of a depleted uranium cube. Its worth was so negative that the reactor was subcritical with it inserted and the reference power could not be obtained. The correction for the degree of subcriticality, based on the source effect measured during the control rod calibration, was 21.5 ± 1.1 Ih, assuming a ±5 percent uncertainty. The autorod was not changed from the reference sample position, but Rod No. 6 was inserted to add 56.4 ± 1.4 Ih. The

reference sample was an empty can worth -0.9 Ih. The drift-correction uncertainty was negligible compared to the other uncertainties.

(ii) Results. The results of central reactivity-worth measurements have been given in Tables I.B.1 and I.B.4. They are discussed briefly below:

(a) Fissile Materials. The fissile samples were sufficiently near to being infinitely dilute that there was no detectable self-shielding. With the assumption that there is none, weighted averages of the measured values give central worths of +441.8 ± 6.7, 529.8 ± 8.5, and 426.3 ± 4.3 Ih/kg Pu (22 w/o ^{240}Pu), Pu (4.5 w/o ^{240}Pu), and U (~93.1 w/o ^{235}U), respectively. The uncertainties are for absolute worths of the plutonium samples and for relative worths of ^{235}U. The sample worths for plutonium were calculated for the entire mass of the material, which included approximately 1 w/o Al. The specific worths when considering plutonium mass only are 447.2 ± 6.7 and 537.2 ± 8.6 for 22 w/o and 4.5 w/o ^{240}Pu, respectively.

(b) B, Ta, and ^{238}U. These materials showed significant self-shielding. The specific worths are shown in Figs. I.B.1, I.B.2, and I.B.3 as a function of the sample-size parameter 4VN/S, where V is the
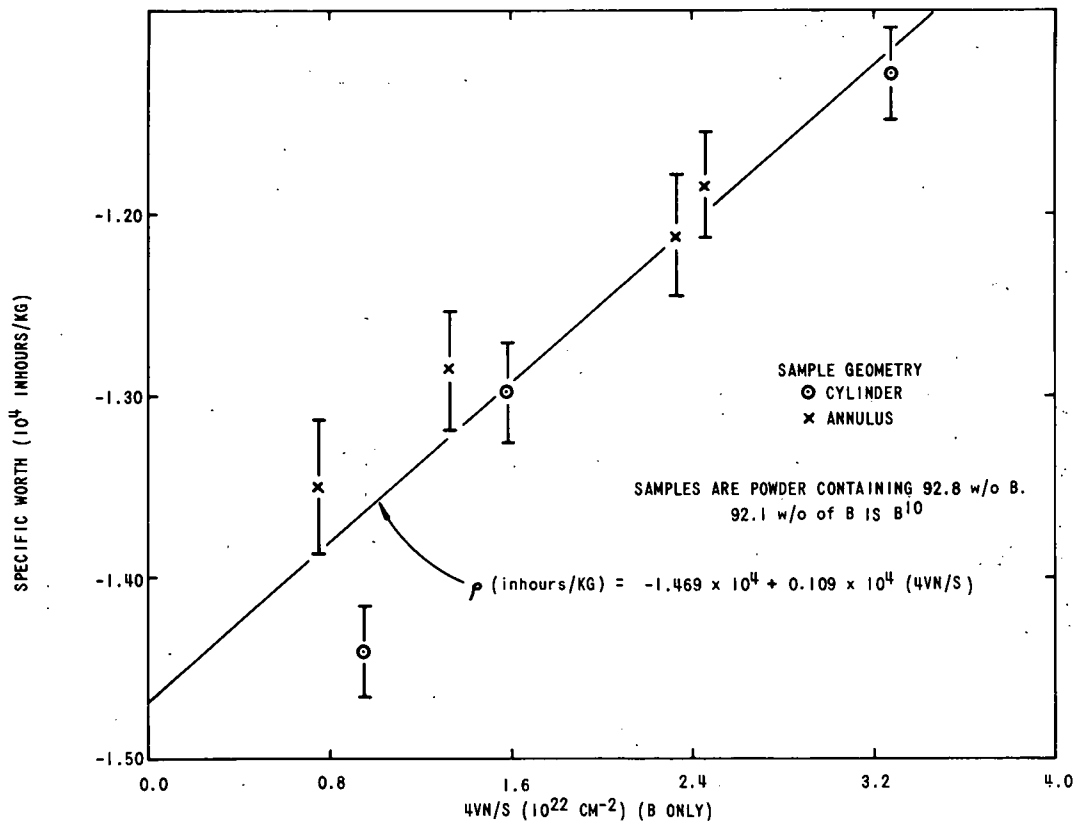
Fig. I.B.1. Boron Worth vs. Sample Size, Assembly 50
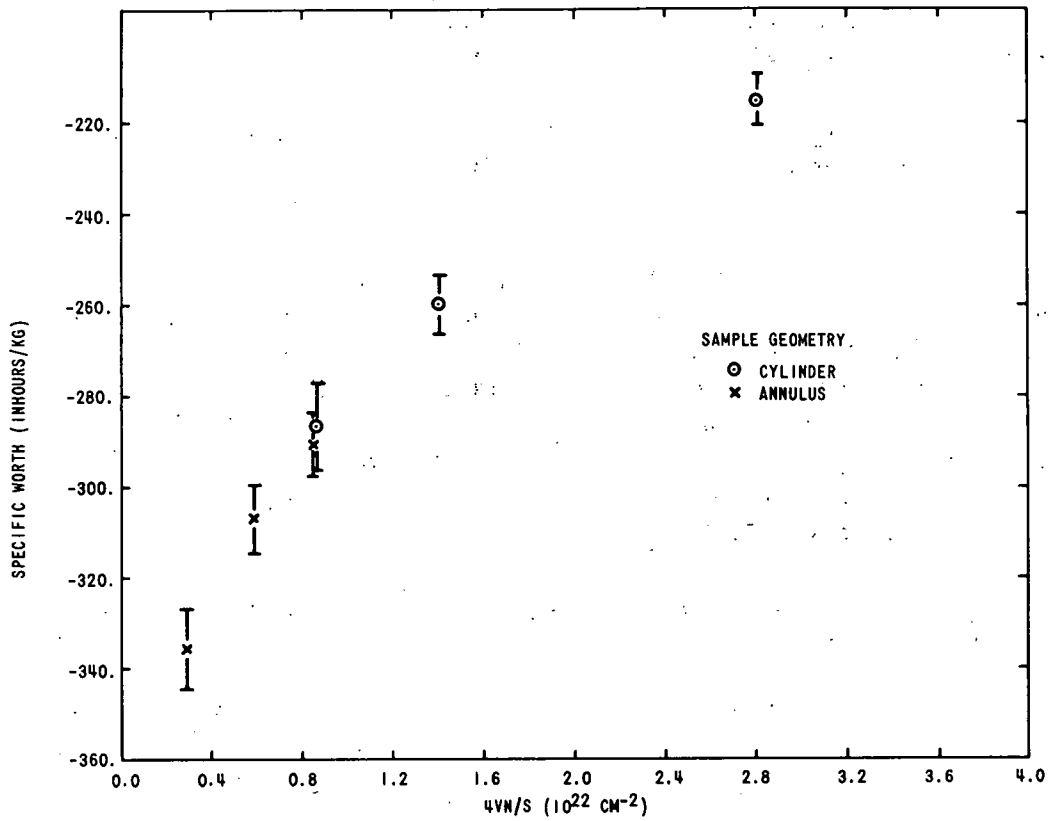
Fig. I.B.2. Tantalum Worth vs. Sample Size, Assembly 50
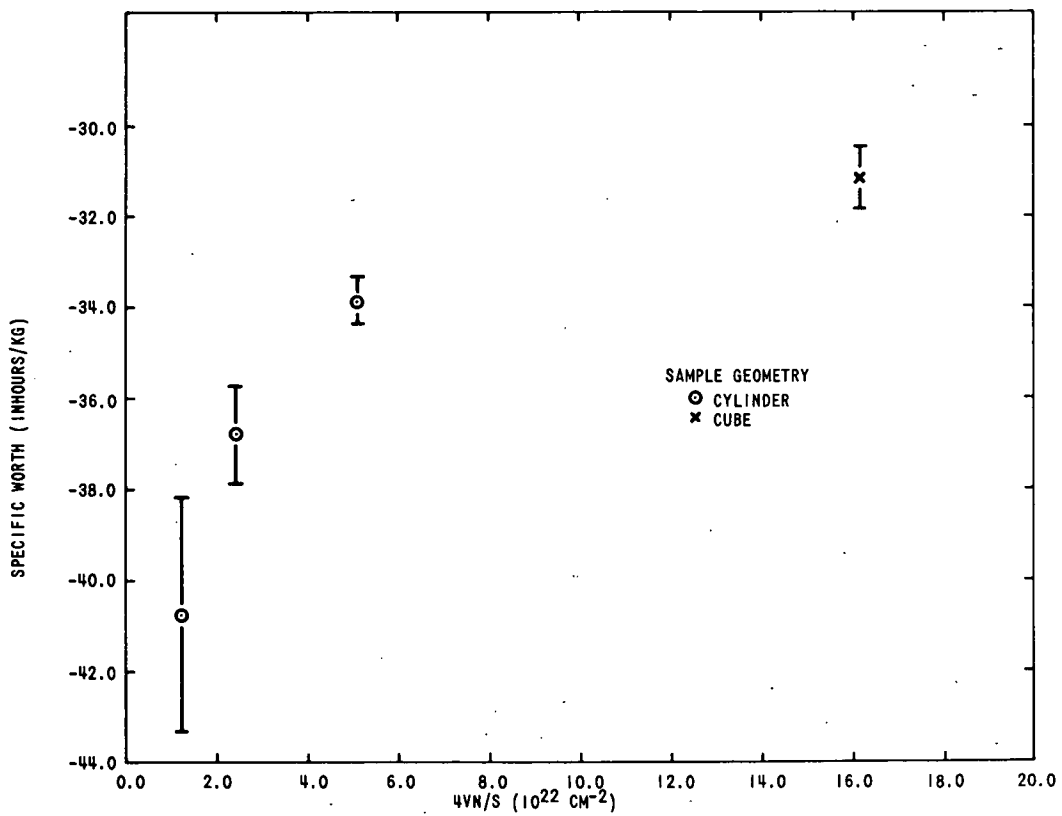
Fig. I.B.3. Depleted Uranium Worth vs. Sample Size, Assembly 50

volume, S the surface, and N the atom density of the sample. The outer surface only was used in calculating the parameter for the annular samples. Theoretical densities were used in determining N for Ta and ^{238}U; the boron powder samples, however, had a varying density which was about 40 percent that of amorphous boron, necessitating the use of densities calculated from the sample masses and volumes. The boron powder mass (92.8 w/o of the total powder) was used to determine the sample density.

A least-squares fit was made for the boron data, giving $\rho(Ih/kg) = -1.469 \times 10^4 + 0.109 \times 10^4 (4VN/S)$, where $4VN/S$ is in units of 10^{22} cm^{-2}.

b. Doppler Coefficient. The modified Doppler equipment needed for the FFTF experiments (Assembly 51) has been fabricated and assembled. Leak checking and installation on the drive carriage will follow.

c. Reactor Technique Development. Fabrication of the sample changer proposed for reactivity traverse measurements is essentially complete. Assembly of the traverse equipment, and bench testing of various modes of operation, will be completed before final determination of parameters for making reactivity traverses.

d. Mockup Studies. Preparations for the FFTF Phase-B critical program in ZPR-3 continued. The drilling of additional access holes for traverses in future FFTF criticals was completed. A new ground was installed between the reactor and the deep water well. The entire reactor-instrument ground system was modified, and two new linear electrometer amplifiers and BF$_3$ detectors were installed to replace existing equipment. All relay contacts were inspected and many were replaced.

After completion of this work, the core and reflector regions shown in Fig. I.B.4 were loaded into the reactor matrix as the first step in Assembly 51, the simple nonsplit cylindrical core of the FFTF series. In the preloading, the core region
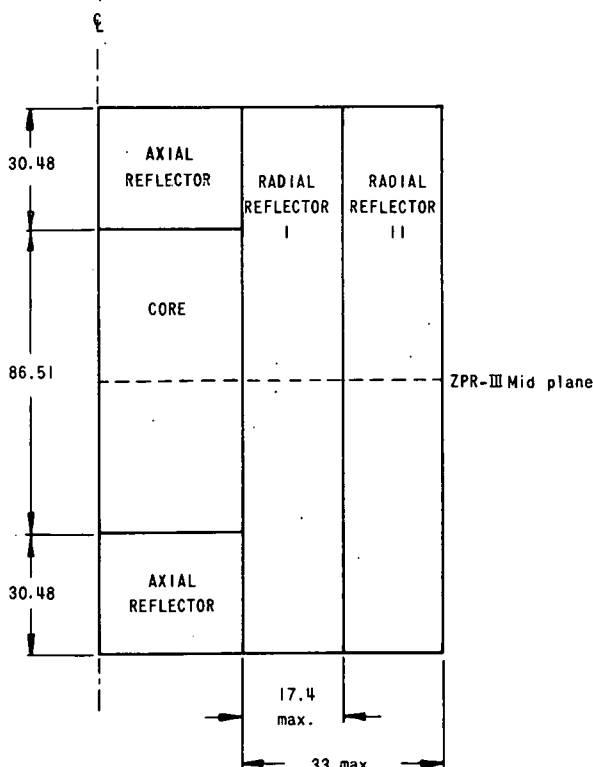
ALL DIMENSIONS IN CENTIMETERS.

Fig. I.B.4. ZPR-3 Assembly 5,
FFTF Phase-B Critical
Assembly 1

was loaded without the plutonium fuel. The approach to critical is being
made by replacing depleted uranium in the core region with plutonium
plates. The approximate composition of each region is listed in Table I.B.5.

TABLE I.B.5. Composition of FFTF Critical Assembly I (ZPR-3, Assembly 51)

atom density (x 10^{-24} cm^3)

Material	Core	Axial Reflector	Radial Reflector I	Radial Reflector II
$^{239+241}$Pu	0.001731			
$^{240+242}$Pu	0.0001706			
^{235}U	0.0000150			
^{238}U	0.007018			
C	0.003113			
O	0.01279			
Al	0.0000553			
Fe	0.01560	0.01046	0.007605	0.07485
Cr	0.003657	0.00259	0.001870	0.00115
Ni	0.001600	0.02893	0.05640	0.00049
Mn	0.0001527	0.0002	0.00023	0.00056
Si	0.0001792	0.0001	0.00009	0.00006
Mo	0.0003275			
Na	0.009256	0.01037	0.00416	

All necessary fuel and materials for Assembly 51 were de-
livered in November.

5. ZPR-6 and -9 Operations and Analysis

a. Integral Studies of Large Systems (W. Y. Kato)

Last Reported: ANL-7391, p. 26 (Oct 1967).

A uranium oxide-zoned core (Assembly 19) has been loaded in
ZPR-9 This assembly consists of three radial core regions and two
radial reflector regions. The outer radius of each region is as follows:

Central Core	26 cm
Buffer	33 cm
Driver	43 cm
Steel Reflector	57 cm
Depleted Uranium Reflector	74 cm

The atom density of each region is given in Table I.B.6. The core height
is 91 cm, to which is added an axial steel reflector of 15-cm thickness
and an outer axial uranium reflector of 15-cm thickness. The volume of
the central region is 192 liters and contains 87 kg ^{235}U. The critical mass
of Assembly 19 was found to be 480 kg ^{235}U.

This assembly will be used for such experiments as: central
and radial reactivity-coefficient measurements, fission-ratio measure-
ments, and central Doppler-effect measurements.

TABLE I.B.6. Atomic Concentrations for ZPR-9 Assemblies 19, 20, and 21

Region	Atomic Densities x 10^{-24}								
	Fe	Ni	Cr	Na	O	Al	C	^{238}U	^{235}U
Core	0.014694	0.001202	0.003035	0.009323	0.014563	-	-	0.005813	0.001156
Buffer	0.007010	0.000793	0.002000	-	0.021732	0.018708	-	0.008259	0.000017
Driver	0.028819	0.003536	0.008196	-	-	-	0.030331	0.000325	0.004553
Steel Reflector	0.077777	0.000891	0.002036	-	-	-	-	-	-
Depleted U Reflector	0.004332	0.000540	0.001140	-	-	-	-	0.03993	0.000081

6. ZPPR Construction (H. Lawroski)

Last Reported: ANL-7391, pp. 30-31 (Oct 1967).

The two remaining major-procurement items for the reactor assembly are now in the final stages of completion. The second rod-drive mounting plate was completed on November 14 and was inspected on November 15 by an ANL representative. The plate was coated and shipped on November 17. The other item consists of the alpha air monitors. The electronics are due by December 18, and the air-sampling pumps are scheduled for delivery by December 6. All other items with the exception of minor nuts and bolts are now stored at ANL-Idaho.

The selection board has recommended a contractor for the installation of the ZPPR reactor assembly and associated equipment. The sample contract was prepared and sent to the AEC for approval on November 16. Since the construction contractor will be late in finishing, arrangements must be made with the installation contractor to begin preliminary work outside the construction area.

The following is a review and updating of the present status of construction.

Placement of the last layer in the gravel-sand roof over the reactor cell, consisting of 2-in. to No. 10 gravel, has progressed to a depth of 6.5 ft; 2 ft more are required for completion. The contractor has completed the weatherproof coating on the mound area with the exception of painting. Cold weather has prevented the painting. The flexboard covering around the backup containment structure has been installed with the exception of the one panel which is being used for entry of gravel fill. Twenty-two of the 24 high-efficiency filter frames have been welded into position. The frame containing the access door is now being installed. The other filter frame will be welded into position as soon as the gravel fill is completed.

All seal connectors have been installed in the mound area. The contractor has completed continuity checks on all wiring between the cell

and the cable-routing room, and between the cell and the workroom. The air piping and electrical controls have been installed to all seal and blast doors with the exception of the two seal doors in the escape tunnel of the reactor cell. The outer seal door of the escape tunnel has been relocated to provide a total of 15-ft clearance between the two seal doors. The original clearance was only 5 ft, which was unacceptable because of congestion between the doors.

The cams for the seal doors in the cell access corridor, in the connecting corridor between the workroom and control room, and in the exit corridor from the workroom and control room, and in the exit corridor from the workroom to the outside have been located for drilling and tapping for mounting screws. Reworking of the contact surfaces between the seal doors and frames has been started in preparation for gluing the rubber seal strips.

Insufficient clearance of the cell-crane trolley drive necessitated rework of the drive train. The specified clearance of 17.5 ft is required for the reactor matrix assembly.

The filter housings for the reactor cooling system have been placed, and the cooling fans have been mounted. The ventilation ducting and refrigeration lines in the cell have been completed. Improper heating coils were rejected and have been replaced in the cell air-handling system. The frangible ceiling grid has been installed.

The two sections of the reactor bed have been lowered 2 ft, placing the bottoms within 2 ft of the reactor-pit floor. The leveling jacks have been positioned and grouted into place with nonshrink grout. Preparations have started for completing the placement of grout in the reactor pit.

The walls and ceilings of the vault, workroom, and inside equipment room of the mound area have been painted. The floors in the vault and inside equipment room have been coated with the epoxy paint.

The air-handling units for the mound area have been operated but not balanced. One of the refrigeration compressors was inoperative, and a replacement oil pump has been ordered to repair the unit.

The support wing of the ZPPR facility is near completion. All tile and trim have been placed. Electrical wiring is essentially complete. The emergency generator was installed and checked out satisfactorily. The cracks in the core cleaning and coating room were repaired, and the floor has been coated with an epoxy paint. The radiochemistry hoods and fuel-coating machine have been installed and connected to the electrical and ventilation systems. The contractor has completed sterilization of the potable water system. The steam, water, and suspect waste systems have

been checked out. The air-handling system has been operating, but has not been balanced. The fan housings for the outside condensers of the refrigeration system were damaged during delivery to the site. This has caused an unacceptable vibration in the housings, which has not yet been corrected.

The biological shield of Argonne Fast Source Reactor (AFSR) has been placed. The rails have been installed for the movable shield in the large experimental hole through the biological shield, and interferences between the movable and fixed shields are being removed.

A reasonable estimate for occupation of the ZPPR facility is early 1968 (approximately mid-January).

A progress meeting was held on November 14 with AEC Chicago, AEC Washington, and ANL personnel. The first informal meeting on the ZPPR Final Safety Analysis Report was held on November 16 in Idaho, attended by AEC Chicago, AEC Washington, AEC Idaho, and ANL personnel. The purpose of the meeting was to discuss preliminary questions and obtain background information. The Final Safety Analysis Report had been sent to AEC on July 28, 1967.

7. ZPR Fuel and Nonfissile Materials--Technical Assistance

    a. **Fuel Element Fabrication Development** (G. D. White and J. T. Dusek)

    Last Reported: ANL-7391, pp. 31-33 (Oct 1967).

Since the modular oxide-core plates for ZPPR are hot pressed five to a stack, the carbon contamination from the graphite molds is a parameter of concern. Specimens of the hot-pressed UO_2 plates were heat treated in a hydrogen atmosphere for 1 hr at 1550°C to reduce the amount of carbon. Specimens of both the hot-pressed plates and the hot-pressed, hydrogen-treated plates were analyzed for carbon. The results are reported in Table I.B.7.

TABLE I.B.7. Carbon Analysis of Depleted UO_2 Plates

Designation	Carbon Content (ppm)	
	As-pressed	H₂ Annealed
5	193	25
10	221	26
26	508	35
3	212	44
8	165	32
24	357	30

Specimens Nos. 5, 10, and 26 are top members of each stack, and Nos. 3, 8, and 24 represent the middle members. Numbers 5, 10, 3, and 8 are from two runs at 1625°C, Nos. 26 and 24 at 1500°C. Representatives of the above-mentioned specimens have been mounted and are now ready for metallographic study.

Steel dies are being designed and ordered for the pressing and sintering of UO_2 and the mixed-oxide $(U,Pu)O_2$ plates. The work on UO_2 will be preliminary to the mixed oxide.

8. ZPR Fuel and Nonfissile Materials--Procurement

Last Reported: ANL-7391, pp. 35-37 (Oct 1967).

a. Process Materials

(i) Plutonium. Approximately 1400 kg of plutonium of varying isotopic composition was blended to 11.5% ^{240}Pu content and cast as 1330 kg of one-kilogram ingots during FY 1967. The work was done at Hanford, Washington, by Isochem Inc. An order for blending and ingoting an additional 1200 kg of plutonium was accepted by the Atlantic-Richfield Hanford Company (Isochem Inc.'s successor) on September 18, 1967. ANL schedules require 686 kg of the plutonium to be blended by January 1968. As of Nov. 30, approximately 238 kg of plutonium ingots had been produced and an additional 276 kg, Blending Lot 14, was approved for ingoting on December 2. Approximately 314 kg of additional plutonium was available, from which Blending Lot 15 will be made to meet the remainder of the January 1, 1968 schedule. Availability of plutonium and blending capacity does not now appear to be an immediate problem. Analytical capability may cause some delay in the acceptance of the material, but it is believed that the slippage in the early part of the NUMEC schedule will provide some slack in the early demand for plutonium.

(ii) Stainless Steel Jackets. The fuel-element jackets consist of rectangular sleeves and two end plugs. The sleeves are made from 1.350-in.-dia by 0.016-in.-wall tubing by flattening and stretch-forming into a rectangular box die by means of an expanding mandrel. The ends of the sleeves must be cut square without turned or burred edges. A special die was developed, which cuts outward from the inside of the jacket sleeve. The outside burr was easily removed by wire brushing. The end plugs were made from formed wire by a series of milling and die-shaving operations. After initial difficulties in obtaining the desired close fit of the end plugs in the jacket sleeves, the tooling was perfected.

The total requirement for the initial Dow order was delivered with greater than 99% acceptance by the vendor. The delivery of jacket components to NUMEC is well ahead of schedule. The numbers of jacket component sets delivered to each vendor by November 30 are given in Table I.B.8.

Jacket sleeves for sodium and sodium carbonate elements are being made by techniques similar to those developed for the fuel elements. The end plugs differ slightly in design from those used for fuel

elements, and are made by stamping and die-drawing operations. A total of 11,500 sets of components for sodium and sodium carbonate elements were made by ANL Central Shops Division. A total of 8,917 were sodium filled. Sodium carbonate tablets were ordered from NUMEC and are to be shipped during early December.

TABLE I.B.8. Jacket Components Scheduled through Dec. 30 and Shipped Nov. 30

Size (in.):	Jacket Sleeves						End Plugs
	1	4	5	6	7	8	
To Dow							
Scheduled	125	804	1151	1066	820	852	-
Shipped	150	804	1151	1066	920	852	9886
To NUMEC							
Scheduled	-	712	1068	712	712	712	-
Shipped	-	712	1068	712	712	712	7832

b. Fuel-element Fabrication. The Dow Chemical Co. has been in fuel-element production since early September 1967. The first month's production gave much lower yields of acceptable elements than Dow expected. This was largely caused by internal casting-shrinkage defects resulting from failure to establish directional solidification and continuous feeding of liquid alloy as the castings solidified. When these conditions were rectified, the yield has improved from less than 50 percent to the present level of about 80 percent of the theoretical possible yield.

Dow has elected to provide chemical isotopic and impurity analyses for each melt and to certify fuel-element composition on the basis of the analyses. Control charts have been maintained for uranium, total plutonium, ^{239}Pu + ^{241}Pu, molybdenum, metallic impurities, nonmetallic impurities, carbon, and americium. Standard deviations were run on subgroups of 25 successive analyses. These are shown in Table I.B.9.

TABLE I.B.9. Evaluation of Dow ZPR Melt Analyses

Data Group		0-25	26-50	51-75	76-100	101-125	126-150	151-175	176-200	201-225
Uranium	Avg	69.02	68.8	68.84	68.86	68.75	68.97	68.99	69.04	68.93
(by difference)	2σ	0.94	0.80	0.38	0.31	1.00	0.16	0.50	0.4	0.50
Plutonium	Avg	28.18	28.50	28.50	28.50	28.51	28.40	28.39	28.31	28.36
	2σ	0.84	0.52	0.32	0.30	0.42	1.06	0.36	0.58	0.50
^{239}Pu + ^{241}Pu	Avg	24.87	25.12	25.16	25.15	25.14	25.06	25.06	24.98	25.04
	2σ	0.76	0.42	0.30	0.28	0.48	0.40	0.32	0.30	0.48
Molybdenum	Avg	2.52	2.49	2.51	2.47	2.52	2.50	2.48	2.53	2.57
	2σ	0.10	0.10	0.14	0.10	0.14	0.10	0.50	0.094	0.02
Metallic Impurities	Avg	677.16	773.8	772.16	724.28	727.56	647.08	501.24	466.52	503.12
	2σ	200.2	219.4	222.8	160.4	128.64	149.00	359.4	327.8	354.6
Nonmetal Impurities	Avg	498.4	411.24	308.72	462.4	452.68	482.28	485.4	547.04	661.08
	2σ	614.2	342.8	234.6	337.8	230.4	393.4	390.6	392.00	319.4
Carbon	Avg	432.72	402.04	295.05	440.56	440.52	470.04	470.6	512.28	625.8
	2σ	519.6	234.00	245.00	325.6	216.4	393.78	386.2	383.6	394.6
Americium	Avg	262.68	296.96	276.05	301.64	275.76	261.68	290.88	275	255.08
	2σ	95.14	66.84	128.92	56.82	74.08	80.6	106.2	70.6	122.00

The compositions appear to be controlled within the limits specified by ANL Specification PF-1600. Carbon has given some difficulty, in part caused by an ultraconservative interpretation of the specification, which limited Dow to a carbon pickup of less than 500 ppm. Reinterpretation of the specification to take credit for 300 ppm carbon in the fuel materials allowed the previously rejected melts to be accepted.

Excessive exposures of personnel to gamma radiation have been a problem at Dow from the start of production. The gamma-radiation levels were particularly high at the vacuum furnace and at the station where crucible shields and machine chips were oxidized. Analysis of scrappings made from the furnace shell showed that the deposited coatings contained very high percentages of [241]Am. The americium content of the ingots has run from less than 100 ppm to over 2000 ppm. The vapor pressure of americium over plutonium has been reported to be 0.03 mmHg at 1139°C, 0.6 mmHg at 1292°C, and 2.95 mmHg at 1436°C.*

Dow has reduced their melt superheat temperatures as low as possible to obtain a homogeneous alloy and casting fluidity. Personnel rotation was used to reduce exposures, and recently the furnaces and furnace gloveboxes were lead shielded. The shielding and furnace cleanup reduced radiation levels at some operator stations by a factor of nearly 100.

Surface dose rates from the fuel alloy are much lower than from the evaporated coatings. These, however, have resulted in hand exposures near the maximum permissible limits in some instances. Hand and body exposures have been reduced by use of local shielding, lead aprons, and lead gloves. A study of the hand and body exposures from zero-power reactor fuel fabrication was recently published.**

The status of fuel-element production at Dow was as follows on December 1, 1967:

Number of casting batches	271
Machined and inspected core plates	2118
Assembled fuel elements	1885
Inspection accepted elements	1796
Elements shipped to Idaho and Illinois	999

Dow has encountered some corrosion problems with about 200 four-inch core plates that were stored in argon-filled polyethylene pouches. The corrosion product is pyrophoric and has been shown to contain uranium-plutonium hydride. The storage conditions have been changed to eliminate this condition.

---

*Nesmeyanov, A. N., (Edited by R. Gary) Vapor Pressure of the Elements, Elsevier Pub. Co. (1963), pp. 345-347.

**Shuck, A. B., "The Fabrication of Plutonium from Highly Irradiated Reactor Fuel," Plutonium as a Reactor Fuel, IAEA, Vienna (1967), pp. 221-236.

The size distribution of accepted and shipped fuel elements was as follows:

Fuel Element Length, in.:	4	5	6	7	8	Total
Dow Accepted Elements	269	903	92	466	66	1796
Shipped from Dow	15	627	15	327	15	999

Nuclear Materials and Equipment Corporation (NUMEC) submitted 50 preproduction dummy elements on September 15, and 27 fuel elements and 23 core plates on October 3. Complete data covering the analysis of these core plates were not received until October 20. Samples representing the top, middle, and bottom of castings were received on October 16, 1967. The NUMEC preproduction elements were evaluated by ANL.

ANL reviewed the NUMEC process specifications and manufacturing instructions, and presented comments on these on November 30, 1967. NUMEC was released for casting production on November 19, 1967, and for welding and assembly of fuel elements November 30, 1967. As of December 1, NUMEC had made eight melts for production (and 32 experimental melts). A total of 51 core plates were considered possible from the eight melts from which 13 core plates had been machined. Eleven of these passed visual and dimensional inspection. The early NUMEC castings have produced a lower yield than expected. This has been largely due to imperfect filling of mold·cavities. Some equipment failures have also been experienced, such as mold heater or thermocouple failure, which have contributed to poor yields.

9. FFTF Critical Experiment Program (P. J. Persiani)

Last Reported: ANL-7391, pp. 37-41 (Oct 1967).

a. Development of Cross-section Set. Set 290001 (see ANL-7391, p. 38) has now been put in proper form for diffusion and transport calculations. It has also been collapsed from 29 groups to 6 groups and designated Set 29601. The lower energy limits of the groups are given in Table I.B.10.

TABLE I.B.10. Lower Energy Limits of Groups of Set 29601

Group	Lower Energy Limit	Group	Lower Energy Limit
1	1.35 MeV	4	4.31 keV
2	183 keV	5	275 eV
3	24.8 keV	6	10^{-5} eV

Computed parameters for ZPR-3 Assembly 51 using Set 29601 without heterogeneity correction are: a critical volume of 305 liters and a critical mass of 209 kg $^{239+241}$Pu. With Set 29001 the corresponding figures are 301 liters and 207 kg.

b. Preplanning Computation of Doppler Coefficient. The core-loading diagram for ZPR-3 Assembly 51 contains three types of fuel pieces: plutonium metal designated Type 1, ZPPR fuel called Type 2, and SEFOR fuel called Type 3. In the computation of the Doppler coefficient it is assumed the heat produced by fissions in each type of fuel does not flow out of the fuel piece. Because the three types of fuel heat up at three different rates, a reference temperature rise is needed, and the Doppler coefficient dk/dT_1 is computed per degree rise of plutonium metal fuel; concomitantly, dT_2/dT_1 and dT_3/dT_1 must be evaluated. It is also assumed that the temperature rise of each type of fuel is not a function of position in the reactor. Thus the coefficient is based on a spatial "average" temperature rise.

The reactivity effect of a temperature change is evaluated for each type of fuel separately by computing k_{eff} through the MACH 1 code and use of cross-section Set 29001 when the temperature of each type of fuel is separately increased to 1000°K while other materials and other fuel types are held at 300°K.

The overall Doppler coefficient is found from

$$\frac{dk}{dT_1} = \left(\frac{dk}{dT}\right)_1 + \left(\frac{dk}{dT}\right)_2 \left(\frac{dT_2}{dT_1}\right) + \left(\frac{dk}{dT}\right)_3 \left(\frac{dT_3}{dT_1}\right)$$

to lead to a -4.33×10^{-6} °K^{-1} change in temperature of the plutonium metal. The Doppler effect is assumed to have a $1/T$ dependence.

c. Preplanning Calculation of Safety-rod Worth for ZPR-3 Assembly 51. Computations of the worth of eight safety rods (two in each of the positions N13, N19, R13, and R19) and with the compositions described as A and B in Table I.B.11 have been completed. Also, the worth was computed for rods made of average core composition.

The composition used in the safety-rod positions for the case of the rods fully out was homogenized empty drawer material. For the rods out 10 in. a rod composition was used with a density reduced by

TABLE I.B.11. Proposed Safety-rod Composition for Assembly 51, atoms/b-cm

Material	Loading A	Loading B
$^{239+241}$Pu	0.002147	0.003220
$^{240+242}$Pu	0.0001020	0.0001530
^{235}U	0.000017	0.000020
^{238}U	0.008119	0.009672
C	0.003119	0.003119
O	0.01413	0.009360
Fe	0.017271	0.01632
Cr	0.003762	0.003970
Ni	0.001646	0.001737
Na	0.008485	0.008596

a factor derived from the small-sample axial worth distribution for [239]Pu given in ANL-7391, p. 40. The actual worths of differential segments of rod length were assumed to be proportional to the small-sample worth of [239]Pu referred to above. Thus the ratio of the worth of the rod out 10 in. to the worth when fully out was assumed to be proportional to the ratio of the integral of the small sample worth from 10 in. to the fully out position divided by the integral of the small-sample worth from zero to the fully out position. This ratio was found to be 0.2481, and the nuclide concentrations for proposed rod compositions A and B were multiplied by this factor in the computation of worth of the rod when out 10 in.

In the case of rods of average core composition, a worth value was obtained for the nuclide concentrations all reduced by 1%, but the computation for rods 10 in. out was not done. For the MACH-1 calculation, which is one-dimensional, the cross-sectional area of the rod was spread into an annular region with an average radial distance from the center equal to that of the rods and with a total cross-sectional area equal to that of the four rod positions. SNARG two-dimensional computations were done in the S_2 approximation, in which four separate rod positions were used.

The results appear in Table I.B.12. The cross-section Set 29001 is appropriate for Assembly 51 and was used in one-group MACH-1 calculations. Because its 29 groups were too many for the SNARG two-dimensional computation, a six-group set, 22612, appropriate to Assembly 48, was used. A group of MACH-1 calculations was made for comparison.

TABLE I.B.12. FFTF Assembly-1 Safety Rods

	MACH 1D Set 29001	MACH 1D Set 22612	SNARG 2D Set 22612
Loading A			
In	k = 1.0000	k = 1.0000	k = 1.0010
Out 10 in.		k = 0.9724	k = 0.9733
	Δk = 0.0277	Δk = 0.0276	Δk = 0.0277
Fully out		k = 0.9401	k = 0.9431
		Δk = 0.0599	Δk = 0.0579
Loading B			
In	k = 1.0000	k = 1.0000	k = 1.0017
Out 10 in.		k = 0.9622	k = 0.9631
	Δk = 0.0376	Δk = 0.0378	Δk = 0.0386
Fully out		k = 0.9262	k = 0.9295
		Δk = 0.0738	Δk = 0.0722
Average Core Loading			
In	k = 1.0000		
1% fuel removed	Δk = 0.000218		
Fully out	Δk = 0.0555		

In all cases the values of Δk for rods 10 in. and fully out are closer together than previous experimental evidence would predict. However, it would appear that the 1.5% Δk total worth required in the eight rods could be met using rods of average core composition.

C. Component Development--LMFBR

1. Sodium Technology Development--Engineering Development
   (S. B. Skladzien)

   Last Reported: ANL-7391, pp. 42-43 (Oct 1967).

   a. Sodium Quality Measurement

   (i) Laboratory Techniques. Characterization of the sodium
in the Building 308 storage tank is continuing. Different methods of
sample-tube precleaning are being investigated to determine whether a
particular cleaning method results in the sodium picking up more or less
contamination from the tubing. Sodium oxide is the reference contami-
nant being measured by mercury amalgamation. Vacuum-distillation-
type analyses are being made on replicate samples as a check.

   (ii) In-line Techniques. Six sodium samples (numbered 11
through 16) were taken from the Sodium Analytical Loop (SAL) and ana-
lyzed for oxygen content. Samples 11L and 12D indicated 15.3 and
17.6 ppm oxygen, respectively, by the atomic absorption spectrophotom-
eter (AAS) analysis method. ("D" and "L" refer to "dip" or "line" type
samples.) These numbers are relatively high; the cause is not known. In
contrast, samples 13D, 14L, 15D, and 16L averaged 8.1 and 7.6 ppm
sodium oxide by the AAS and titration-analysis methods, respectively.

   To date, 122 plugging runs have been made; the more
recent of these runs were with varied flow and cooling rates. The results
showed a plugging-temperature spread of 30°F for the same system con-
dition. A faster flow (which creates slower cooling) seems to give a higher
plugging temperature with a more definite flow break on the recorder
trace. We have found that the sharp break occurring at the higher flow
coincides with the oxygen content found by chemical analyses (titration and
AAS). The chemical analyses, in turn, agree with the latest solubility
data* for oxygen content in sodium at the temperature where the break
occurs.

   The operating temperature of the SAL was reduced from
600 to 310°F for 10 days to locate the reason for the erratic output of the
resistivity meter. The loop that includes the resistivity meter was kept
at 300°F and flowing when the vacuum-insulation shroud and heat-reflection
shields were removed. Faulty mechanical connection of the copper lead
wires at the measuring point was found to be the cause of the problem.
Since these connections were silver-soldered, resistance measurements
have been constant and correct.

---

*LA-3607, Quarterly Status Report No. 1 on Advanced Plutonium Fuel Program for period July 1 through
Sept. 30, 1966; Project 802--Measurement of Impurities and Development of Quality Control Techniques
for High-Temperature Sodium-Coolant Systems.

During the same period of 310°F loop operation, two 250-W cartridge heaters in the main vessel were replaced by two 750-W heaters. The heaters were changed to achieve more precise temperature control and faster reheat after plugging runs.

The responses of the resistivity meter and the United Nuclear oxygen meter cell No. 2 were checked with a 1°C change in temperature. The temperature change between 313.42 and 314.42°C was measured by a precisely calibrated platinum resistance thermometer located within the resistivity meter and was controlled within ±0.03°C. A 1°C change equals 0.75 micro-ohm for the resistivity meter and 1.1 mV for the oxygen meter. Oxygen cell No. 1 was not tested because it has been producing sudden voltage changes as high as 9 mV. The cause has been traced to the sensor proper; although this cell does not behave consistently, it is useful for test purposes.

Six gallons of 300°F sodium from the EBR-II Model Tank have been transferred to the 19-gal makeup tank on the SAL.

2. Reactor Mechanisms Development--Materials Evaluation

    a. Physicochemical Mechanics of Materials (F. A. Smith)

    Last Reported: ANL-7391, pp. 43-44 (Oct 1967).

Three thin 0.2-μ foils of Type 304 stainless steel were received from Stanford Research Institute for exposure to various sodium environments. One of the three experimental foils has been held in a Mark-I holder in static 1200°F sodium for 7 days. Procedures are being developed for construction of the Mark-I sample holder, sodium insertion, sample removal, sample-sodium removal or cleaning, and sample shipment.

When adequate procedures for handling the thin foils have been developed, 12 additional thin foils will be exposed to sodium and then will be examined with a transmission electron microscope.

    b. Out-of-core Neutron-detection Systems (T. P. Mulcahey)

    Last Reported: ANL-7279, p. 66 (Nov 1966).

Wide-range and intermediate-range circuits are being developed and will be tested in a special thimble in EBR-II. Environment and performance requirements for FFTF and future LMFBRs serve as development and test goals so that suitable neutron-flux measurement systems will be available for such reactors.

The counting-mean-square voltage approach to neutron-flux detection systems shows particular promise when applied to a Liquid Metal Fast Breeder Reactor where large residual gamma fluxes caused by sodium activation are almost always present. By combining the excellent gamma-discrimination capabilities of counting circuitry with the inherent discrimination obtained from a mean-square voltage signal, a single fission counter may be utilized to measure up to 10 decades of reactor power accurately. For investigation and evaluation of the counting-mean-square voltage approach, two commercial prototype reactor instrument systems have been ordered.

Both systems are wide-range channels operating from a single fission counter and may be able to measure up to 10 decades of neutron flux in the presence of a gamma background of $>10^5$ R/hr. With one system, the full 10-decade range will be indicated on a single log-power meter or recorder, as will the reactor period; this system electrically combines a log-countrate signal, available for the lower 5 decades, with a log-average-magnitude-squared (AMS) signal, generated over the upper 5 decades, to produce a single output indication. The other system produces two separate 7-decade outputs, one of which is a log-count-rate signal while the other is a log-true-mean-square (TMS) signal; separate reactor period outputs are generated from each channel signal.

A linear power channel is included as a part of both systems. The dc signal required for this channel is derived directly from the same fission counter. Safety trip, calibration, trip test, and detector excitation voltage circuits are a part of the complete system designs.

The delivery of both these instrument systems is expected by March 1968.

c. <u>Fuel-pin Thermocouple</u> (G. F. Popper)

Last Reported: ANL-7371, pp. 71-72 (Aug 1967).

(i) <u>Electrical Insulators</u>. To determine the cause of changes in color and some crystal formations, thoria samples that have been heated are being analyzed for both contaminants and changes in stoichiometry. Analysis with a laser microprobe has begun.

Problems in obtaining source materials of sufficient purity have delayed delivery of samples of the vitrified beryllia and hafnia insulation.

(ii) <u>Thermoelement Properties</u>. Since the failure of BTC-1 (see Progress Report for July 1967, ANL-7357, pp. 72-74), other W-3% Re/W-25% Re bare-wire thermocouples have been constructed and

tested. Each has failed similarly to BTC-1 and within 48 hr at 2400-2500°C. The cause of the failures, which have occurred with each lot of W-3% Re/ W-25% Re wire tested, is being determined.

(iii) <u>Material Compatibility</u>. Another tantalum-UO$_2$ compatibility sample is ready for testing. This sample, identified as TU-3, has the same construction as TU-2 and will be tested under the same conditions (see Progress Report for April 1967, ANL-7329, p. 41).

d.   <u>Fission-Gas Pressure Transducer</u>   (J. R. Folkrod)

Last Reported: ANL-7391, p. 44 (Oct 1967).

(i)   <u>NaK-filled Capillary System</u>. The miniaturized (1/8-in. bellows) system is ready for final cleaning and assembly. It then will be filled with NaK.

(ii) <u>Null-balance System</u>. The MSA null-balance system has been delivered and is being tested. With this system, the simulated fission-gas pressure is slowly increased and the reference gas pressure is observed for comparison. Both pressures are sensed by pressure transducers; the signals are recorded on a strip chart. Testing so far is at room temperature; eventually, the null-balance device will be heated to 1200°F. It appears that the reference gas reads about 4 psi greater than the simulated gas pressure over the range from 0 to 75 psig. Occasionally, the probe did not contact the bellows; then the reference gas pressure was considerably off, causing a sudden jump in pressure and a step in the curve.

e.   <u>In-core Flowmeter</u>   (G. F. Popper)

Last Reported: ANL-7391, pp. 44-48 (Oct 1967).

(i)   <u>Thermal and Mechanical Tests of Magnetic Materials</u>. The B-H tester is now operational. This instrument will be used to examine the changes in shape of the magnetic material hysteresis loop due to temperature (and, possibly, radiation) effects.

Figure I.C.1, which shows the reversible effects of an Alnico-8 rod magnet that has a length-to-diameter (L/D) ratio of 8, represents typical results obtained using the lavite furnace assembly and magnetometer. The lavite furnace, however, has developed serious cracks because of temperature cycling. A castable ceramic material is being considered as a possible replacement for the lavite furnace body.

(ii) <u>Prototype Magnetic Flowmeter</u>. The calibration loop has been repaired. The flowmeter will be calibrated.
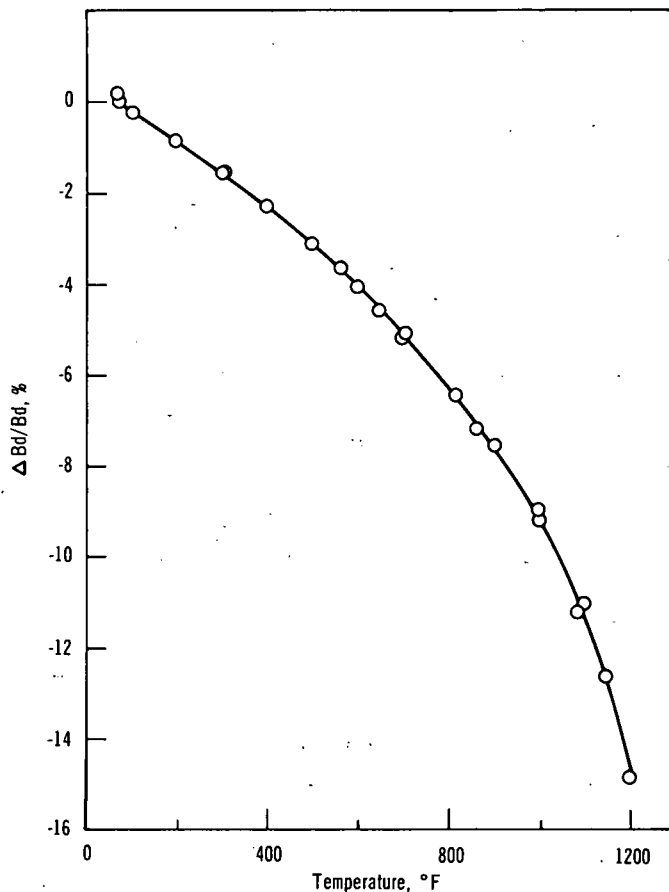
Fig. I.C.1

Reversible Changes of Remanence of an
Alnico-8 Rod Magnet Whose Length-to-
Diameter Ratio is 8

(iii) Magnet Irradiation Tests. Excessive time and effort would
be required to use a mockup irradiation capsule to define more accurately
the gamma heating rates in the EBR-II. Instead, the magnet irradiation test
will be based on the following criterion. The irradiation-capsule thermal
shields will be sized to produce a magnet temperature of 1200°F with the
largest gamma heating rate to be expected at a reactor power of 50 MW.
Thus, with the present uncertainty about gamma heating rate (see Progress
Report for October 1967, ANL-7391, p. 47), the magnets will operate at a
maximum temperature between about 850 and 1200°F, but under no con-
ditions could they exceed 1200°F. Melting-point capsules will be examined
after the irradiation test to determine the actual operating temperature.
With this decision, experiment description and hazard analysis can be
completed.

f.   Signal-lead Connectors for Sodium Service   (A. P. Grunwald)

Last Reported: ANL-7382, p. 70 (Sept 1967).

A test has been started to determine the time an electrical
connector can be left opened in a sodium vapor environment before the
occurrence of serious loss of insulation resistance between connector pins
and the metallic body of the connector. A Physical Sciences Corporation

36-pin high-temperature plug (previously selected as the FARET prototype design*), welded into the top of a 2-in.-dia x 3.5-in.-high stainless steel capsule containing 35 g of sodium in an argon atmosphere, is being tested in an instrument-controlled electric furnace. Insulation resistance at various temperatures is being determined by the series-voltmeter method with a 0-185-V dc power supply. Approximately 90% of the test data has been taken and is being analyzed.

g. <u>Method of Locating Failed Fuel</u> (F. Verber)

Last Reported: ANL-7371, p. 74 (Aug 1967).

A sodium-recirculating system is being designed to demonstrate that fission gas can be separated from circulating sodium and measured to locate a failed fuel element. To determine the sensitivity and response time of the fission-gas detection, a small amount of krypton gas containing krypton-85 (10.4-yr half-life) will be injected in the sodium loop; krypton that arises above the sodium will be detected with a Geiger-Muller counter at a stainless steel window.

System design drawings are being prepared and materials and components are being acquired. Figure I.C.2 shows the flow diagram for the system. The enclosure of the 1-in. pipe (with six 1/2-in.-dia holes) inside the 4-in. pipe section (see enlarged view) of the sodium-recirculating system reasonably approximates the FFTF in-reactor counterpart. At this time, design emphasis is toward achieving a reliable piston-type gas injector.

3. <u>Fuel Handling, Vessels, and Internals</u>

a. <u>Core Component Test Loop (CCTL)</u> (R. A. Jaross)

Last Reported: ANL-7391, p. 48 (Oct 1967).

The 4-in. gate valve for flow control is ready for installation in the pressure vessel. A tentative arrangement of the test FFTF fuel subassembly in the vessel is being drafted; because the estimated 60-psi pressure drop across the subassembly will produce an upward force of 1880 lb, the grid-plate assembly will be attached positively to the vessel. A preliminary design has been selected for the elevator that will be assembled within the vessel for dynamic material corrosion and stress tests; however, means for removing corrosion samples while the loop is operating require further study.

---

* Popper, G. F., and Knox, A. E., <u>FARET In-core Instrument Development</u>, ANL-7161 (July 1966).
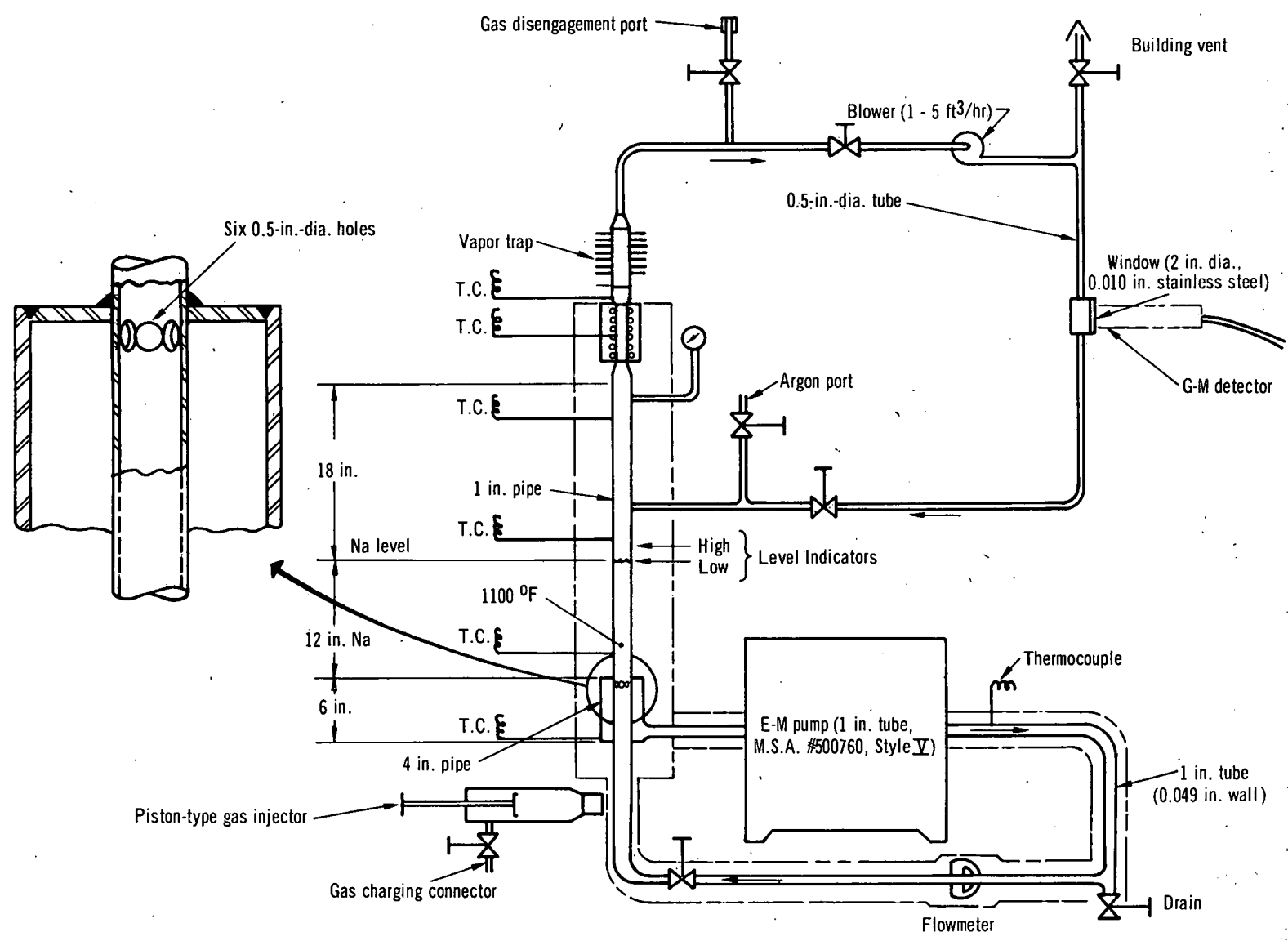
Fig. I.C.2. Flow Diagram of Loop for Testing Principle of Failed-fuel Locator

(i) <u>Stresses in Piping.</u> High-temperature strain gauges are being used to determine the stresses in the loop during operation (see Progress Report for September 1967, ANL-7382, pp. 71-72). Apparently anomalous readings from the 87 gauges on the loop led us to investigate gauge accuracy under controlled conditions. Thus rokide-bonded free-filament strain gauges were tested on an unstressed Type 304 stainless steel specimen that was heated to various temperatures in a furnace.

After the desired furnace temperature was established and stabilized, strain readings were taken periodically over a 2-hr period, the time that might be needed to take readings on the loop piping. Drift during the 2 hr is negligible at temperatures up to about 1000°F; however, a drift at 1190°F was noticeable, being about 500 μin./in./hr. In addition, the variation of strain readings with temperature was much greater than we expected. Most disturbing is the fact that the two identical gauges indicated different strains at the same temperature. More gauges will be tested to determine the extent of the problem.

D. EBR-II

1. Research and Development

    a. Reactor Experimental Support--Reactor Analysis and Testing
        (R. R. Smith)

        Last Reported: ANL-7391, pp. 51-60 (Oct 1967).

        (i) Nuclear Analysis

            (a) Run 26B. After 90 MWd of reactor operation in
Run 26A, the Mark-II oscillator rod was installed in control-rod position
No. 8 (5A3). A loading readjustment was made which included replacing a
half-worth driver subassembly in position 4B3 with a full-worth driver sub-
assembly, and a full-worth driver subassembly in position 6C1 with a half-
worth driver subassembly. This new loading was designated 26B. During
Run 26B, six separate power-reactivity decrement (PRD) measurements
were made.

            Data on PRD from Run 26B were corrected and are
presented in Table I.D.1. No significant change in PRD occurred during
Run 26B.

TABLE I.D.1. Power-reactivity Decrement (PRD) for Run 26B

Date	Total Integrated Power for Run 26 (MWd)	Control-rod-bank Position (in.)	PRD, Ih Normalized to 11.00-in. Rod Bank
10/14	100	11.00	40.6
10/15	122	11.00	41.8
10/17	185	11.00	40.3
10/20	252	11.00	38.5
10/27	555	11.50	40.2
11/19	1050	12.75	42.4

            Because of the added emphasis on more precise deter-
mination of reactivity effects, a new nonmechanical period-measuring device
has been designed. It is initially intended to serve as a backup to the present
system, with the expectation that it will prove more reliable and eventually
become the principal period-measuring device.

            (b) Measurements of Transfer Function. The transfer
functions at 22.5, 30, and 41.5 MW were remeasured near the end of Run 26B
under high rod-bank conditions (12.75 in.). The resulting data are being
normalized and feedback is being calculated.

Data were obtained at the start of Run 26B on measured phase and amplitude at 500 kW and at 22.5, 30, and 41.5 MW, at control-rod bank positions of 11.00 and 12.75 in. Examples are given in Figs. I.D.1 and I.D.2. The calculated zero-power data are given as the solid line. Analysis indicates that for the 30- and 41.5-MW data, the normalization at 8.8 cps introduces a decided shift in the amplitude. Normalization at 4 to 6 cps would appear to be more consistent with the 22.5-MW operation and with what is expected based on the reactor response as indicated from the results of rod-drop measurements. The source of this discrepancy is under investigation.

(c) Feedback Data from Rod-drop Experiments. The reactivity feedback was established from the results of rod-drop experiments at reactor power levels of 25, 35, and 45 MW with the control rods banked at a nominal 13.00-in. position during Run 26A. The results of a typical calibration from five sets of measurements are given in Fig. I.D.3. The solid line represents an attempt to improve the quality of the calibration by an initial smoothing of power-recording data. It is still unclear whether or not such data conditioning significantly improves the quality of the calibration. In any event, the calibration established from raw data has been found to be sufficiently accurate and is being used in feedback analyses.
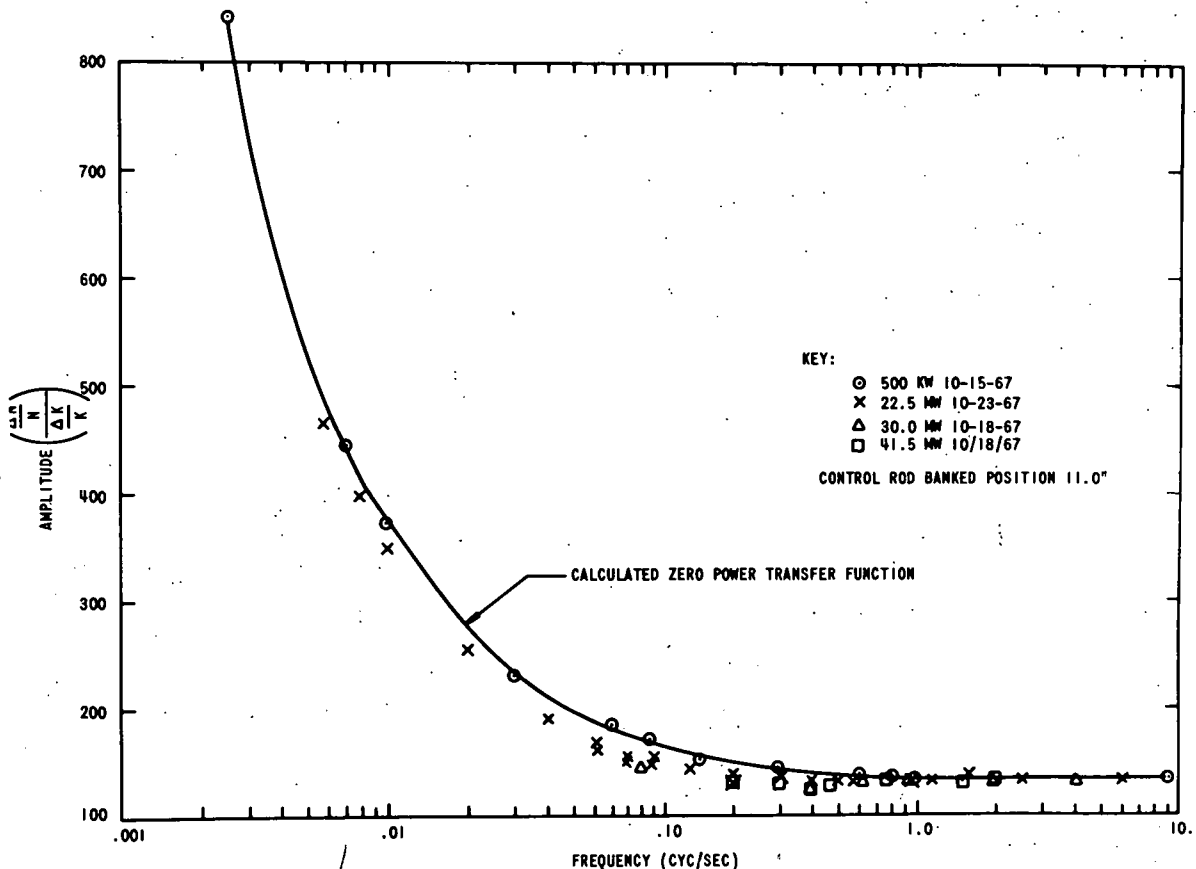
Fig. I.D.1. EBR-II Transfer-function Amplitude
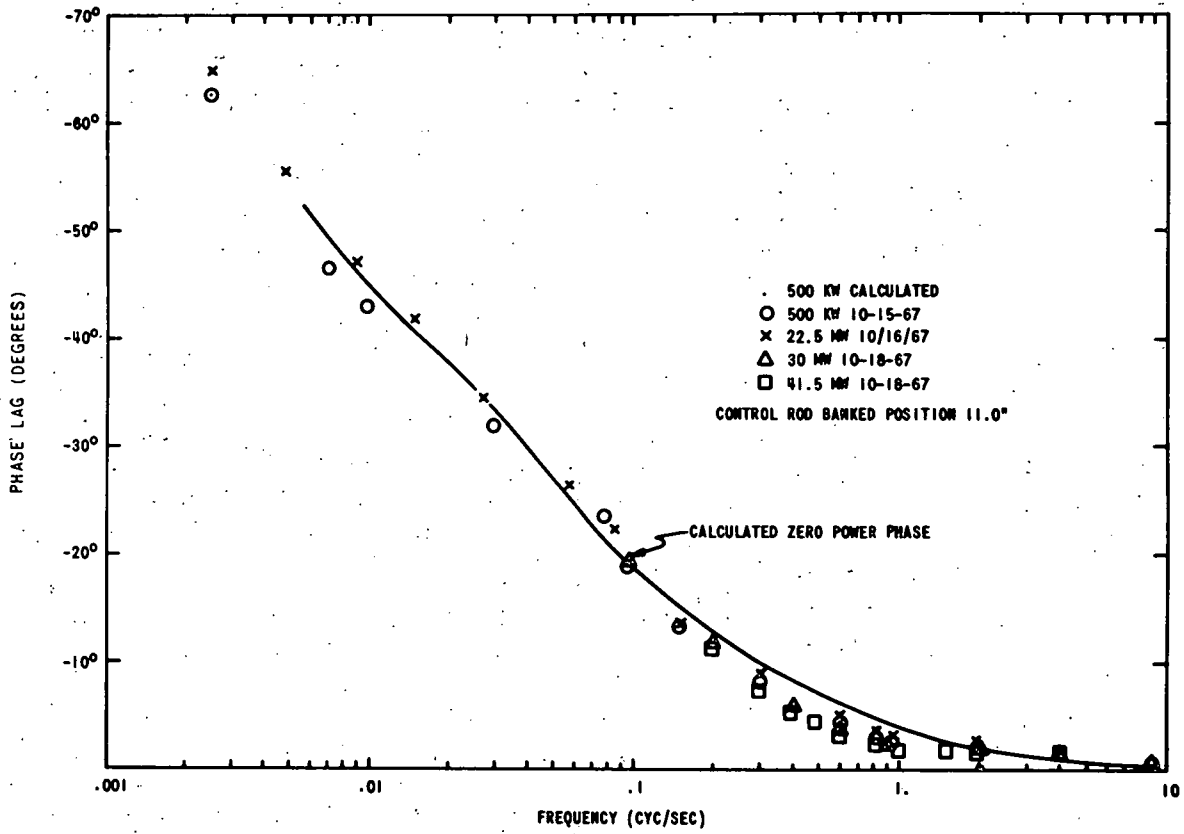
Fig. I.D.2. Phase Lag of EBR-II Transfer Function
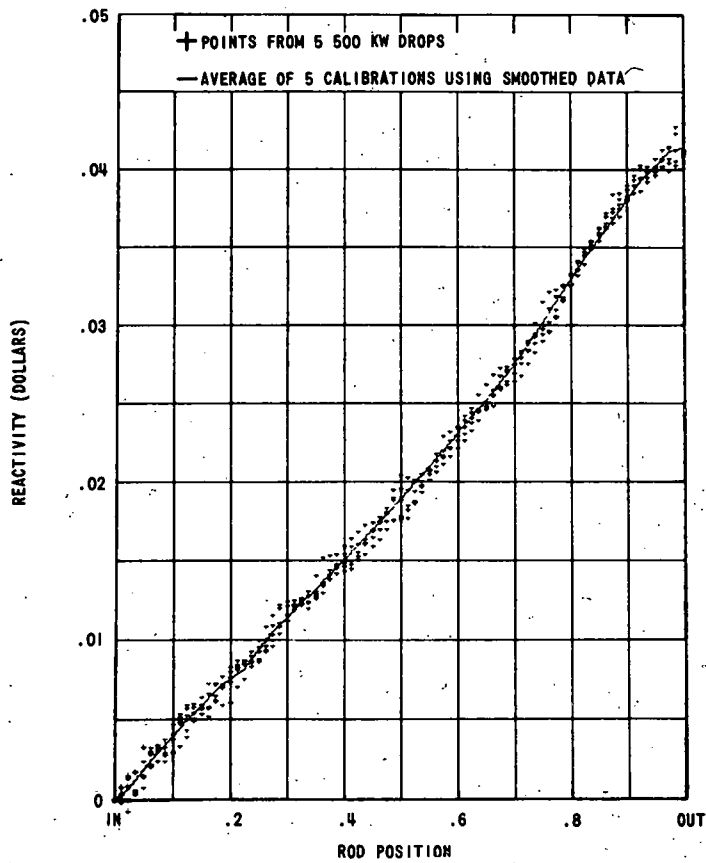
Fig. I.D.3

Stainless Steel Rod Calibration
for Rod-drop Experiments

It appears that the worth of the drop rod changes when the reactor power is raised from the calibration level of 0.5 MW. Evidence indicating such a change is given by the behavior of the calculated feedback during the initial 0.3 sec of the measurements. Without exception, the calculated feedback is negligible until the drop-rod travel is complete, at which time the feedback rises abruptly. It seems that the reactivity worth of the drop rod increases by an amount which is just sufficient to cancel the feedback during this period of time. It is significant that a change of as little as 2 percent in drop-rod worth causes a significant error in assessing the magnitude of the prompt feedback. The effect of such changes in the calculated feedback one second after drop, however, is probably not more than 15 percent.

The data for the 25- and 35-MW drops during Run 26A are given in Figs. I.D.4 and I.D.5. The 45-MW results are nearly identical to those cited for Run 26A in the Progress Report for October 1967, ANL-7391, pp. 57-58, for the 11.00-in. rod-bank position. The 25-MW data in Fig. I.D.4 indicate the existence of a strong delayed positive component of the power coefficient following the more prompt, and equally strong, negative component. At the end of the first second, the power has dropped about 5 percent and the feedback is $0.0035; although the power drops almost 5 percent more at the end of 10 sec, no additional feedback is obtained during the latter interval. The delayed positive coefficient is apparently strong enough to offset any additional feedback from prompt negative effects; however, net feedback is still uniformly negative and sufficiently strong for good control characteristics.
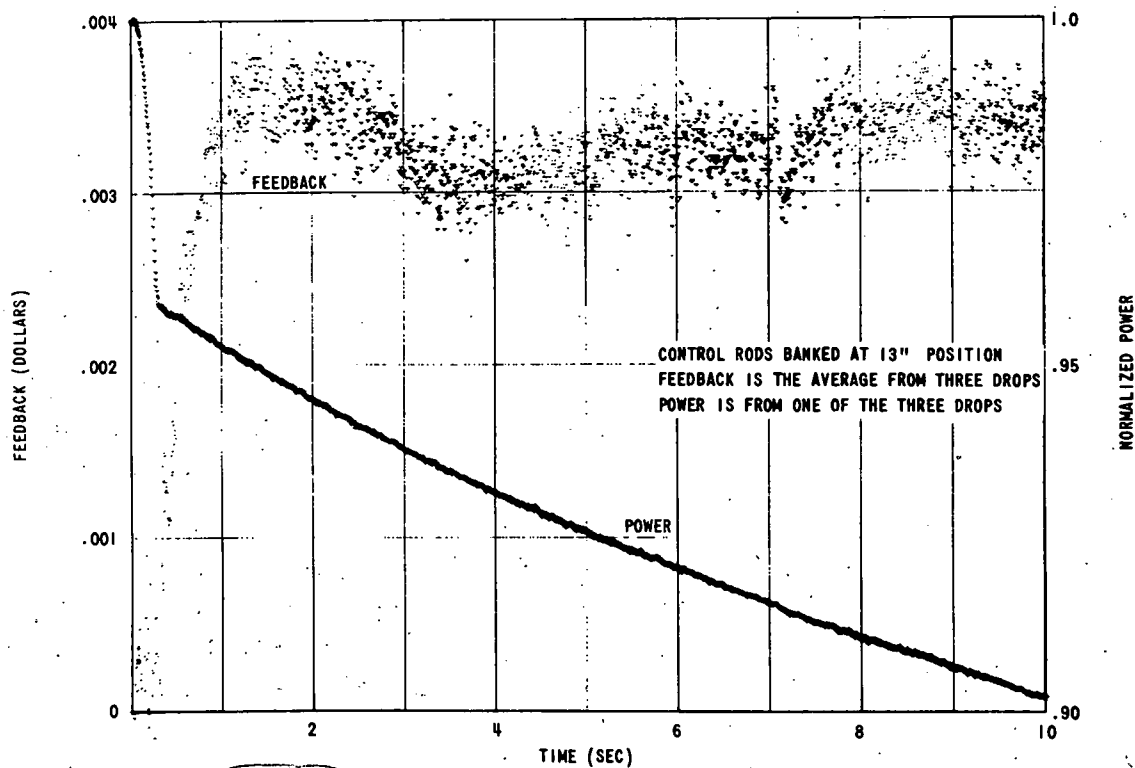
Fig. I.D.4. EBR-II Rod-drop Experiment at 25 MW during Run 26A
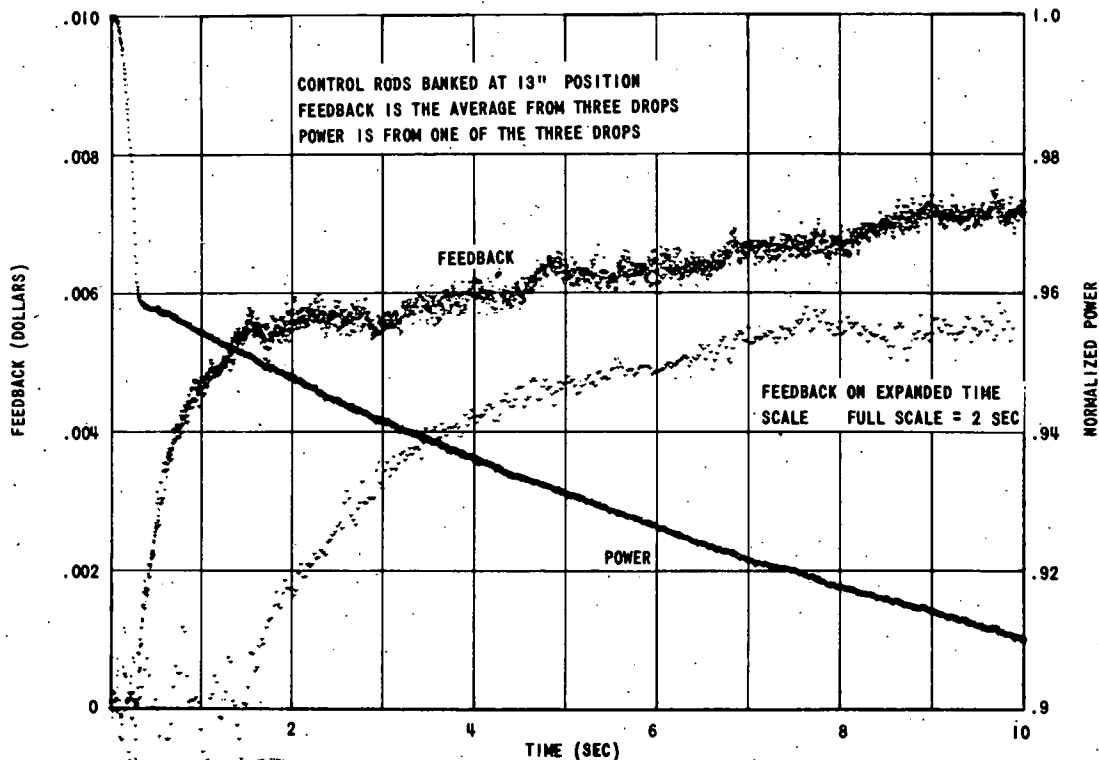
Fig. I.D.5. EBR-II Rod-drop Experiment at 35 MW during Run 26A

The same effect may be seen, but to a lesser extent, in the 35-MW results of Fig. I.D.5. In this case, the feedback continues to increase after the initial action of the prompt component, but the increase is considerably less than it would have been had the delayed positive effect not been present.

The rod-drop results are qualitatively consistent with the results of oscillator and static power-coefficient measurements. It is important that the value of the static power coefficient near 25 MW is the result of a delayed positive coefficient which is suppressed at higher and lower powers. The rod-drop results demonstrate clearly that there is no significant reduction in the prompt negative coefficient in this intermediate power range.

Attempts are being made to establish a set of feedback terms which will be consistent with the results of transfer function and static power-coefficient measurements.

(d) Reduced-flow Experiments. Criticality measurements at full and reduced flow were made in Run 26A and at the beginning and end of Run 26B. The last of these represented about 1000 MWd of burnup as compared to the beginning of the run. Experimental data from these measurements are given in Table I.D.2.

TABLE I.D.2. Reduced Flow Experiments

Approximate Clock Time	ΔT (°F)	Reactor Power Q (MW)	Flow Fraction R (%)	Reactivity Rod Worth (Ih)	Bulk Sodium Temp Correction (Ih)	Burnup Correction (Ih)	Excess Reactivity (Ih)[a]
				Run 26A			
September 27, 1967:							
1025	121.8	41.5	100	52.6	0	0	52.6
1200	66.0	22.5	100	63.2	0.5	0.3	64.0
1350	69.5	22.5	95	64.6	0	0.45	65.0
1425	73.5	22.6	90	65.8	0	0.6	66.4
1550	88.0	22.5	75	65.6	0.3	0.75	66.6
1742	122.8	22.6	54	←———————(Scrammed--no reading) ————————→			
2208	122.0	22.5	54	59.3	0.5	1.35	61.1
				Run 26B--Start			
October 19, 1967:							
0915	122.8	41.9	100	36.4	0.3	0	36.7
1700	65.9	22.5	100	55.2	0.3	0.4	55.9
1800	74.2	22.8	90	55.3	0.2	0.6	56.1
1900	93.1	23.8	75	53.0	0.16	0.8	54.0
2000	117.5	24.1	60	46.2	0.08	0.9	47.2
2100	131.6	24.2	54	42.1	-0.02	1.1	43.2
2235	123.6	30.7	73	40.1	0.14	1.4	41.6
2330	97.8	30.0	90	44.1	0.4	1.5	46.0
				Run 26B--End			
November 6, 1967:							
1700	120.9	41.2	100	54.0	0.1	0	54.1
1845	121.6	29.9	72	58.6	0.6	0.3	59.5
2100	66.2	22.6	100	67.7	-1.2	0.6	67.1
2200	73.1	22.4	90	68.7	0.5	0.8	70.0
2330	88.7	22.7	75	68.6	0.4	0.9	69.9
0115	111.5	22.8	60	64.8	0.6	1.2	66.6
0215	122.9	22.6	54	63.2	0.4	1.2	64.8
0415	121.7	14.9	36.2	67.0	-0.6	1.5	67.9

[a]Corrections for rod-bank expansion have not been applied.

In Run 26A, the reactor power was leveled with care at each point, but no standardized averaging procedure was used. In Run 26B, the procedure was adopted of leveling the power and holding the power level constant by moving control rods, taking readings at 1-min intervals over at least a 20-min period, and averaging these results to establish the critical position. The values listed in Table I.D.2 for ΔT, rod reactivity worth, and bulk sodium corrections represent averages over a 20-min period determined in this manner. The flow rate (percent) is read directly from the average of the two high-pressure flowmeters. The reactor power level Q is then computed from the average ΔT and the percent of full flow, R, using Q = 34.1 $\Delta T/R$. Rod reactivity worth is taken from tabular values multiplied by a calibration factor determined from a period measurement. Reactivity values are then adjusted for bulk sodium temperature (1 Ih/°F) and burnup during the experiment (0.15 Ih/MWd) to give the excess reactivities given in the last column.

The adjustments to the data thus far are straightforward, but further interpretation of the results must include consideration of the significant effects of hysteresis and differences in rod-bank position. (Hysteresis effects were discussed and illustrated in the Progress Report for August 1967, ANL-7371, p. 10. Although the source of these effects has not been identified, enough data have been collected to conclude that reactivity differences as large as 3 to 5 Ih can be introduced, depending on the recent operating history of the reactor.)

In the reduced-flow experiments, the established procedure is to take the first data point at a nominal 41.7 MW and then reduce power to a nominal 22.5 MW. Because of hysteresis, the difference in reactivity between these initial points may not be comparable to the corresponding points on a normal power-coefficient curve measured during ascending power. The subsequent course of the experiments involves reduction of flow, which increases the coolant temperature differential across the core. Although little is known about the hysteresis associated with flow changes, it seems reasonable to assume that the effect of ascending temperatures as flow is reduced will lead to a reactivity condition which can be roughly compared with the normal ascending power-coefficient curves. Thus, the 41.7-MW, full-flow condition can be compared with the 22.5-MW, 54-percent-flow condition with reasonable confidence.

The rod-bank expansion corrections have been calculated to be 9.39, 12.64, and 8.04 Ih for the rod-bank configurations of Run 26A, 26B-start, and 26B-end, respectively, all calculated at full power and full flow. The rod-bank expansion correction at other conditions is assumed to be proportional to reactor power and inversely proportional to flow rate, i.e., proportional to the rise of sodium temperature. This adjustment must be taken into consideration for any physical interpretation of the power and flow coefficients in terms of their components.

Since the nominal 22.5-MW, 54-percent-flow point was not always measured at the precise nominal power, some correction must be made in order to compare one run with another. For this purpose, a semiempirical power coefficient of about 3 Ih/MW has been computed and is believed to be appropriate for small adjustments at 54-percent flow.

After all necessary corrections are made, the reactivity differences between the 41.7-MW full-flow and 22.5-MW 54-percent-flow conditions appear to be 8.8, 11.3, and 11.6 Ih for the three measurements made throughout the course of the run, each with an uncertainty factor of at least ±1 Ih. The steady, small increase suggests a trend with burnup which will be watched for confirmation in future measurements.

(ii) Thermal and Hydraulic Analysis

    (a) Modification of the HECTIC-II Heat-transfer Program. The HECTIC-II heat-transfer program is being modified so as to permit detailed computations of fuel, cladding, and coolant temperatures in half-loaded driver subassemblies.

    (b) Melt-wire Temperature Studies. To obtain more definitive information relevant to power generation in the stainless steel-reflector region, plans are being formulated for the incorporation of melt-wire temperature indicators at the exit of a Row 7 stainless steel subassembly. From a knowledge of the flow rate (determined by water calibration studies) and the temperature differential across the subassembly, it will be possible to estimate with reasonable accuracy the specific power-generation rate. Such information is vital for the proposed reorificing of stainless steel-reflector subassemblies. However, since there is apparently some difficulty in obtaining melt wires having the proper range of melting temperatures, the capability of performance of this technique is uncertain.

(iii) Safety

    (a) Postirradiation Inspection of Fuel Subassemblies Discharged from Run 25. Straightness, twist, and button dimensions were measured on additional subassemblies discharged from Run 25. No deviations from specifications for straightness and twist were found. Small deviations, however, were noted for the dimensional checks across the buttons. Button dimensions are listed in Table I.D.3 (for the methods of button measurements see the Progress Report for October 1967, ANL-7391, p. 59). Since specifications require 2.318 ± 0.001 in., and since the reproducibility of measurements has been shown to be ±0.001 in., it is clear that small changes in dimensions across the buttons have occurred. An attempt is being made to correlate deviations from specifications with orientation of the subassembly.

TABLE I.D.3. Summary of Postirradiation Measurements of Button Dimensions

Subassembly	Grid Location	Flat Position	Preirradiation Results (in.)	Postirradiation Results (in.)
B-342	6B1	1-4	One set, 2.320	2.319
		2-5	Others in spec	2.311
		3-6		2.311
B-343	6E3	1-4	One set, 2.323	2.317
		2-5	Others in spec	2.321
		3-6		2.315

TABLE I.D.3 (Contd.)

Subassembly	Grid Location	Flat Position	Preirradiation Results (in.)	Postirradiation Results (in.)
B-345	6A4	1-4	One set, 2.321	2.319
		2-5	Others in spec	2.318
		3-6		2.315
B-346	6B3	1-4	One set, 2.322	2.316
		2-5	Others in spec	2.318
		3-6		2.318
B-347	6F3	1-4	In spec	2.321
		2-5		2.317
		3-6		2.318
C-262	3F1	1-4	In spec	2.324
		2-5		2.321
		3-6		2.319
C-270	3A2	1-4	One set, 2.315	2.314
		2-5	Others in spec	2.317
		3-6		2.315
C-276	4F1	1-4	One set, 2.321	2.315
		2-5	Others in spec	2.315
		3-6		2.318
C-282	3D2	1-4	In spec	2.316
		2-5		2.320
		3-6		2.320

b. Nuclear Analysis Methods Development (P. J. Persiani)

Last Reported: ANL-7391, pp. 61-66 (Oct 1967).

(i) EBR-II Physics Analysis. Calculations have been made of subassembly worths in Run 26A, utilizing the SNARG two-dimensional simulation (see ANL-7391, p. 61), and the improved 6-group cross-section set 23806 in place of the older 23606 set. Since the computations are based on exact experimental compositions, differences appear between subassemblies of the same type, such as driver fuel and experimental.

The Run-26A base configuration for determination of subassembly worths was made critical by a simulated banking of the 11 fueled control rods in Ring 5. It was found that the replacement with follower composition of 48.75 v/o of each of the fueled control rods was necessary. The corresponding replacement fraction for the Run-26A core with depleted

uranium blanket in place of the stainless steel blanket in Rings 7 and 8 was 28.98 v/o, while that for the stainless steel blanket in Rings 7-14 was 78.46 v/o. Consequently, the Run-26A subassembly worths are not readily comparable with those calculated for Run 25D, in which the fueled control subassemblies are left at 100 v/o while criticality was achieved by varying the enrichment of all driver fuel subassemblies. In particular, the fueled control subassembly worths in Run 26A measured a different quantity than those of Run 25D.

Table I.D.4 presents Run 26A subassembly worths. Of the worths which are roughly comparable to the Run-25D values, the replacements of Assembly 6B1 produced a 20% greater reactivity effect than in the analogous replacements reported for Run 25D, whereas the interchanges of fuel for experimental, and experimental for fuel, subassemblies have approximately twice the previous effect and are no longer symmetric.

TABLE I.D.4. EBR-II Subassembly Worths
(SNARG, Two-dimensional, Twofold Symmetry, xy Geometry)

Replacement	Run-25D Δk	Run-26A Δk
Foll for 5A1(FC)	-	-0.00236
Foll for 5A3(FC)	-	-0.00255
Foll for 5B1(FC)	-	-0.00220
Foll for 5B3(FC)	-	-0.00243
6B2(D) for 6B1(SB)	+0.00253	+0.00303
5D1(MR) for 6B1(SB)	-0.00037	-0.00044
6B5(x) for 6A3(D)	-0.00216	-0.00437
6A3(D) for 6B5(x)	+0.00217	+0.00379

Subassembly Types:
D	Driver Fuel	SB	Steel Blanket
x	Experimental	MR	Modified Reflector
FC	Fueled Control	Foll	FC Follower

(ii) Development of EBR-II Cross-section Set. The preliminary evaluation of cross-section sets 238 and 23806 has shown that the uses of reflector-weighted cross sections improves the results of EBR-II neutronic calculations. The value of k_{eff} which has been obtained to date for various arrangements of EBR-II are given in Table I.D.5. Although the data have not been completely analyzed, some improvements in the results are seen.* The worth of the blanket as calculated with set 23806 was approximately 1.6% Δk as compared to ~2.5% with set 23606. The measured value is about 1% Δk.

_____

*After the proper corrections are made, the value of k_{eff} for Run 26A at 45 MW is almost unity; previously the k_{eff}'s have been ~3% too high.

TABLE I.D.5. Values of k_{eff} Calculated for
Various Arrangements of EBR-II in Run 26A
by SNARG and CANDID Using Set 23806

Case	Description	SNARG	CANDID
1	700°F	1.0313	0.9982
2	45 MW	1.0294	0.9965
3	Case 2 Blanket	1.0118	0.9804
4	Case 3 with 5 Full Subassemblies Replacing 5 Half-subassemblies	1.0325	1.0005

The calculations predict the worth of substituting full- for half-loaded subassemblies to be 170 Ih, which is close to the prediction based on experiment. The relation between the SNARG and CANDID results are approximately that which was expected. However, an error in the CANDID code has been found, and no conclusion can be drawn until the code is corrected. Also, an error in the input composition for these calculations is being corrected, but no significant difference in the results is expected therefrom. The flux and power distributions still must be examined in the evaluation.

The effect of the number of core regions used in the neutronic one-dimensional, cylindrical calculations was investigated for Run 25 of EBR-II. The Idaho Division has developed an accurate, 15-radial-region representation of the EBR-II core. Their representation was compared to a simple representation in which each hexagonal ring of the core corresponds to a radial region. The values of k_{eff} calculated with the two representations agreed within 0.2% k. A study of the flux and power distribution is under way.

(iii) Core Size and Composition Analysis for EBR-II Power-coefficient Investigation. A systematic study was undertaken to investigate the effects of changes in the core configuration and composition of EBR-II on the power coefficient. In this study the following changes were examined to determine their influence on the linear components of the power coefficient:

1. core size and its accompanying change in core composition;

2. substitution of stainless steel for depleted uranium in Rows 7 and 8;

3. control-rod position;

4. burnup in the core;

5. burnup in the core and blanket.

The systems used in this study are described in Table I.D.6. The dimensions and the compositions in the noncore regions are the same as for EBR-II. The homogenized composition of the core, which was varied to achieve criticality, is approximately that of EBR-II core. The temperatures assumed for the materials in the regions of the reactor at zero and 45-MW operation are the same as those used in the study of the power coefficients for Runs 24 and 25.

TABLE I.D.6. Cases of the Systematic Study

Case No.	No. of Subassemblies	Radial Blanket Material	Control-rod Position (in.)	Burnup[a]	
				Core Only	Core + Blanket
1	91	Depleted Uranium	14.00	0.0	0.0
2	70	Depleted Uranium	14.00	0.0	0.0
3	90	Stainless Steel	14.00	0.0	0.0
4	90	Depleted Uranium	10.86	0.0	0.0
5	90	Depleted Uranium	14.00	1.0	0.0
6	90	Depleted Uranium	14.00	1.0	1.0

[a]Burnup (atom percent) normalized to reactor center.

All calculations were performed with two-dimensional diffusion-theory codes, using a collapsed six-group cross-section set derived from the MC^2 code. For all six cases the values of the neutron multiplication k_{eff} were calculated for the system operating at zero and 45 MW. It should be pointed out that the temperatures and the corresponding material densities and dimensions of the system for 45-MW operation were taken to be the same for all cases. In interpreting the results of the study it should be realized that the temperatures would be different for the 70- and 91-subassembly cores (Cases 1 and 2) at 45 MW. The reactivity defect due to dimensional changes (axial fuel and radial structural expansion) were obtained from the difference in the multiplication of the systems at zero and 45 MW. The reactivity worths of density changes were calculated with a first-order perturbation code.

Comparison of the results of Cases 1 and 2 shows the effect of core size and the corresponding core composition. The influence of

substitution of steel for depleted uranium is determined from Cases 1 and 3, while the effect of control-rod position is found by comparing the results of Cases 1 and 4. The results of Cases 5 and 6, as compared to Case 1, provide information on the effects of burnup in the core and in the core and blanket, respectively.

The effect of the changes on the power coefficient were divided into five components: core fuel expansion, sodium in the core, sodium in the axial reflector, sodium in the radial reflector (or blanket), and radial structural expansion.

The results of the systematic study are presented in Table I.D.7 in terms of $(\Delta k/k) \times 10^5$. It is seen that the total reactivity defect, as well as that of each component, is negative for all of the cases. The magnitude of reactivity loss with power for each component, except for the sodium in the small radial blanket, is at least 20 Ih between zero and 45 MW. The values of $\Delta k/k$ for the individual components do not deviate greatly among all the cases evaluated. The values for each component (except for the radial blanket in Case 3) fall within ±5% of each other. This is also true for the value of the total reactivity defect, which indicates that deviations in the values of $\Delta k/k$ for the individual components tend to cancel. Based on the small deviations of the results for Cases 1, 3, 4, 5, and 6, it may be concluded that the influence of control-rod position, radial blanket material (steel or depleted uranium), and burnup in the core and blanket are small.

TABLE I.D.7. Reactivity Defect for the Six Cases of Table I.D.6 in Units of $10^{-5} \Delta k/k$

Case	k_{eff}	Core Axial	Sodium Core	Sodium Axial Reflector	Sodium Radial Blanket	Sodium Total	Structure	Total
1	0.9999995	-54.0	-55.6	-59.8	-10.1	-125.5	-152.5	-332.0
2	0.9999664	-57.4	-55.2	-53.8	-11.3	-120.3	-150.7	-328.4
3	1.0261572	-51.4	-56.9	-63.9	-5.6	-126.4	-163.0	-340.8
4	0.9953970	-50.2	-63.5	-56.2	-10.1	-129.8	-146.8	-326.8
5	0.9916931	-46.4	-55.4	-59.6	-10.1	-125.1	-147.0	-318.5
6	0.9928010	-49.8	-55.1	-59.5	-10.1	-124.7	-151.2	-325.7

The reactivity effects of Cases 1 and 3 may be compared on the basis of two cores having the same height but different radii. The stainless steel reflector in Rows 7 and 8 reduces the neutron radial leakage and effectively simulates a core having a larger radius. Therefore the core-size effect on coefficients can be studied in terms of Cases 1, 2, and 3, with the Case-3 core the largest. The trend of the axial expansion effect of the core does reflect the behavior of the radial-leakage-dependent coefficients, which are expected to decrease as the core size increases.

This expected trend is maintained in the radial-blanket component of the sodium effect, which is less important in a system of lower radial leakage.

The increased axial cross-sectional area of the larger-diameter cores effectively increases the worth of the sodium in the axial reflector region. This expected trend is consistent with the computed effects. Generally, then, although the individual power-coefficient components do change with core size, the somewhat compensating trends of these components appear to result in an insignificant overall change in reactivity effects.

The reactivity effect due to structural expansion is dependent on the total area of core leakage, and for slight changes, such as between Case 1 and 2, the effect is negligible. In the core configuration of Case 3, the stainless steel in Rows 7 and 8 constitute a more effective reflector than a uranium blanket, so that a change in its reflective properties should result in an increased reactivity effect. However, again it is found that even this component does not significantly change the total overall reactivity coefficient for these sample EBR-II core configurations.

The additional effects of the control-rod and burnup characteristics of the simulated 91-subassembly core again indicates that the trends of the reactivity effects are in the anticipated direction, but the magnitudes of the differences must be considered negligible.

Currently under study is the effect on the reactivity feedbacks resulting from the replacement of the axial blanket by the stainless steel reflector.

Of greater importance in the core-size effect may be, not the changes in the reactivity coefficients themselves, but the changes in temperature distribution between small and large cores. The difference in the values of $\Delta k/k$ for Cases 1 and 2 is small; however, the temperatures used in Case 2 were not representative of an actual 70-subassembly core. Therefore, since higher temperatures would be expected in a smaller core for the same power level, the results suggest that the overall reactivity decrement may be more negative for the 70-subassembly than for the 91-subassembly core.

In order to account more quantitatively for the reactivity coefficients observed in the actual EBR-II configurations, a detailed study of these coefficients has been initiated for Runs 16, 24, 25, and 26. The study is to be performed using the actual operating thermal conditions as well as the actual core configuration and subassembly compositions.

c. Reactor System Testing, Surveillance, and Evaluation
(B. C. Cerutti)

Last Reported: ANL-7391, pp. 66-67 (Oct 1967).

(i) Startup Feedwater Pump. Fabrication of the new centrifugal startup feedwater pump is proceeding satisfactorily. Delivery is expected late in January 1968.

(ii) Mark-II Oscillator-rod Drive. Operation of the oscillator-rod drive system continued with restrictions in effect for reactor power levels above 25 MW. Lower limits of 0.1 cps at 30 MW and 0.3 cps at 41.5 MW were placed on the frequency to prevent rubbing of the oscillator in the thimble. A plan was formulated for changing some of the adjacent subassemblies to obtain a more uniform radial distribution of temperature around the oscillator-rod thimble when the reactor is at power; this change should reduce or eliminate the rubbing. Fuel handling to accomplish this plan is now in progress.

(iii) Fuel Unloading Machine (FUM) and Argon Cooling System (ACS). Some operational problems have recently been encountered with the FUM and ACS. A study has led to recommendations for revision of procedures and also outlines the possible causes of some of the difficulties. To prevent further water contamination of the FUM, the IBC should be purged when it is received from the FCF.

The two spare molecular sieves were modified and installed in the ACS system. Baffles were installed along the top of each unit to prevent channeling of the flow over the top of the pellet filter material and to ensure that the sieves perform as designed. The buildup of sodium oxide in the argon compressor and FUM in the past has required excessive maintenance on these units.

Design work on the new FUM jaw position, elevation, and sense-indication system continued. All preliminary assembly and installation layouts were completed; detail drawings are approximately 75 percent complete.

(iv) Cooling Tower for EBR-II Plant Auxiliary System. Design work on the auxiliary cooling tower and the plant changes required to accommodate it are now complete. The design package is now ready for submission for bids.

d. Higher Power Operation (R. E. Rice)

Last Reported: ANL-7391, pp. 67-68 (Oct 1967).

The engineering package has been prepared for the plant modification on reorificing of fuel subassemblies for higher flow rates in Rows 4, 5, and 6.

A second prototype Row-6 driver subassembly with the tri-fluted axial blanket was flow tested as a configuration with six 0.297-in. inlet holes, which is the hole size specified for the proposed reorificing of driver subassemblies for this row. The flow rate of 800°F sodium is 78 gpm at 41 psi.

Three prototype subassemblies with increased flow rates have been fabricated. Core-type subassemblies C2127 and C2128, with the top row of inlet holes enlarged to 0.359 in., will be installed under thermocouple locations in Rows 4 and 5. These subassemblies should have flow rates of 100 gpm in Row 4 and 87 gpm in Row 5. Inner blanket core-type subassembly B389 with the inlet holes enlarged to 0.297 in. will be installed under the thermocouple in Row 6. The flow rate for this subassembly is estimated to be 78 gpm. The outlet temperatures from these prototypes will be monitored and compared with those taken when standard driver subassemblies were in those positions.

    e.   <u>Fuel Swelling and Driver Surveillance</u> (F. G. Foote and R. R. O'Boyle)

Last Reported: ANL-7391, pp. 68-78 (Oct 1967).

    (i)   <u>Mark IA--Investigation of Anomalous Fuel Swelling</u>

    (a) <u>Effect of Pressure upon Fuel Swelling</u>. Six fuel pins from the P-1 (pressure-effect specimens) capsule have been declad. All were in a condition of advanced swelling. After the sodium had been melted away, much of each pin was too fragile to permit meaningful measurements of diameter and length. Only the density of the more solid remainder of each pin was determined (see Table I.D.8). The relationship between fuel swelling and in-reactor pressure is plotted in Fig. I.D.6. Despite the advanced state of deterioration of the fuel pins, a trend to lower swelling with increasing pressure is evident.

TABLE I.D.8. Density Data for P-1 Pressure Specimens of Melt 409

Specimen No.	Cast Pin No.	Mean In-reactor Fuel Temp (°C)	Mean[a] In-reactor Pressure (psia)	Preirradiation Density (g/cc)	Postirradiation Density (g/cc)	ΔV/V (%)
1	53-5	560	54[b]	18.03	9.70	86
2	53-11	560	160	17.99	10.23	76
3	53-1	560	213[b]	18.05	10.49	72
4	53-7	560	486	18.01	9.74	85
5	53-3	560	876	17.99	11.17	61
6	53-9	560	1599	18.01	11.47	57

[a]Effects due to fuel swelling or gas evolution have not been included.
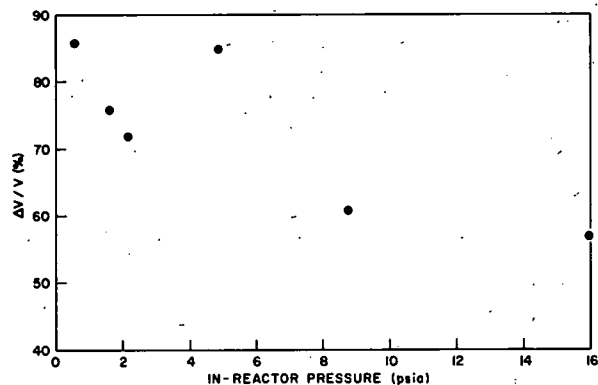[b]Pressure up to clad rupture only.

Fig. I.D.6. Effect of Pressure on
Swelling, Capsule P-1

The examination of capsule P-2 has not progressed beyond the stage reported previously (see ANL-7391, p. 70) because of the work on P-1.

Capsule P-3 was returned to the reactor. Burnup was 0.6 a/o (158 MWd or 38% of P-1) by November 9, when it was removed for neutron radiography.

(b) Effect of Heat Treatment upon Swelling. Capsule H-1, which contained six heat-treatment specimens, was inserted into the reactor in time for startup on October 25 and has accumulated 0.4 a/o burnup. Some overheating has been experienced.

The fuel-pin loading for capsule H-2 is being encapsulated. This fuel consists of six 1-in. pin sections from the Idaho EUF melts bearing additions of silicon and iron. These specimens, like those in H-1, will be irradiated without cladding for comparison with the SL type of material.

(c) Hot Laboratory Examination of Irradiated Fuel. A complete transverse cross section of U-5 w/o Fs irradiated in EBR-II to 0.76 a/o burnup was examined by electron microprobe analysis to determine the distribution of alloying elements in the fuel following irradiation. The specimen was cut from the midlength of pin 71 irradiated in subassembly C180 to a maximum subassembly burnup of 0.82 a/o.

Previously,* optical and electron microscopy and X-ray diffraction results for nineteen irradiated specimens taken from three different fuel pins were discussed. The report showed that (1) there are no apparent structural differences between the three material types (SL, MR, and MRC) at magnifications to 18,000 times, and (2) optical and electron microscopy show no evidence of either prior gamma grain boundaries or of intermediate phases (U$_2$Ru and U$_2$Mo) known to precipitate in unirradiated U-5 w/o Fs under the same thermal conditions. The apparent lack of these phases suggested the possibility that molybdenum and ruthenium are put into a metastable gamma solid solution during irradiation, similar to that known to occur in U-Mo alloys. One object of the microprobe examination was to determine the distribution of molybdenum and ruthenium in the fuel following irradiation.

The specimen examined was sliced from the midlength of the fuel pin and reduced in thickness to 0.004 in. Gamma activities

---

*Reactor Development Program Progress Report for August 1967, ANL-7371, pp. 24-25.

measured 12 in. from the mounted specimen were 300 mR/hr hard and 5000 mR/hr hard and soft. Two regions on the fuel-pin cross section were examined: one region near the surface of the pin, irradiated at a calculated temperature of 480°C, and one region near the center of the pin, irradiated at a calculated temperature of 550°C. The microprobe X-ray data showed that on a micron scale the distribution of molybdenum and ruthenium is not uniform in the matrix. In the center of the pin, the molybdenum concentration varied periodically between 1 and 7 w/o, and the ruthenium concentration varied between 1/2 and 6 w/o. The typical peak-to-peak distance for both elements is about 4 μ. The amplitude and the period of the concentration variation were less in the cooler (480°C) circumferential region of the fuel than in the center. These data suggest that precipitation and growth of U_2Ru and U_2Mo occur in U-5 w/o Fs during irradiation on a scale comparable with that observed in the unirradiated fuel when heat treated at the same temperature. After heat treatment at 500°C for 28 days, the typical sizes of U_2Ru and U_2Mo precipitate particles are 1.0 and 0.5 μ, respectively. Some evidence of prior gamma grain boundaries is indicated by the heavy precipitation of molybdenum and ruthenium that occurs periodically at about 25-μ intervals. A striking feature of the optical and electron metallography of these alloys after irradiation is the lack of discrimination of gamma and precipitate boundaries either by electrolytic or cathodic etching.

Carbide inclusions in the matrix having a typical size of 3 μ were found to contain about 46 w/o zirconium and 30 w/o uranium. No iron, silicon, or aluminum was detected in the inclusions. Hence, it appears that much of the zirconium in the alloy (typically 0.08 w/o) is contained in the uranium-zirconium carbides. Neither silicon nor aluminum were detected in the matrix; however, a uniform distribution of approximately 0.1 w/o iron was detected.

ERRATA: In Table II.E.9, Trace-element Analyses-- EBR-II, Mark-IA Fuel, on pp. 72-75 of ANL-7391 (Oct 1967), the element numbers for Casting Batches 4080 and 4081 were interchanged. The numbers should be 14 and 22, respectively.

f.   Mark-II Driver Fuel-element Development   (J. H. Kittel)

Last Reported: ANL-7391, pp. 79-81 (Oct 1967).

Three capsules containing EBR-II Mark-II fuel elements were received from Idaho. The capsules had been rejected because of incomplete weld penetration of the closures. One capsule (209) was successfully repaired by welding. The defective weld was in the upper portion of the capsule, away from the sodium. The defective welds in the other capsules (204 and 214) were at the bottom, where the sodium was located. Even though the bottom end plugs were inserted 3 in. deep into the capsule tube, and the main body of the sodium was 3 in. away from the weld, sodium

apparently penetrated the weld area because the heat of welding caused the sodium to melt and to be ejected. The two capsules will be stripped and the fuel elements recovered for re-encapsulation.

Two spare capsules (227 and 273) have passed the necessary bond-inspection requirements and were shipped, along with capsule 209, to Idaho as replacements for capsules 204 and 214. An extra capsule, 269, was sent for contingency purposes.

Drawings for the stagnant sodium TREAT capsule have been reviewed for possible use with the Mark-II element. Only the Mark-II fuel pins in the 24- and 26-in. lengths are to be tested. A number of stagnant sodium TREAT capsules (18 in. long) are available that were designed for testing Mark-IA and -IB fuel pins. Nevertheless, it will be possible to utilize several major parts. The components requiring changes are being redesigned to accommodate the longer fuel-pin lengths.

A tentative program for testing Mark-II fuel pins has been outlined.

g. **Equipment--Fuel Related** (E. Hutter)

Last Reported: ANL-7391, pp. 81-84 (Oct 1967).

(i) **New Control-rod Subassemblies**

(a) **Control Rod of Greater Worth.** The study to design an absorber-type control rod with gas-collecting chambers above and below the absorber continued. A material is being sought with porosity that will permit helium to pass through and out of the subassembly without allowing sodium to enter the B_4C section. Tests on an impervious grade of thoria-yttria oxide indicated that it was not permeable to helium or sodium. On the other hand, tests of aluminum oxide showed that it is permeable to both helium and sodium. Sintered metallic samples will be tested.

(ii) **Engineering Consultation**

(a) **Modification of Core Gripper Assembly.** The design modification of the core gripper assembly consists of replacing the welded gripper-guide assembly with a single-piece assembly and adding hexagonal sections to the sensing rod and to the outside of the jaw-actuating tube. These modifications will prevent the seal-bellows assembly from being damaged by inadvertent torsional loading during handling and assembly. Drawings for the modification have been completed and checked; a spare core gripper will be fabricated to this design.

(b) **Bypass-flow Irradiation Subassembly.** Rather than modifying a Mark-A irradiation subassembly to obtain irradiation at higher

than normal EBR-II operating temperatures (see Progress Report for October 1967, ANL-7391, p. 83), it has been decided to modify a Mark-C irradiation subassembly, which has a bypass flow path and mixer, to satisfy the particular requirements of the experiment.

(c) Power Coefficient. A hypothesis for explaining recent changes observed in power coefficients has been proposed (see Progress Report for October 1967, ANL-7391, pp. 83-84). Briefly, the hypothesis states that the changes are due largely to replacement, adjacent to the core, of depleted-uranium blanket subassemblies with stainless steel reflector subassemblies, and to consequent differences in the thermally induced bowing of the reactor subassemblies as a whole.

To substantiate this hypothesis, both a simple and an advanced bowing model are being developed. The simple model describes the change of core radius with power by use of three connected linear algebraic equations in which the constants are related to (1) the movement of subassemblies due to unrestrained bowing, (2) the ratio of stiffness of the core under compression to stiffness of the innermost row of blanket-reflector subassemblies under bending, and (3) the clearances between subassemblies at their top ends and at their spacer-button locations. With this model, core-radius values are multiplied by a reasonable $\Delta k/\Delta r$ constant to get reactivity predictions. Results from the simple model strongly support the bowing hypothesis.

For the advanced bowing model, a computer code designated BOW* calculates the detailed movements of each row of subassemblies; thus, reactivity predictions can be obtained by multiplying the radius values for each row by an appropriate $\Delta k/\Delta r$ factor. This model takes into account the bowing interactions between subassemblies much more precisely than the simple model. Clearances between subassembly lower adapters and lower-grid-plate holes are considered in addition to those clearances specified above for the simple model. Preliminary results from the advanced model also lend justification for the bowing hypothesis.

h. Reactor and Primary Coolant System (B. C. Cerutti)

Last Reported: ANL-7391, pp. 84-87 (Oct 1967).

(i) Design for Sodium Drain Tank. The design of the primary-sodium-storage facility continued. A study of the feasibility of draining the primary tank by pressurizing and of utilizing a vacuum assist in the drain tank indicates that the primary tank can be safely pressurized to 8 psi, which is a pressure higher than that required to accomplish draining. The use of an EM pump for draining the tank is also being evaluated.

---

* Bump, T. R., Effect of Reactor Temperatures on Bowing of EBR-II Subassemblies, Trans. Am. Nucl. Soc. 10(2), 661 (1967).

(ii) <u>Primary-tank Pressure-Vacuum Relief.</u> The design work and the engineering submittal for the primary tank pressure-vacuum relief modification are nearly complete. Upon completion of drawings the entire engineering package will be issued for review.

(iii) <u>General Improvements</u>

(a) <u>FERD Loop Plugging Meter and Sampling System.</u> The installation of the FERD loop plugging meter and sampling system was completed. Operational testing of the systems is in progress. Two sodium samples were taken, and a third sample run is in progress.

(b) <u>New Plugging Meters for the Primary and Secondary Sodium-purification Systems.</u> Piping drawings for the new plugging meters for the primary and secondary sodium-purification systems were completed. Installation drawings for the new plugging meters are being prepared. Components for the plugging meters are being procured.

(c) <u>New Sodium-sampling System.</u> Piping installation drawings for a new sampling facility for the primary-sodium-purification system are essentially complete. Sodium-sampling capabilities will be greatly improved as a result of this new design, which will permit flow-through samples to be taken before and after the crystallizer.

(d) <u>Surge Tank for Primary-sodium-purification System.</u> The engineering package for a new surge tank for the primary sodium-purification system is complete. Copies have been issued for review.

(e) <u>Blanket-gas Monitor.</u> Bids were received from two vendors for components for the new blanket-gas monitor. Neither bid met the specifications required for compatibility with the three-pen Leeds and Northrup recorders now on order. The vendors indicated that their systems could be modified to meet the specifications, and new bids were requested.

(f) <u>Control-rod Lifting Platform.</u> Redesign of the mechanical interlocks for the control-rod lifting platform was completed, and the necessary parts were fabricated and installed. The system was then rewired into the fuel-handling console, and electrical and mechanical checkout was satisfactorily completed. Revision of drawings is in progress.

(g) <u>Improved Bulk-sodium-level Transmitter.</u> Testing of the new bulk-sodium-level transmitter in the primary tank was completed. During a shutdown, the central shaft and bellows were partially removed for inspection. No sodium deposition was found, and the unit was reassembled. The new unit will replace the present level transmitter, which has been unreliable.

(h) <u>Transfer-arm Position-indicator Lights</u>. A set of lights which duplicates the transfer-arm position-indicator lights on the fuel-handling console was added to the transfer-arm column. The new set of lights permits the transfer-arm operator to determine when electrical-circuit interlocks associated with the transfer arm have been completed, without leaving the transfer-arm area.

(i) <u>Instrumentation for New Plugging Meters for the Primary- and Secondary-sodium Purification Systems</u>. Basic design sketches were completed for the instrumentation and control circuits for the new plugging meters for the primary- and secondary-sodium systems, and detail drawings were started. Preparation of test procedures, design reports, and installation details is in progress.

(iv) <u>Sodium Sampling Pump and Filter</u>. All the specially fabricated parts have been received; the pump and filter are being assembled. The water test rig has been completed.

i. <u>Secondary Sodium and Power Systems</u> (B. C. Cerutti)

Last Reported: ANL-7391, p. 87 (Oct 1967).

(i) General Improvements

(a) <u>Feedwater System</u>. Several vendors of control valves were consulted, and the selection of a replacement bypass valve for the feedwater-regulating valve will be based on an evaluation of their recommendations.

(b) <u>Turbine Generator</u>. Minor adjustments have improved the action of the initial-pressure governor on the turbine generator. A complete checkout has not yet been accomplished.

(c) <u>Sodium Boiler</u>. Bids have been requested on replacement safety valves for the steam drum.

(d) <u>Low-level Alarm for Condensate Storage Tank</u>. A low-level alarm has been added to the condensate storage tank to warn of low condensate level, which would allow air to enter the main condenser through the condensate-makeup system.

(e) <u>Steam-trap Drain and Vent in Sodium Boiler Building</u>. Prefabrication of the piping for the steam trap drain and vent in the sodium boiler building continued.

(f) <u>Analyzer for Oxygen in Secondary Sodium</u>. Work continued on the installation of the economizer for the secondary-sodium oxygen analyzer.

j.   New Subassemblies Design and Experimental Support (E. Hutter)

Last Reported: ANL-7382, pp. 36-37 (Sept 1967).

(i) Mark-II Core. Design of the Mark-II (24-in. element) and Mark-IIA (26-in. element) fuel subassemblies has been completed; the drawings have been reviewed and approved. To increase the capability for fuel burnup, more volume is provided to accommodate fuel swelling and released fission gas by making the fuel elements longer and decreasing the diameter of the fuel pins. Also, the rod-type fuel-pin restrainer is eliminated by dimpling the fuel-element jacket tube. To compensate for the smaller diameter of the fuel pin, fuel enrichment is increased.

The lengthened fuel element increases pressure drop through the fuel section. Thus, to maintain the desired overall hydraulic-flow characteristics, the pressure drop through the upper and lower shield sections has been decreased by redesigning the upper and lower shield assemblies; they are stainless steel central-plug shields through which coolant flow alternates between the perimeter and the center. Because the fuel elements in the Mark-IIA subassembly are 2 in. longer than those in the Mark-II subassembly, the Mark-IIA upper shield is 2 in. shorter.

The Mark-II and Mark-IIA irradiation characteristics and their effect on the reactor vessel are being studied. Because the new subassemblies have less axial blanket shielding than do the Mark-I and Mark-IA subassemblies, it is expected that the reactor cover and grid plates will be irradiated more strongly when the new subassemblies are used. However, re-evaluated total doses calculated by the MAC computer code indicate that the absolute total-dose values are lower than originally computed. On this basis, the shielding characteristics of the new subassemblies are acceptable. Tests have shown hydraulic aspects of the new subassemblies to be acceptable.

(ii) Irradiation Subassemblies

(a) Mark C. To fill an early need of experimenters for a 19-element Mark-C subassembly that can accommodate 0.250-in.-dia irradiation capsules, the Mark-C19A subassembly has been designed; the outside diameter of each element is 0.328 in. instead of the 0.290 in. of the elements in the standard Mark-C19 subassembly. Drawings for the Mark-C19A subassembly are being completed.

k.   Instrumented Subassembly (E. Hutter)

Last Reported: ANL-7391, pp. 87-88 (Oct 1967).

(i) Subassembly Attachment and Lead Severance. The preliminary-design cutting tool (see Progress Report for September 1967, ANL-7382, pp. 37-38) was tested by cutting 330 leads in room-temperature

air. The constraint of limited space was given particular attention; transparent plastic mockups of the actual cutting area were used so that the operation could be observed. Stainless steel-sheathed, aluminum oxide-insulated leads and 3/16-in.-OD x 0.016-in.-wall stainless steel tubes were cut while positioned in the top-end fixture of the instrumented subassembly. Observation showed that a change in the angle of cutting-tool contact was needed so the cut leads would pass behind the cutter and not interfere with the next cut. The angle was increased from 0 to 15°, which gave the lead a satisfactory side thrust during cutting.

Prooftests were conducted in 700°F sodium with test apparatus that closely simulated the instrumented-subassembly configuration.

Stainless steel-sheathed, aluminum oxide-insulated leads were severed in 12 simulated cutting operations. In all, two hundred four 1/16-in. leads, sixty 1/8-in. leads, and twelve 3/16-in. x 0.016-in.-wall tubes were cut; torque requirements were 8, 18, and 15 ft-lb, respectively. These results compared favorably with those obtained during single-lead cutting operations (see Progress Reports for March 1967, ANL-7317, pp. 15-19, and September 1967, ANL-7382, pp. 37-38). All tests resulted in clean, sharp cuts, with no metal-chip formation. The AISI-SAE-TI cutting tool remained keen through all tests and retained its hardness although cycled 12 times in 700°F sodium.

To date, over 900 leads have been cut, half in 700°F sodium. These tests show that both leads and tubes can be cut reliably in room-temperature air or in 700°F sodium. The cutting operation is actually a shearing process and leaves no metal chips. The torque required to cut the leads is nominal and can be applied with simple mechanisms. Leads were severed more easily in 700°F sodium than in room-temperature air because of the lower yield strength of the stainless steel sheath at this elevated temperature.

(ii) Operating Mechanism. A mechanism is being designed to raise the extension tube and attached subassembly so they will clear the core when the shield plug is rotated during normal fuel-handling operations. As presently conceived, the operating mechanism will be located over a specific control-rod opening. The design permits the mechanism guidance and drive arrangement to be located between the centerline of the control-rod opening and the outside surface of the existing control-rod center-support column. Thus the subassembly and extension tube package can be installed and removed with a minimum of disassembly of the mechanism and structural support (only the elevator-arm assembly need be removed for withdrawal of the subassembly).

Structural support for the operating mechanism is obtained by attaching the lower end of the mechanism to the side of the existing center-support column. Since the upper end of the mechanism structure will

extend 69 in. above the top of the center column to provide the 8 ft of rise for the elevator arm, a structural support will be required at the upper end of the operating mechanism. This support must accommodate the 4 in. of relative motion which exist between the center-support column on the lifting platform and the surface of the rotating plug; it also must provide sufficient clearance between the top of the mechanism structure and the bottom of the cover-lifting drive motor located directly over the center column.

The present design of the extension column incorporates an external configuration and dimensions identical to the existing center column, thus permitting its attachment to the top of the center column. The extended length of the center column will permit continuous support for the linear bearing way which guides the elevator over the 8 ft of travel. The drive mechanism and motor arrangement will be mounted on the top of the extension column.

The use of an extension column will require the disassembly and removal of the pneumatic cylinders, hoses, and related electrical connections on the 12 control rods. This disassembly is necessary to expose the top of the air tank located in the upper end of the center-support column. The bolt holes in the mounting flange of the air tank and in the top face of the center column will be enlarged to accommodate the larger bolts necessary to hold the extension column rigidly to the center column.

Access slots in the sides of the extension column will allow the upper ends of the flexible pneumatic lines to exit from inside the column for connection to the control-rod air cylinders. Reassembly of the air cylinders and dashpots to the center-support column and connection to the control drives can then be completed.

1. Packaged Loop (B. C. Cerutti)

Last Reported: ANL-7391, p. 88 (Oct 1967).

The feasibility study of the packaged loop continued. A survey of prospective materials for the fabrication of the loop is being completed. Effort is being applied to the problems of flow, heat transfer, and insertion and removal of the in-core thimble.

m. Process Chemistry (D. W. Cissel)

Last Reported: ANL-7391, pp. 89-96 (Oct 1967).

(i) Sodium Coolant Quality Monitoring and Control

(a) Primary Sodium

(1) Sampling. Primary sodium samples were taken in Pyrex beakers ("cup-and-spigot" method) and extrusion vessels

(flow-through method) and submitted for analysis. The sample system was out of service from October 30 to November 14, 1967, for repair and modification of the "cup-and-spigot" sampler. A malfunction had resulted in the burning of a beaker sample within the sampler (see Sect. I.D.1.m.(2) below).

(2) Studies of Cesium Segregation. A sodium sample was taken in an extrusion vessel containing an orifice designed to distribute sodium flow next to the wall and create a spiral flow pattern in the vessel. The sample was frozen with liquid nitrogen while sodium was flowing through the vessel. The purpose of the sample was to study the effect of increased sodium velocity at the vessel wall on the segregation of cesium in the sodium. The sample was partitioned and analyzed by the method previously reported (see Progress Report for June 1967, ANL-7349, pp. 37-39). The results are shown in Table I.D.9 along with results from previous samples which were reported in Table II.E.16, ANL-7391, p. 91.

TABLE I.D.9. Ratios of ^{137}Cs/^{22}Na for
Extruder-partitioned Samples of Primary Sodium

| Aliquot No. | No Mixing | | Magnetic Mixing, Quick Chill (<40 sec) | Flow Mixing | |
	Slow Chill (60 min)	Quick Chill (<40 sec)		Without Orifice, Quick Chill (<40 sec)	With Orifice, Quick Chill (3 min)
1	0.06	0.06	0.10	0.15	0.18
2	0.08	0.05	0.17	0.17	0.12
3	0.09	0.07	0.15	0.17	0.14
4	0.09	0.07	0.16	0.15	0.13
5	0.07	0.07	0.15	0.16	0.12
6	0.07	0.07	0.12	0.10	0.12
7	0.07	0.06	0.09	0.06	0.09
8	0.04	0.03	0.05	0.23	0.04
Bottom	0.02	0.15	0.13	0.20	0.23
Vessel Wall	12.9	12.7	10.3	14.3	9.4
Whole Sample	-	-	0.26	0.26	0.47

Cesium segregation in the sodium was not substantially changed by the increased mixing provided by the orifice.

(3) Tin, Bismuth, and Lead Analyses. Additional analyses for tin, bismuth, and lead in both historical and current samples of primary sodium have been made by the Idaho Chemistry Laboratory and by Chemical Engineering and Reactor Engineering Divisions in Illinois.

The following conclusions have been drawn from these analyses:

1. A sharp increase in tin and bismuth concentration occurred in July 1965. The most probable source is the tin-bismuth alloy which forms a gas seal around the primary tank rotating plugs (see ANL-7391, p. 93).

2. Tin is distributed rather uniformly in sodium samples, and the concentration has remained constant at 15-20 ppm since the increase in July 1965.

3. In historical sodium samples, bismuth is concentrated at the bottom of the aluminum sample cups. Bismuth concentration in the sodium has dropped from an estimated 20-25 ppm following the increase in July 1965 to 1-3 ppm at the present time. The bismuth is believed to have been removed by the cold trap.

4. Lead is distributed rather uniformly in historical samples, and the concentration has remained constant at about 10 ppm since 1963.

No further analyses for tin and bismuth in historical samples are planned, but both impurities will be monitored routinely in the future. One additional historical sample for 1963 will be analyzed for lead.

A set of three EBR-II primary-sodium samples has been analyzed for bismuth and tin. The bismuth and tin were separated by coprecipitation with iron as the carrier element. After the precipitates were redissolved, the final concentrations were determined by atomic absorption. The analyses showed:

Sample Date	Bi (ppm)	Sn (ppm)
5-29-67	2.0	9.7
6-21-67	3.2	18.8
7-26-67	2.6	14.9

Unfortunately, these analyses had been initiated before bismuth segregation in sodium samples was found to be a problem (see ANL-7391, p. 93). However, the sodium-sample segments, each of which was about 25 g and 1.5 to 1.75 in. long, were taken from about the middle of the aluminum tubes that had been used to transport the sodium from the EBR-II. These values agree with those obtained on primary-sodium samples for which the total sample was analyzed.

An earlier set of samples yielded bismuth values ~1 ppm lower than these and tin values that also were lower. Whether there was still some bismuth segregation in these samples at the present low (~2.5 ppm Bi) level is not known. However, the sodium taken for the earlier analyses did come from the upper region of the sample tubes.

(b) Expanded Sampling Capabilities for Primary and Secondary Sodium

(1) Primary Sodium. The primary "cup-and-spigot" sampler was modified and improved to provide more reliable and convenient operation. On one occasion a 10-g sample of sodium burned in the sample chamber. To prevent a recurrence, the gas seal on the access lid of the sampler was modified to provide a more positive seal. The sodium inlet was routed through the chamber walls rather than the lid to make sample recovery more convenient. At the same time, provisions were made for filling two 10-ml beakers simultaneously. With these modifications completed and the sampler back in service, it should be possible to implement a sampling schedule which will meet routine analysis commitments.

Design work continued on modifications to the primary sampling system (see Progress Report for September 1967, ANL-7382, p. 41).

(c) Effect of Recycling Type 304L Stainless Steel Tubes. The Type 304L stainless steel tubular specimens that previously had been (1) exposed to 1100°F sodium for 7 days, (2) cleaned, (3) stored for either 10 or 120 days in normal (humid) or dry air, and (4) tested for changes in electrical resistivity, have been returned to flowing 1100°F sodium for 7 days, removed, cleaned, and their effective electrical resistivities have been measured.

(1) Normal-air Storage. Figure I.D.7 compares the effect on corrosion of storing samples either 10 or 120 days in normal air between 7-day exposures to 1100°F sodium. The resistivity (a measure of corrosion effect) of all of the 120-day-stored specimens increased with exposure to reagent. The data spread
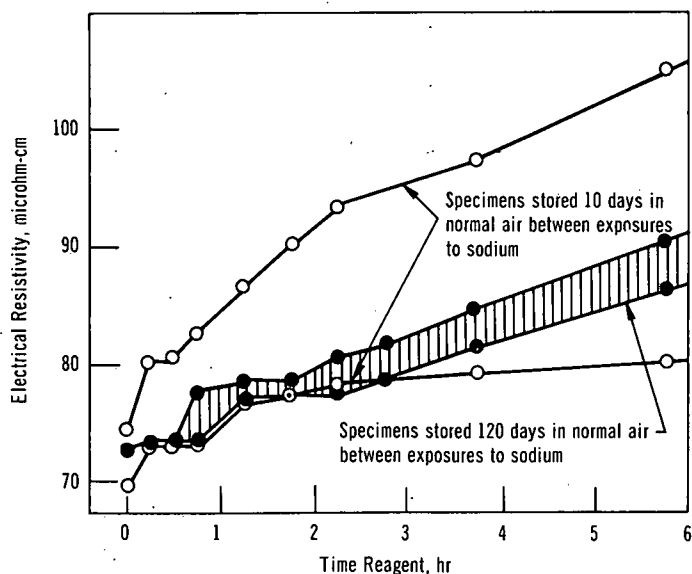

Fig. I.D.7. Effect of Re-exposing to 1100°F Sodium for 7 days Specimens of Type 304L Stainless Steel That Had Been Stored 10 or 120 days in Normal Air After Earlier Similar Exposure to Sodium, as Indicated by Resistivity Changes during Exposure to Strauss Reagent in Accelerated Corrosion Test

is smaller for the 120-day specimens than for the 10-day specimens. For any given time of exposure to reagent, the most corroded of the 120-day specimens had a greater resistance than any of the 10-day samples.

The resistivity of specimens stored for 120 days with no re-exposure to sodium reached a plateau at 78 microhm-cm at 1-6 hr in reagent (see ANL-7391, p. 95, Fig. II.E.13), in contrast to the continued resistivity increase to 90 microhm-cm after the re-exposed specimen is in the reagent for 6 hr.

(2) Dry-air Storage. The samples whose data are presented in Fig. I.D.8 were handled in the same way, except that they were stored in dry (CaSO$_4$-desiccated) air.

The resistivity increases in both Figs. I.D.7 and I.D.8 indicate the general desirability of not re-exposing Type 304L stainless steel to sodium after any storage in air. But the swift rise in resistivity of the 120-day dry-air stored specimens, as shown in Fig. I.D.8, leads to the conclusion that re-exposure of Type 304L stainless steel that has been exposed to dry air for an appreciable time should particularly be avoided.

Fig. I.D.8   Effect of Re-exposing to 1100°F Sodium for 7 days Specimens of Type 304L Stainless Steel That Had Been Stored 10 or 120 days in Dry Air after Earlier Similar Exposure to Sodium

Photomicrographs of the tube specimens that had been stored in dry air for 120 days between sodium exposures show gross loss of metal from both the outer and inner surfaces, indicating severe generalized erosion or corrosion. This contrasts with the nominal intergranular effects of the reagent on the samples that had not been exposed to sodium a second time.

n. Experimental Irradiations and Testing (D. W. Cissel)

Last Reported: ANL-7391, pp. 97-102 (Oct 1967).

(i) Experimental Irradiations

(a) Status of Experiments in EBR-II. The status of all experimental irradiations in EBR-II as of November 30 is shown in Table I.D.10.

TABLE I.D.10. Status of EBR-II Experimental Irradiations, November 30, 1967

Subassembly	Date Loaded	Capsule Content and Number of Capsules ( )		Experimenter	Approx Accum Exp (MWd)	Goal Exp (MWd)
XG02	7/16/65	UO_2-20 w/o PuO_2	(1)	GE	12,597	13,650
		Stainless Dummies	(18)			
XG03	7/16/65	UO_2-20 w/o PuO_2	(2)	GE	12,597	19,450
		Stainless Dummies	(17)			
XG04	7/16/65	UO_2-20 w/o PuO_2	(2)	GE	12,597	39,000
		Stainless Dummies	(17)			
XG05	9/3/65	UO_2-20 w/o PuO_2	(9)	GE	12,020	13,750[a]
		U-15 w/o Pu-10 w/o Zr	(1)	ANL		
		U-15 w/o Pu-10 w/o Ti	(1)	ANL		
		UC-20 w/o PuC	(3)	ANL		
		Structural	(5)	GE		
XA08	12/13/65	UC-20 w/o PuC	(8)	ANL	10,198	19,600
		Structural	(11)			
XO10	3/24/66	UO_2-20 w/o PuO_2	(4)	GE	9,528	19,600
		Structural	(11)	ANL		
		Structural	(4)	PNWL		
XO12	8/10/66	UO_2-20 w/o PuO_2	(19)	NUMEC	5,828*	20,600
XO15	11/15/66	PuO_2-UO_2	(11)	NUMEC	4,173	11,000
XO16	1/13/67	Structural	(9)	ANL	2,853	5,400
		Structural	(10)	GE		
XO17	11/15/66	PuO_2-UO_2	(11)	NUMEC	4,173	6,500
		(PuU)C	(3)	UNC		
		Mk-1A (Metal)	(5)	ANL		
XO18	12/6/66	Structural	(3)	GE	3,483	21,300
		Structural	(1)	PNWL		
		Structural	(2)	ANL		
		Structural and Heavy Metal Fission Yield Samples	(1)	ANL		
XO19	1/13/67	UO_2-20 w/o PuO_2	(7)	GE	2,853	12,500
		$(U_8Pu_2)C$	(3)	UNC		
		Structural	(8)	PNWL		
		Graphite	(1)	PNWL		
XO20	1/13/67	Mixed Oxides	(9)	GE	2,853	25,000
		Mixed Carbides	(3)	UNC		
		Structural	(4)	PNWL		
		Structural	(2)	ANL		
		Graphite	(1)	PNWL		

*This was reported in July 1967 as 7,528 instead of 4,528, and in October as 7,765 instead of 4,765.

TABLE I.D.10 (Contd.)

Subassembly	Date Loaded	Capsule Content and Number of Capsules ( )		Experimenter	Approx Accum Exp (MWd)	Goal Exp (MWd)
XO21	2/27/67	Structural	(7)	PNWL	2,853	24,400
XO22	2/27/67	Structural	(7)	PNWL	2,853	5,900
XO25	10/10/67	Structural	(19)	GE	1,213	5,000[b]
XO26	10/11/67	Structural	(7)	NRL	1,213	3,500
XO27	11/22/67	UO_2-PuO	(18)	GE	184	~7,200
		Structural	(1)	PNL		
XO28	11/22/67	U-Pu-Zr	(19)	ANL	184	~9,200
XO30	10/10/67	Thermocouple Matl.	(2)	PNWL	1,213	No Limit
		Graphite	(3)	PNWL		
		Structural	(1)	PNWL		
XO31	11/22/67	UO_2-PuO_2	(19)	PNL	184	~2,200
XO32	11/22/67	UO_2-PuO_2	(19)	PNL	184	~11,000

[a]This goal exposure is a new value.
[b]Nominal; actual exposure will be established on the basis of best interests of LMFBR program.

Subassemblies XO27, XO28, XO31, and XO32 were loaded into the reactor on November 22 at the end of Run 26B in grid positions 4-B-3, 4-D-3, 6-C-1, and 6-F-1, respectively.

Safety and operational approval was given for these subassemblies by the Idaho Division Director in July (XO27), October (XO28), and November (XO31 and XO32).

(b) Procurement and Inventory Control of Experimental Hardware. The remaining inventory of certified Type 304 stainless steel bar stock has been received from ANL, Illinois. This completes the transfer of experimental capsule hardware to the Idaho Division.

Orders were placed for 5000 ft of 0.806- and 0.290-in.-OD Type 304 stainless steel tubing which will supplement the stock received from ANL, Illinois.

Orders for experimental capsule hardware were filled for Westinghouse, and a partial order was shipped to the General Electric Co.

Negotiations and bid evaluations are in progress to select an outside shop to fabricate experimental capsule hardware from ANL-supplied stock. Outside shop fabrication will provide an available stock of the various end fittings required for experimental capsules and will prevent any delay in supplying these items to the experimenters.

The 37 capsules containing ANL Mark-II U-Fs alloy were wire wrapped in preparation for assembly into a Mark-B37 subassembly designated XO29.

(c) <u>Other Work</u>. Flow tests were performed with the following irradiation subassemblies: XO27, containing GE-E1H oxide-fuel specimens; and XO31 and XO32, containing PNWL oxide-fuel specimens.

The HECTIC-II code, which takes account of coolant mixing, has been modified to calculate the temperature distributions in the Mark-B37 irradiation subassembly. Temperature distribution was calculated for XO29, a Mark-B37 subassembly array with ANL-MET-encapsulated Mark-II driver fuel specimens, with the flow rate specified for approaching the desired maximum clad temperature.

A test melt-wire capsule was made with follower weights of borated stainless steel. This capsule will be neutron radiographed in subassembly-top-adapter and axial-blanket locations to determine the capability for definition with these borated stainless followers. This test capsule will also be heated at 1100°F for one week and examined metallurgically to establish the compatibility of melt-wire and capsule material.

(ii) <u>Nondestructive Testing</u>

(a) <u>Capsule Examinations</u>. Replacement capsules have been received from ANL for the three Mark-II U-Fs-alloy capsules which were rejected for incomplete weld penetration. These three, and a spare unit, were inspected and found to be acceptable for insertion in the reactor. After wire wrapping, these capsules will be assembled into a Mark-B37 subassembly designated XO29.

Two repaired capsules, designated Nos. 36 and 38, from the GE-E1H series were inspected to determine their suitability for inclusion in experimental subassembly XO27. Capsule No. 36 was found to have a tubing-wall defect which measured 11 percent of the capsule-wall thickness. As a result, XO27 was reassembled with a PNL materials capsule substituted for capsule No. 36, which is being retained for further evaluation and possible insertion at a later date.

Nineteen capsules of the UNC uranium-plutonium carbide series have been inspected, and one was returned for weld rework.

(b) <u>Other Nondestructive Testing</u>. Coils have been completed for the eddy-current bond testing equipment. Preliminary tests indicate good sensitivity for sodium-level and bond-void detection.

(c) <u>Antimony-Beryllium Neutron Source</u>. An EBR-II antimony tetroxide source was irradiated in the MTR for one cycle in order to obtain neutron-flux measurements and a number of neutron radiographs from the neutron source in the development of sources for future use in the

FCF Argon Cell. Preliminary measurements indicated a neutron flux of $5^{-10} \times 10^4$ n/cm²-sec at the outside end of the collimator. Evaluation of collimator apperture openings and configuration remain to be completed in order to fix the final design.

(iii) Handling and Examination

(a) Irradiated Capsules from XO11. No further handling or examination of capsules from XO11 was done by the Idaho Division. Capsule F4F has been returned to GE for positive verification of integrity of the capsule wall. The 13 capsules remaining in Idaho, all of which appear to be in satisfactory condition, are in the FCF Air Cell awaiting transfer to the Argon Cell for storage until return to the reactor or other final disposition.

No formal reports have been received from the investigations proceeding on the six capsules returned to sponsors. The unofficial status of these capsules is as follows:

(1) 5P-9 and 5P-12. PNL has completed metallography on both capsule walls. The microstructure appears to be normal with some expected indication of the temperatures at which they had operated. No corrosion or other surface effects were visible.

(2) HOV-4 and HOV-10. ANL-MET is preparing equipment to inspect capsule-wall integrity to determine if either capsule leaked fission products to the primary coolant while being irradiated in XO11. Both capsules contain failed fuel elements. No inspection data are yet available.

(3) F4D and F4F. GE has not started metallographic analysis of the F4D capsule wall, but the schedule calls for metallography to be completed by November 30, 1967, and a formal analysis report to be sent to ANL-ID by December 4, 1967.

Capsule F4F containing a failed fuel element is to be leak tested under a vacuum at elevated temperatures. The equipment for this test is being prepared.

(b) Testing of Procedures for Removal of Sodium from a Subassembly.

(1) Metallographic Examination of Capsule Wall Material (Type 304 Stainless Steel) from Capsules Irradiated in Subassembly XG06. GE has completed a metallographic analysis of F2Q, a typical capsule from the F2 series. Their results include the following:

1. The grain structure was lightly sensitized.

2. Grain size was estimated at ASTM-7 (this compares very favorably with the grain size in samples of as-received tubing with the same preirradiation heat treatment).

3. There was no evidence of attack, compositional changes, or changes in the mode of precipitation to either the outer surface (contacting the flowing primary coolant) or the inner surface (static bond sodium contact) of the capsule wall.

The conclusion was that the Type 304 stainless steel is normal considering the temperature history of the material.

(2) Cyclical Testing of Type 304L and 304 Stainless Steel Tubing Exposed at 1100°F, Washed in Water, and Stored in Air. Phase IV of this program, the 120-day air storage after soaking in sodium, is still in progress. After examination of the samples following the 120-day storage period, the program will be completed. However, arrangements are being made to examine some of the tube samples by electron microprobe in an attempt to determine whether sodium has penetrated into the tube wall. This latter examination may be possible in late December or January.

(3) Cyclical Testing of Stressed Capsules (Type 304 Stainless Steel) at EBR-II. Experimental subassembly X900, containing pressure-stressed tubing samples, was removed from the primary sodium and washed for the third time. Another set of seven stressed samples will be removed and the subassembly will then be returned to the primary tank for the fourth cycle.

The apparatus for measuring and depressurizing the helium gas used to stress the capsules operated successfully. The sample tubes from cycles one and two were measured and depressurized, and are presently being subjected to metallographic examination.

(c) Demonstration of Sodium-bond Integrity. Data have been accumulated from work of the Idaho and Metallurgy Divisions which support the theory that melting and freezing of sodium bonds between fuel-element claddings and inner capsule cores while the capsules are maintained in the vertical position does not cause deterioration of these bonds. Work continues toward summarizing the data for presentation to the EBR-II Irradiations Review Committee.

(iv) Safety Review of Experiments. The following experimental proposals were reviewed for safety and operational approval recommendation in EBR-II:

(1) Subassembly XO29, a Mark-B37 type subassembly, containing Mark-II encapsulated fuel pins for irradiation in Row 4; this is an ANL-MET experiment;

(2) Subassembly XO31, a Mark-A-type subassembly containing 19 capsules of mixed-oxide fuel for irradiation in Row 6; this is a PNL (FFTF) experiment;

(3) Subassembly XO32, exactly like XO31, except slated for longer exposure.

o. FCF Process Analysis and Testing (M. J. Feldman)

Last Reported: ANL-7391, pp. 102-103 (Oct 1967.).

(i) Operational Analysis. The initial phase of time study of the production activities was completed. A computer program is being prepared to analyze the data gathered.

(ii) Test and Analytical Methods. An investigation was completed as to the condition of the sodium bond in irradiated driver-fuel elements from subassemblies that are removed from EBR-II and disassembled in the Vertical Assembly-Disassembly machine (VAD). The purpose of the investigation was to determine the effects of maintaining the elements in a vertical attitude at all times during removal from EBR-II, transfer to the FCF, and dismantling of subassemblies in the FCF air cell.

The investigation involved pulsed eddy-current bond tests on a total of 192 elements from three subassemblies. In order to obtain data for elements showing various degrees of irradiation swelling, and hence, various sodium-bond annuli thicknesses, the subassemblies selected for examination represented three levels of fuel burnup. Subassembly identities and pertinent information are as follows:

(1) C-257 was irradiated in reactor grid position 3B2 to a maximum fuel burnup of 0.79 a/o.

(2) C-272 was irradiated in reactor grid position 4D1 to a maximum fuel burnup of 0.94 a/o.

(3) C-274 was irradiated in reactor grid position 5C4 to a maximum fuel burnup of 1.18 a/o.

Fuel elements were bond tested in the "as-received" condition at cell ambient temperature and at temperatures well above the melting point of sodium. Following completion of these tests, elements

were given a rebonding treatment using the FCF impact bonding technique and then bond tested again at cell ambient temperature and at elevated temperatures. Table I.D.11 summarizes the data obtained for the three subassemblies. Included are data on the numbers of voids and on sodium levels at the described temperatures.

TABLE I.D.11. Summary of Bond-testing Data for Elements from Subassemblies Handled in Vertical Orientation at All Times Following Irradiation in EBR-II

Subassembly No.		C-257	C-272	C-274
Burnup (a/o):	Max	0.79	0.94	1.18
	Avg	0.68	0.78	0.95
No. of Elements Tested		91	10	91
Number of Voids (average and range)				
"As Received" (cell temp)		14 (7-18)	11 (9-16)	14 (8-22)
"As Received" (elevated temp)		5 (2-9)	5 (3-8)	8 (3-15)
After Bonding (cell temp)		4 (0-9)	4 (1-9)	5 (0-9)
After Bonding (elevated temp)		4 (0-7)	4 (3-7)	5 (3-9)[a]
Sodium Level (average and range) (in.)				
"As Received" (cell temp)		1.13 (0.96-1.27)	1.32 (1.20-1.55)	1.32 (1.08-1.70)
"As Received" (elevated temp)		1.21 (1.02-1.39)	1.40 (1.31-1.59)	1.34 (1.10-1.60)
After Bonding (cell temp)		1.05 (0.85-1.20)	1.20 (1.03-1.37)	1.22 (0.92-1.40)
After Bonding (elevated temp)		1.18 (0.94-1.35)	1.35 (1.21-1.49)	1.35 (1.07-1.45)

[a]Average of 13 elements.

From the data in Table I.D.11, the following observations can be made:

(1) Irradiated driver-fuel elements from the three sub-assemblies (maximum burnup range from 0.79 to 1.18 a/o) were found to have voids in their bond annuli when received in the FCF from EBR-II and eddy-current bond tested at cell temperature. In general, the numbers and sizes of voids in the elements were comparable to those observed previously when the horizontal subassembly-dismantling technique was employed.

(2) Approximately one-half of the "as received" voids disappeared when the elements were bond tested at temperatures above the melting point of sodium. This reduction is attributed to the elimination of shrinkage-type voids in the sodium bonds. These voids were probably introduced into the bonds during uncontrolled cooling conditions that existed in the subassemblies during their withdrawal from the primary-sodium tank and transfer and sodium-removal operations in the FCF.

(3) Subjecting of elements to a single rebonding cycle (consisting of 500 impacts at 450°C) was not effective in eliminating all the bond defects. This observation held true both for bond testing at cell temperature and for bond testing at elevated temperatures following the rebonding treatment.

(4) Since the range of fuel burnup represented by the three subassemblies was approximately 0.8 to 1.18 a/o, a considerable range of fuel swelling (to about a 14-percent volume increase) was expected. Examination showed, however, that the fuel irradiated to 0.8 a/o in C-257 swelled about 3 percent, while the fuel irradiated to 1.18 a/o in C-274 swelled only about 4 percent. As a result, only limited information on the number of bond defects in elements as a function of the amount of fuel swelling (and, hence, as a function of sodium-bond annuli-thickness variations) was obtained from this investigation.

(5) Voids in the fuel-element bonds appeared to be reasonably equally distributed over the length of the fuel pins. Past experience, however, has indicated that voids are fewer in regions of maximum fuel swelling. These observations were made on pins which swelled by approximately 14 volume percent.

No explanation can be given at this time regarding the mechanisms of formation and possibilities for elimination of real voids in the element sodium bonds. Shrinkage-type voids, on the other hand, are readily explainable from the handling operations involved and can be eliminated by heating techniques.

p. **FCF Equipment Improvement** (M. J. Feldman)

Last Reported: ANL-7391, p. 104 (Oct 1967).

(i) **Auxiliary Equipment.** The previously submitted preliminary proposal for the construction of the Interim Subassembly Storage Area (see Progress Report for September 1967, ANL-7382, p. 52) was revised and resubmitted to AEC Chicago for approval of funds.

Loading and unloading of the transfer cask for this storage area will require an in-cask subassembly grapple. A model of one proposed grapple system has been completed. In order to test the system, a model of the cask cavity has also been constructed. The models have been assembled, and mechanical and pneumatic testing has been started.

(ii) **Repair and Decontamination.** Work continued on the engineering of the decontamination and repair facilities for manipulator and process equipment.

q. **Hot Fuel Examination Facility (HFEF)--Feasibility and Cost Study** (N. J. Swanson)

Last Reported: ANL-7391, p. 104 (Oct 1967).

Contract negotiations with the architect-engineer (Norman Engineering Co., Los Angeles) have been completed. Members of the firm have visited the EBR-II site for technical discussions and general orientation.

The first of a series of meetings between HFEF project personnel and PNL Fuel Examination Facility design personnel, to aid both groups by discussion of mutual problems, was held at EBR-II. The PNL facility is being designed as a part of the FFTF complex.

The preliminary cost estimate for HFEF has been completed and work has started on the Feasibility and Cost Study.

r. **Superheater and EM Pump Study and Test** (R. A. Jaross)

Last Reported: ANL-7391, pp. 104-105 (Oct 1967).

(i) **Superheater Vibration Study.** The superheater tube has been approximated as a uniform clamped-clamped beam of length ℓ = 25.125 ft with three interior supports located at distances a, b, and c from the tubesheet nearest the sodium inlet. The two different support configurations resulting from the different baffle spacings obtained when the shell is considered in halves are defined as:

Configuration I: a = 9.25 ft; b = 15.75 ft; c = 22.25 ft;

Configuration II: a = 6.0 ft; b = 12.5 ft; c = 19.0 ft.

The natural frequencies of free vibration of a uniform beam can be expressed as

$$\omega_n^2 = \left(\frac{EI}{\rho A}\right) \lambda_n^4,$$

where EI is the flexural rigidity, ρA is the virtual mass per unit length, and λ_n are the eigenvalues (roots of the frequency equation). For the superheater tube

$$\omega_n = 506\ \lambda_n^2,$$

where λ_n has the units ft^{-1}.

A computer code was written to allow evaluation of the eigenvalues. The results for the first three natural frequencies are given in Table I.D.12 for the two support configurations. These natural frequencies will be used in subsequent analyses for resonant phenomena instability and fatigue.

TABLE I.D.12.   Eigenvalues and Natural
Frequencies of Superheater Tubes.

n	Configuration I		Configuration II	
	$\lambda_n(ft^{-1})$	$f_n(cps)$	$\lambda_n(ft^{-1})$	$f_n(cps)$
1	0.452	16.4	0.528	22.4
2	0.563	25.5	0.622	31.2
3	0.669	36.0	0.726	42.5

s.   Reactor Improvements, Nuclear Instrument Test Facility
(B. C. Cerutti)

Last Reported: ANL-7391, p. 105 (Oct 1967).

The following were accomplished:

(1) A preliminary design layout of the insert for the high-temperature "O" thimble was started. Letters of inquiry have been sent to six electric-furnace manufacturers for information needed to complete the layout and design in the heater and related insert area.

(2) A preliminary design layout of a high-temperature "O" thimble and thimble extension was initiated.

(3) A partial conceptual layout of a proof-test facility for the new thimble, the thimble insert, and associated equipment was made.

t. Feasibility Study of Fuel Failure Detection--Chemical and Mechanical Methods

(i) Trace Elements Analytical Techniques (C. E. Crouthamel)

Last Reported: ANL-7391, pp. 106-107 (Oct 1967).

Activity has centered primarily on an examination of the literature in an effort to pinpoint the selection of tagged elements which appear most applicable. Recent information indicates that cesium dissolved in sodium is readily absorbed on substrates such as stainless steel. Bismuth appears to undergo extensive segregation when solutions of bismuth in sodium are cooled.

A spark-source mass spectrometer will be used in the tagged-element study. Shipment of the mass spectrometer, scheduled for the first of November, has been rescheduled for sometime in December. Laboratory space for the spark-source mass spectrometer is under construction.

Construction is also proceeding on the laboratory facility for the matrix-isolation studies on tagged elements. An inert-atmosphere box and its attendant purification system have been acquired and will be installed in the facility as soon as construction permits.

(ii) Tag-confirmation Study (F. A. Cafasso)

Last Reported: ANL-7391, p. 107 (Oct 1967).

The conceptual design of the small-scale experimental loop for circulating liquid sodium, has been completed, and the engineering design has been started. Selected pieces of equipment for the loop have been requisitioned.

(iii) Mechanical Failed-fuel Locator (E. Hutter)

Last Reported: ANL-7391, pp. 108-109 (Oct 1967).

The study to provide a mechanical method to detect fission-gas leakage from a specific subassembly is continuing. Two approaches to the concept of monitoring fission-gas pressure during reactor

operation by means of a sampling mechanism in a control-rod position were studied: (1) continuous sampling of liquid sodium and (2) dip sampling of frozen sodium.

(a) Continuous Sampling of Liquid Sodium. A method of providing liquid-sodium samples to an external apparatus was investigated; it would permit continuous analysis for the presence of solid matter from a failed fuel element. An experimental water loop was assembled to study pressure distribution and siphoning effects in a closed loop; a mockup fission-gas separator was installed in an adjustable water stream that simulated primary-pump operation. An additional loop, operating on the siphoning principle, was assembled; it consisted of a vacuum chamber connected by a tube to the fission-gas separator 6 ft below the vacuum chamber, and an exit tube. Circulating gas introduced into the water stream provided additional turbulence to assist in releasing trapped fission gas. Both loops operated satisfactorily.

(b) Dip Sampling of Frozen Sodium. This method of providing a small sample of sodium for analysis is much simpler than continuous liquid-sodium sampling, which has problems of clogging, shielding, and heating. The gas-sampling system (see Progress Report for October 1967, ANL-7391, pp. 108-109) would have to be modified to allow insertion of a small open-top container on the end of a rod. The container would be positioned in the sodium flowing through the fission-gas separator. When desired, the container could be withdrawn for analysis of the sodium.

u. EBR-II Materials--Coolant Compatibility (J. E. Draley, principal investigator; work by N. Balai and R. V. Strain)

Last Reported: ANL-7391, p. 109 (Oct 1967).

(i) Corrosion of SURV-I Surveillance Specimens. With but two exceptions, tantalum and Berylco 25 (beryllium-copper), small weight losses were found after irradiation exposure in coolant sodium (see Table I.D. 13). The specimens were in the SURV-I materials-surveillance assembly in Row 12 of EBR-II from March 1965 to March 1967, during

TABLE I.D.13. Corrosion Losses by SURV-I Specimens

Material	Average Initial Weight (g)	Weight Losses (mg)		Comments
		Average	Range	
Aluminum-Bronze	16.06	1.7	0.5-2.6	
Berylco-25	17.97	151.2	126.2-177.0	3 samples[a]
Stellite-6B	18.09	1.4	1.1-1.7	
Tool steel T-1	18.68	4.2	0.6-8.9	18-4-1 cutting steel
Inconel-X	17.74	1.6	0.2-3.3	
Tantalum	36.20	13.1	3.8-22.4	2 samples
Type 17-4PH SS	16.69	1.1	0.7-1.5	Hardened
Type 304 SS with boron	16.78	3.1	2.0-4.2	2.1% natural boron
Type 304 SS (warehouse)	16.85	1.3	0.0-2.1	3 samples typical stock
Type 347 SS	16.94	1.1	0.0-1.7	3 samples
Type 416 SS	16.29	2.4	1.6-2.9	Hardened
Type 420 SS	16.50	1.8	1.2-2.6	Hardened

[a]A fourth sample lost only 3.4 mg and is not included in the average.

which the reactor operated 15,000 MWd. The nominal size of a specimen was 0.875 in. by 0.437 in. in diameter. Except where noted, the results in Table I.D.13 are from four specimens of each material.

(ii) Mechanical Properties of Irradiated SURV-I Materials. Data on preirradiation mechanical properties of the materials were augmented by results from spare specimens prepared concurrently with those for the SURV series. Partial load-strain curves (to 0.5% elongation) for both the unirradiated and the irradiated materials were obtained and reviewed. The curves for irradiated tantalum and aluminum-bronze reveal an approximately 50% increase in the modulus of elasticity.

Annealed and moderately work-hardened Type 304 stainless steel were not affected in the irradiation cycle; weld-metal ductility of Type 308 stainless steel was slightly reduced. Hardened Inconel-X and Type 17-4PH stainless steel overaged with accompanying losses in ductility; Inconel-X was weakened but the 17-4PH (a precipitation-hardening alloy) was strengthened. The tensile strength of tantalum was almost doubled at the partial expense of its ductility; however, the irradiated metal is still ductile. The aluminum-bronze apparently aged in a manner similar to that displayed by Inconel-X. The softening of hardened Type 420 stainless steel is believed to be a long-time annealing effect.

Although surveillance specimens were irradiated in two environments, sodium and helium, evidence for environmental effects is inconclusive. The conventional mechanical properties (strength, ductility, and hardness) pertinent to reactor safety are summarized in Tables I.D.14 and I.D.15.

Measurement of postirradiation hardness proved to be an unreliable indicator of material performance otherwise. For example, the hardening of Type 17-4PH stainless steel reflected its strengthening, but aluminum-bronze hardened and lost tensile strength; the annealing of the previously hardened Type 420 stainless steel was undetected by hardness measurements.

(iii) Effects of Irradiation on Hardening of SURV-I Specimens. The average Vickers Hardness Number for at least five indentations on irradiated samples is reported in Table I.D.15. All of the hardness tests (including those on the control samples) were made on the same Tukon microhardness tester. The machine was calibrated (within 3% of values for a standard test block) before and after testing each sample.

The approximate neutron exposures at specimen center lines were calculated from titanium flux wires. These values are approximate because they are based only on the variation in flux axially in the reactor and they are not corrected for the attenuation of the neutrons across the diameter of the subassembly.

TABLE I.D.14. Strength and Ductility of SURV-I Materials (Average and Range for Three or More Specimens)   Pg 90

| Exposure | | | Strength (10^3 psi) | | | | Ductility (%) | | | |
| | | | Tensile | | Yield Point | | Elongation | | Red. of Area | |
Fluence[a]	Temperature	Environment	Average	Range	Average	Range	Average	Range	Average	Range
			Aluminum-Bronze							
0	Room	Air	103.3	102-106	48.7	47-51	29.7	28-31	41.3	40-44
8×10^{18}	EBR-II	Na	98.7	96-101	58.0	55-60	11.3	10-13	11.3	10-13
9×10^{18}	EBR-II	He	97.5	95-100	57.2	54-61	9.7	9-10	11.2	9-19
			Inconel-X							
0	Room	Air	170.0	168-171	96.0	91-99	24.0	21-26	23.7	21-26
8×10^{18}	EBR-II	Na	159.3	157-160	130.3	127-133	17.5	15-20	18.5	14-21
8×10^{18}	EBR-II	He	157.2	152-161	129.0	124-132	18.2	16-24	18.5	13-27
			Tantalum							
0	Room	Air	51.3	47-56	36.3	32-41	56.7	54-63	95	90-99
1×10^{19}	EBR-II	Na	97.1	89.7-103	96.1	89-101.5	20.7	16-24	86.2	80-89
1×10^{19}	EBR-II	He	100.1	89.6-106	96.5	92-104	16.2	15-18	69.7	69-70
			Type 17-4PH Stainless Steel							
0	Room	Air	174	172-176	168.3	166-171	17.3	17-18	53.3	52-54
1×10^{19}	EBR-II	Na	214.7	211-221	204.5	201-208	12.2	12-13	41.5	38-44
1×10^{19}	EBR-II	He	212.2	209-216	204.0	194.5-209.5	9.7	3-13	29.7	8-40
			Type 304 Stainless Steel Warehouse Stock							
0	Room	Air	111	101-123	85.0	75-98	40.3	34-46	58.3	49-69
8×10^{18}	EBR-II	Na	117	104-128	92.0	77.9-104	39.0	35-45	63	57-68
8×10^{18}	EBR-II	He	108	104-118	79.0	78-80	42.7	36-46	70.7	67-77
			Type 304 Stainless Steel (EBR-II cover plate)							
0	Room	Air	80.7	80-82	33.7	33-34	74.0	72-77	79.0	75-82
1×10^{19}	EBR-II	Na	79.2	78-80.4	35.0	33.0-38.3	70.0	69-71	80.5	79-82
1×10^{19}	EBR-II	He	79.8	79-80	34.3	33-40	70.3	68-72	75.0	71-80
			Type 304 Stainless Steel Welded with Type 308L Stainless Steel							
0	Room	Air	87.7	87-88	47.7	47-48	37.7	33-42	59.0	57-61
9×10^{18}	EBR-II	Na	90.1	89-91	51.9	50-53.3	26.3	25-29	54.0	45-60
9×10^{18}	EBR-II	He	88.9	88-89.9	51.5	47-60	29.2	23-34	51.0	46-59
			Type 420 Stainless Steel							
0	Room	Air	224.1	207.0-228.4	170.1	164.0-180.3	5.7	5.0-6.0	35.7	30-44
9×10^{18}	EBR-II	Na	209.8	200-227	173.8	157-183	12.2	9-16	40.5	34-44
9×10^{18}	EBR-II	He	201.2	198-202.8	171.3	169-173	9.0	6-12	40.5	33-43

[a]Exposure averaged from vertical dispersions of samples in reactor. Total exposure was between 5×10^{18} and 1.2×10^{19} n/cm^2 [2.2×10^7 sec at 45 MWt].

TABLE I.D.15. Irradiation Hardening of EBR-II Materials (SURV-I)

Material and Sample No.	Distance from the Top of Tube (in.)	Approximate % of Maximum Integrated Flux	Approximate Total Integrated Flux (n/cm^2 x 10^{-19})	Vickers Hardness No. (500-g Load)
Aluminum-Bronze				
Control				191
1	22-7/16	44	0.6	224
2	16-13/16	78	1.1	213
3	8-3/16	99	1.4	223
4	25-7/16	26	0.4	202
Stellite				
Control				371
1	21-9/16	50	0.7	425
2	12-15/16	99	1.4	485
3	7-5/16	90	1.3	453
4	24-9/16	31	0.4	428
Inconel-X				
Control				372
1	17-11/16	73	1.0	375
2	12-1/16	99	1.4	353
3	3-7/16	75	1.1	376
4	20-11/16	55	0.8	399
Type 420 Stainless Steel				
Control				358
1	16-13/16	78	1.1	372
2	8-3/16	99	1.4	403
3	25-7/16	26	0.4	397
4	19-13/16	63	0.9	377

TABLE I.D.15 (Contd.)   *Pg 91*

Material and Sample No.	Distance from the Top of Tube (in.)	Approximate % of Maximum Integrated Flux	Approximate Total Integrated Flux (n/cm^2 x 10^{-19})	Vickers Hardness No. (500-g Load)
T-1 Tool Steel				
Control				710
1	12-15/16	99	1.4	672
2	7-5/16	90	1.3	646
3	24-9/16	31	0.4	681
4	12-15/16	99	1.4	696
Type 347 Stainless Steel				
Control				148
3	20-11/16	55	0.8	162
4	12-1/16	99	1.4	166
Type 416 Stainless Steel				
Control				275
1	8-3/16	99	1.4	314
2	25-7/16	26	0.4	306
3	19-13/16	63	0.9	294
4	8-3/16	99	1.4	277
Berylco 25 (Beryllium-Copper) Control				320
1	7-5/16	90	1.3	161
2	24-9/16	31	0.4	165
3	12-15/16	99	1.4	176
4	7-5/16	90	1.3	176
Borated Type 304 Stainless Steel				
Control				237
1	3-7/16	75	1.1	270
2	17-11/16	73	1.0	268
3	12-1/16	99	1.4	231
4	3-7/16	75	1.1	244
Type 17-4PH Stainless Steel				
Control				298
2	16-13/16	78	1.1	363
Type 304 Stainless Steel				
Control				141
1	24-9/16	31	0.4	143
2	12-15/16	99	1.4	143
3	7-5/16	90	1.3	143
Tantalum				
Control				121
1	17-11/16	73	1.0	161
2	12-1/16	99	1.4	209
3	3-7/16	75	1.1	210

Even though all samples were exposed to the primary sodium during irradiation, most exhibited no surface hardening or softening. The individual hardness numbers varied in a random fashion across sections of several of the samples. The variation was probably due to the dispersed precipitates in the alloys.

The most striking result of the hardness measurements was the reduction in hardness of the beryllium-copper (Berylco-25) samples. This is a precipitation-hardening alloy that has been reported to increase in hardness upon irradiation. Possibly the sodium environment is responsible for the softening; surface corrosion was observed on all four Berylco-25 samples. The microstructure of these samples also changed considerably. Grain-size reduction appears likely, but optical metallography has not clearly defined what has occurred.

The T-1 tool-steel samples also became softer during the irradiation. This was probably due to the tempering effect of the ~700°F operating temperature of the subassembly. The stainless steel samples were all stress relieved near 900°F as a final heat treatment, but the tool steel samples were not stress relieved.

The Inconel-X, the borated Type 304 stainless steel, and the unmodified Type 304 stainless steel did not undergo appreciable hardening during the irradiation.

The remainder of the samples (aluminum-bronze, stellite, Type 420 stainless steel, Type 347 stainless steel, Type 416 stainless steel, 17-4PH stainless steel, and tantalum) all became appreciably harder during irradiation. Generally, the hardness of these samples increased with the neutron exposure of the samples. However, it is not possible to determine a direct correlation between the two because of the inexactness of both hardness measurements and the neutron exposure values.

2. **Outside Fuel Procurement** (C. E. Stevenson)

Last Reported: ANL-7391, p. 110 (Oct 1967).

a. **Mark-IA-IB Fuel Procurement**

(i) **Fuel Elements.** The fuel-element contractor, Aerojet-General Corp., is making good progress in procuring materials, and in constructing and installing equipment for element fabrication. The alloy-preparation and injection-casting furnaces are being installed. Control equipment and accessories for these furnaces are being fabricated. Both furnaces were expected to be ready for operation by the end of November. The initial shipment (45 kg) of 52-percent-enriched uranium was received, and sampling and analyses began. One 5.5-kg "button" was returned to the supplier because of poor surface condition.

Aerojet completed development and assembly of pulsed eddy-current equipment, similar to that used by ANL, for inspection of fuel-element tubing in order to detect defects corresponding to 10 percent of the tubing wall thickness. The equipment was initially used with samples of defect-containing tubing supplied by ANL, and natural defects whose depth was 0.8-1.0 mil were detected, as indicated by sectioning and micrography. The equipment was then installed in the production line, but the sensing coil appeared to have suffered some damage in the transfer. A new coil was fabricated, and it appears to give satisfactory results. The tubing supplier, the Matthey Bishop Co., delivered an initial lot of tubing (982 ft) to Aerojet for evaluation before embarking on production. Defect standards for Argonne approval will be prepared from tubing in this lot. Evaluation of the tubing indicated that the defect level being experienced was higher than appeared desirable and that some process difficulties had been encountered which could be overcome. Bishop has agreed to supply Aerojet with a second 1000-ft lot for evaluation before commencing the production run.

In order to develop specification limits for tensile and burst-test strength applicable to tubing procurement, data were obtained by Argonne

on samples of Type 304L stainless steel tubing previously procured for fuel-element fabrication. The samples had all been subjected to pulsed eddy-current inspection to detect and eliminate sections whose defects exceeded 10 percent of the wall thickness. The data represent products of three suppliers, but are not believed to be fully representative of the range of material obtained, since only a small portion of this material was used for sampling. The data obtained are summarized in the following table:

Tensile and Burst Strength of EBR-II Fuel-element Tubing
(Type 304L Stainless Steel, 0.156-in. ID, 0.009-in. Wall Thickness)

Supplier		Tensile Test (ASTM A370-65)				Burst Test	
		No. of Samples	Ultimate Strength (psi)	Yield Strength (0.2%) (psi)	Elongation, (Percent)	No. of Samples	Burst Pressure (psi)
A	avg	15	98,000	45,450	57	16	8,580
	range		91,320-102,440	37,300-60,600	51-65		8,000-9,100
B	avg	2	89,670	36,060	66	2	8,100
	range		89,020-90,310	35,410-36,700	66-7		8,000-8,200
C	avg	2	101,340	50,110	57	3	8,250
	range		100,080-102,580	47,770-52,440	55-60		7,750-9,000

Additional specifications for the fuel element tubing were derived from these data, from literature data on Type 304 stainless steel (including elevated temperature properties), and from service requirements for the fuel elements. Specification changes were prepared and have been submitted to RDT for review.

With regard to the procurement of other cladding components, an order was placed by Aerojet for wire for the spiral wrap, additional restrainers were delivered, and the tip fabricator was reported to be making progress toward submitting a "first part" lot by mid-November. The wire-to-tube welding procedure is substantially developed, and tests of the wire-to-tip weld were initiated. Equipment was installed for the tip-to-tube weld. Procedures for tube deburring and tip insertion were completed. Aerojet also submitted an outline of the Fabrication Procedures manual for ANL review.

(ii) Subassembly Hardware. Final negotiations were completed on a contract for the fabrication of over 500 sets of hardware preassemblies and other hardware components, and the vendor commenced work planning on the contract.

3. Operations--Reactor Plant (G. K. Whitham)

   Last Reported: ANL-7391, pp. 111-117 (Oct 1967).

   a. Operations. Operation at 45 MW continued through November 5, except for two days during which oscillator experiments were conducted at reduced power levels. On November 6, additional reduced-flow and reduced-power experimental data were obtained, followed by further oscillator experiments at 22.5 and 30 MW. Power was reduced to 50 kW on November 8, prior to taking another set of power-reactivity-decrement measurements to 45 MW. During the raising of reactor power after a critical-position measurement at 50 kW, a high lubricating-oil temperature in the motor-driven feedwater pump was noted (see Sect. I.D.3.b.(i).(b)). The reactor and pump were shut down, and inspection of the pump revealed that the inner thrust bearing had failed. The reactor was restarted and power raised to 15 MW using the startup feedwater pump and to 20 MW using the turbine-driven feedwater pump. The power coefficient between 15 and 20 MW appeared to be very slightly positive, but the reactivity change observed was about equal to the uncertainty of measurement. After lowering power to 15 MW to obtain additional data, the reactor was shut down pending further consideration of the matter.

   Further maintenance was then performed on the motor-driven feedwater pump, and the annual leak-rate test of the emergency airlock was carried out. Biweekly, monthly, and quarterly interlock checks were completed, and the periodic test of emergency power system and bus-tie circuit breakers was conducted.

   Following consultation within ANL and agreement on a plan of action, the reactor was restarted on November 12 to continue power-coefficient measurements. Shortly after power reached 20 MW, the primary-system bulk-sodium temperature began increasing. The operator tried to control the temperature by adjusting secondary flow, but it soon became apparent that this was ineffective, and the reactor was shut down. It was found that because of a malfunction of the steam-drum water-level recorder-controller (and alarm), the drum had been boiled dry and most of the water in the evaporators had been lost. The secondary-sodium level in the surge tank was lowered to stop natural convection and conserve the remaining water in the steam system. Cooldown of the primary tank was begun. After the sodium lines, evaporators, superheaters, and steam drum had cooled sufficiently, feedwater at 350°F was slowly added to re-establish normal steam-drum water level.

   Cooldown of the primary tank was continued until the bulk sodium temperature approached 450°F. Secondary-sodium temperatures simultaneously were controlled between 350 and 420°F. Sodium level in the surge tank then was raised very slowly toward the operating level and minimum

flow in the forward direction was established. Finally, the secondary-sodium flow was gradually increased until normal plant heatup conditions were attained. The reactor was used to heat the bulk sodium from 600 to 700°F.

The power-reactivity decrement was measured before the reactor was reloaded for Run 26C.

b. Operational Support and Maintenance

(i) Plant Maintenance.

(a) No. 2 Heater. A leak in the upper sight glass of the No. 2 feedwater heater required replacement of gaskets, mica, and viewing glasses.

(b) Motor-driven Feedwater Pump. High lubricating-oil temperature noted during startup of the motor-driven feedwater pump caused a shutdown for disassembly and inspection of the pump bearings.

The inner thrust bearing, which had failed, was replaced with a new set of inner thrust-bearing shoes and a new inner thrust collar. The balance-drum clearances, the suction strainer, both lube-oil pumps, the balance line, the oil-supply check valve, and the Δ oil strainers were checked, but nothing abnormal was found. Some water was found in the oil; the oil sump was completely drained and cleaned. If water had caused the bearing failure, the journal bearings would have probably been damaged also. The journal bearings showed no evidence of any damage; therefore, the cause of the failure remains undetermined. The pump is now operating normally.

(c) Startup Feedwater Pump. Lifting of the pressure-relief valve on the startup feedwater pump resulted in cracking of its inlet pipe. The piping was repaired by replacement with schedule 160 pipe. The leaking No. 1 suction valve was removed, the head was remachined to provide a better sealing surface, and the valve was reassembled and replaced.

(d) Turbine-driven Condensate Pump. The outboard journal bearing on the turbine-driven condensate pump failed. This failure was apparently due to steam blowing out of the shaft seals, causing water to condense in the bearing housing. A new bearing was installed, the shaft seal was adjusted, and the unit was restored to service.

(e) Main Turbine. The main turbine initial-pressure governor was realigned and reset and is operating satisfactorily.

(f) <u>Steam Drum.</u> Because of a small leak, new studs, mica, and gaskets were installed on the east steam-drum sight glass.

(g) <u>Reactor-building Rotary Crane.</u> A bearing in a wheel on the reactor-building bridge crane failed, and was replaced with a new bearing assembly.

(h) <u>Reactor-building Shield Cooling Exhaust.</u> The control valve on the air-exhaust damper (R8-DM-726) of the shield-cooling system was disassembled and inspected because of sticking on switch-over of the Nos. 1 and 2 exhaust blowers, but no specific defect was found. New bearings and seals were installed, alignment was checked, and the unit was reassembled. The valve is now functioning satisfactorily.

(i) <u>Primary Motor-Generator (M-G) Couplings.</u> The frequency generator on the M-G set for the No. 2 primary sodium pump malfunctioned. A rebuilt frequency generator was installed as a replacement.

Disassembly of the spare M-G eddy-current coupling was completed.

(j) <u>Argon Cooling System for Fuel Unloading Machine (FUM).</u> Spare molecular sieves for the FUM argon cooling system were modified by installing baffles to prevent gas from bypassing the sieve material. The spare sieves were installed but an operational check has not been made.

A bearing failed in the motor which drives one of the 10-hp ac blowers for the FUM argon system, and a spare motor was installed. A new motor has been ordered as a spare.

(k) <u>Fuel Unloading Machine (FUM).</u> A crack developed in the carriage-drive clutch support of the FUM. The clutch support was re-welded and reworked. The rail-guide roller bearings were inspected and found worn, and replacement bearings were ordered. Following breakage of the cable for the argon hose take-up reel, which resulted in unwinding of the springs inside the reel housing, the cable was repaired and the springs were rewound. The FUM gripper was removed, cleaned, checked, and reinstalled.

(l) <u>Leak-rate Test of Reactor Building Containment.</u> The annual leak-rate test was performed on the emergency air lock.

Door	Leak-rate (Std cu ft/24 hr)
No. 1 (outer) door and lock	4.3
No. 2 (inner) door	2.9

Annual leak-rate tests were performed on electrical penetrations Nos. 9, 10, 13, 23, 24, 25, 27, 29, 31, 35, 36, and 26 (vacuum breaker). All penetrations had a leak rate of less than 0.1 std cu ft/24 hr; thus all leak rates were within acceptable limits.

(m) <u>Control-rod Drives</u>. The roller clutch for the latch of No. 12 control rod was replaced with a new unit. The lower jaw assembly was cut off the control rod drive which was recently removed from position No. 7. The tubing will be kept for stock for fabricating a spare drive assembly if needed.

(n) <u>480-V Electrical System</u>. The semiannual emergency power test, EP-1, was performed satisfactorily. This is a test of the performance of the emergency power-generating equipment and associated switchgear, and 480-V bus-tie breakers.

A new 1000-A breaker was installed for the 480-V power supply to the Lab and Office Building, replacing the original 400-A breaker. The 400-A breaker will be kept as a spare.

Two new breakers, Nos. 3 and 4, were installed to replace breakers that were malfunctioning in the secondary-sodium surge-tank heater supply, but the new breakers do not function properly. The difficulty is believed due to the high ambient temperature. The manufacturer is sending, at no charge, two breakers calibrated at 50°C.

(ii) <u>Spare Parts</u>. Delivery of the spare FERD loop EM pump is delayed until December. Purchase orders for inventory additions to spare parts were placed for the following components:

(a) a packing kit for repairing the air cylinders for the shield-cooling exhaust damper;

(b) a complete set of internal parts for the desuperheater cooling-water bypass valve, P5-VC-619A;

(c) high-tensile studs for the steam-drum gauge glasses;

(d) a motor, speed reducer, and brake for the main core gripper and holddown elevation drive.

c. <u>Operator Training</u>. Five technicians completed individual Systems Training Qualification. Two of these men have now completed all five system qualifications and were designated EBR-II Reactor Plant Operators.

Systematic updating and filing of information on systems and components is continuing to provide better information service to operating personnel.

d.   Operating Manual.   Operating Manual revision bulletins Nos. 62 and 63 were issued.   Bulletin No. 62 is the revised continuous power supply section of Division IX.   Bulletin No. 63 is a new section covering operation of the Fuel Element Rupture Detector.

Drafts for revisions to the boiler feedwater treatment, plant cooling, water treatment, and water-sampling stations sections of Division VI were completed.   Revised plugging-run procedures for both primary and secondary systems were drafted, and work started on sodium sampling procedures.   Drafting of a new section covering operation of the fission gas monitor continued.

Work continued on revisions of the Normal Operating Procedures section of Division II.

e.   Planning and Scheduling.   Many short-range schedules to coordinate maintenance activities with the reactor experimental program were prepared and revised as needed.   Work continued on the annual reactor operating schedule.

4.   Operations--Fuel Cycle Facility   (M. J. Feldman)

a.   Hot-line Operation.   Routine operations were conducted, but production rates were hampered by lack of fuel, lack of subassembly-storage space, and the requirements of experimental programs.   Table I.D.16 summarizes the production activities.

TABLE I.D.16.   Production Summary for Hot Line

	11/1/67 through 11/30/67	Total This Year
1. Subassemblies Received:		
Core, Control, Safety	10	64
Other	3	127
2. Subassemblies Dismantled (for processing)	12	72
3. Subassemblies Dismantled (for examination, etc.)	3	40
4. Subassemblies Fabricated (includes one made with unirradiated fuel)	7	150[a]
5. Subassemblies Transferred to Reactor;	0	84
Subassemblies Sent to Storage in L&O Vault and Interbuilding Corridor	6	34
6. Elements Decanned:		
From Irradiated Subassemblies	1,091	6,012
Rejects	0	876
Other	0	0
Total Decanned	1,091	6,888

Melt Refining

	Irradiated Fuel	Recycle Material	New Fuel
7. Number of Runs	8	6	0
8. Average Pour Yield, %	92.7	93.7	-
1967 to date (Total)	48	74	52

TABLE I.D.16 (Contd.)

	11/1/67 through 11/30/67	Total This Year
Processing		
9. Injection-casting Runs (Total Number)	13	161
10. Elements Processed:		
Accepted	829	13,895
Rejected	84	1,827
11. Elements Welded	846	22,781
Rewelded	0	17
12. Elements Leak-tested:		
Accepted	757	13,141
Rejected	32	293
13. Elements Bonded (including recycle)	766	16,648
14. Elements Bond-tested:		
Accepted	577	13,361
Rejected	47	823
15. Elements to Surveillance	147	759
Number of Subassemblies	9	56
Waste Shipments		
16. Cans to Burial Ground	5	92
17. Oxide and Glass Scrap to ICPP	1	52

[a]Corrected values to include hot-line production only.

Fuel in the form of irradiated subassemblies was received from the reactor, and two-shift operations were initiated at reprocessing stations to get the fuel into the process stream as soon as possible. Additional effort was required for these operations because of the dimensional measurements required on the subassemblies prior to dismantling. The 18 core-type, 6 control-type, and 1 safety-type subassemblies removed after Run 25 have all been examined for (a) overall straightness, (b) twist, and (c) hex-tube dimensions on, directly above, and directly below the buttons.

The last of three shipments of iron-contaminated fuel was sent to the Idaho Chemical Processing Plant (ICPP) for reprocessing.

The Mark-IB experimental program was inaugurated and is scheduled for completion by the start of reactor Run 27. This program calls for fabrication of experimental subassemblies containing fuel elements which were made up from selected batches of fuel and with the Mark-IB restrainers; these restrainers are smaller than those previously used, in order to increase the volume of the gas plenum in the fuel element.

b. Cold-line Operation. The cold-line equipment is now available for routine operations. A summary of the month's production data is given in Table I.D.17.

One depleted-uranium ingot containing 2 w/o silicon was prepared for use as a master alloy in the silicon-addition program (for both hot and cold lines). The injection casting of this ingot was unsuccessful: incomplete filling of the Vycor molds occurred, and the Vycor that was in

contact with the metal shattered severely. Whether this is an isolated failure or a result of particular properties of this alloy has not yet been determined. Another ingot is being prepared.

TABLE I.D.17. Production Summary for Cold Line

	11/1/67 through 11/30/67	Total This Year
1. Alloy-preparation Runs		
New Fuel	5	11
Remelts	3	5
Total	8	16
2. Injection-casting Runs	7	13
3. Fuel Pins Processed		
Accepted	536	937
Rejected	12	110
4. Elements Welded	558	859
Rewelded	0	0
5. Elements Leak Tested		
Accepted	554	852
Rejected	4	7
6. Elements Bond Tested		
Accepted	499	706
Rejected	39	106
7. Subassemblies Fabricated	5	8

The redesigned coil-support plate for the injection-casting furnace was examined after about 12 usages. No sign of warping was detected.

The cold-line assembly machine (CLAM) is operational. Two subassemblies were successfully assembled by use of this machine.

A pneumatic straightener has been fabricated to correct any deformations of the element tips that may have occurred during the bonding operation.

The top-loading and -unloading transfer cask was found satisfactory in a leak test and in tests of compatibility with the FCF. Preparations are under way to determine the heat-transfer characteristics of the cask and to carry out test transfers of subassemblies between the FCF and the ICPP. The ICPP has designed and is fabricating the necessary equipment to unload the cask at the water storage basin.

c.   Maintenance and Repair.   The bridge drive motor on the Air Cell crane was replaced. No problems have been encountered with the operation of the crane since this motor was replaced.

d.   Operator Training.   A refresher course on criticality considerations in cold-line operations was given to all personnel assigned to these operations. A lecture-demonstration course on unusual fires, i.e. sodium, alcohol, or metal, was started for all FCF operations personnel.

e.   Operating Manuals and Reports. Five new sections of the FCF Operating Manual were issued as accepted portions of the manual. Five revised sections were approved for issuance.

Revisions of the criticality procedures and rules for handling fissionable material in the FCF were submitted for approval.

f.   Product Analysis

(i)   Chemical Analyses.   The number of fuel-production analyses on cast-pin and ingot samples, together with the average values and range, are given in Table I.D.18.

TABLE I.D.18. Production Fuel

Analyzed for	Number	Average Value	Range
U (total and isotopic)	18	94.06	93.25-95.34
^{235}U		52.19	51.81-52.54
Pu (total and isotopic)	5		
Mo	37	2.45 w/o	2.34-2.76
Ru	32	1.91 w/o	2.75-2.11
Pd	25	0.195 w/o	0.150-0.235
Rh	28	0.292 w/o	0.266-0.394
Zr	35	0.077 w/o	0.028-0.118
Nb	27	0.013 w/o	0.005-0.023
Fe	41	439 ppm	86-1500
Al	9	183 ppm	48-585
Si	25	375 ppm	130-800
C	7	294 ppm	145-580

Total Analyses: 289

In addition to production analyses, top, center, and bottom samples from cast pins made from depleted uranium-5 percent fissium alloy were analyzed to determine homogeneity. The results are in Table I.D.19.

TABLE I.D.19. Average of Four Analyses

Element	Top (w/o ± 1σ)	Center (w/o)	Bottom (w/o)
Mo	2.39 ± 0.08	2.35	2.38
Ru	1.79 ± 0.06	1.78	1.87
Rh	0.280 ± 0.006	0.279	0.278
Pd	0.194 ± 0.006	0.190	0.201
Zr	0.048 ± 0.004	0.050	0.041
Nb	0.020 ± 0.003	0.018	0.015
Fe	88 ppm	88 ppm	92 ppm

No significant variation was observed.

(ii) Postirradiation Analysis of EBR-II Fuel. A total of 309 Mark-IA driver-fuel elements from 9 spent subassemblies representing 21 casting batches of FCF-produced fuel and 5 batches of ANL-Chicago-produced fuel were subjected to postirradiation examinations in the FCF. These examinations were conducted in order to obtain irradiation swelling data for the U-5 w/o Fs alloy on a batch-to-batch basis. Included in the examination procedures were element dimensional surveys, sodium re-bonding, sodium bond and level testing, and gamma spectrometry. Also included in this effort was the examination of U-5 w/o Fs alloy that had been subjected to three irradiation cycles in EBR-II and two reprocessing cycles in FCF. Data from these examinations are now being assembled for analysis and reporting.

The ICPP is continuing the corrosion testing program to determine whether the stainless steel cladding of EBR-II fuel elements which had been exposed to in-reactor sodium would become defective as a result of being stored in a water storage basin. No additional results are available.

The ICPP is carrying out a leach test in which a small piece of declad EBR-II fuel is being exposed to ICPP storage-basin water. The leach rate for cesium-137 after 51 days of exposure to the water is essentially the same as reported (~0.20 μCi/cm^2-day) after 16 days of exposure.

PUBLICATIONS

LIQUID-METAL FAST BREEDER REACTORS-- CIVILIAN

Neutron Spectrum Measurements in ZPR-3, -6, and -9 Using Hydrogen-Recoil Proportional Counters
E. F. Bennett and R. Gold
Trans. Am. Nucl. Soc. 10(2), 577 (Nov 1967)   Abstract

Performance of Mixed Carbide Fuel Rods under Fast-Reactor Conditions
F. L. Brown, L. A. Neimark, B. J. Koprowski, J. H. Kittel, J. E. Ayer, and O. L. Kruger
Trans. Am. Nucl. Soc. 10(2), 473 (Nov 1967)   Abstract

Effect of Reactor Temperatures on Bowing of EBR-II Subassemblies
T. R. Bump
Trans. Am. Nucl. Soc. 10(2), 661-662 (Nov 1967)   Abstract

Effects of Other Power-Plant Parameters on Fuel-Element Lifetime
T. R. Bump
Trans. Am. Nucl. Soc. 10(2), 664 (Nov 1967)   Abstract

Solid-State Drive Circuit Considerations for Paper-Tape Punches
C. E. Cohn
Rev. Sci. Instr. 38, 1662 (Nov 1967)   Note

The Effect of Radial Heat Transfer on the Temperature Distribution in EBR-II Stainless Steel Reflector Subassemblies
R. A. Cushman
Trans. Am. Nucl. Soc. 10(2), 661 (Nov 1967)   Abstract

Neutron Radiography in the EBR-II Fuel Cycle Facility Using an Isotopic Neutron Source
D. C. Cutforth and V. G. Aquino
Trans. Am. Nucl. Soc. 10(2), 442 (Nov 1967)   Abstract

Postirradiation Thermal Properties of a Uranium-Fissium Alloy as a Function of Burnup
R. A. DiNovi
Trans. Am. Nucl. Soc. 10(2), 475 (Nov 1967)   Abstract

Diagnostic Radiochemistry Following the Recent EBR-II Fission-Product Release
E. R. Ebersole and R. Villarreal
Trans. Am. Nucl. Soc. 10(2), 634 (Nov 1967)   Abstract

Experience with Glovebox Inert Atmosphere Control System
    W. F. Holcomb
        Nucl. Eng. Design 6(3), 213-216 (Oct 1967)

Carburization of Type 304 Stainless Steel in Liquid Sodium
    W. F. Holcomb
        Nucl. Eng. Design 6(3), 264-272 (Oct 1967)

On-Line Transfer Function Analysis of EBR-II
    R. W. Hyndman, M. R. Tuck, and F. S. Kirn
        Trans. Am. Nucl. Soc. 10(2), 696 (Nov 1967)   Abstract

A Qualitative Consideration of Nuclear Excursion Initiated by a Shock Wave
    V. Z. Jankus
        Trans. Am. Nucl. Soc. 10(2), 695 (Nov 1967)   Abstract

Analysis of the Die-Away of Prompt Neutrons with Two-Group Time-
Dependent Solution of the Diffusion Equations in Reflected Reactors
    R. A. Karam
        Trans. Am. Nucl. Soc. 10(2), 593 (Nov 1967)   Abstract

Effect of the Stainless Steel Reflector on the Power Coefficient of EBR-II
    F. S. Kirn, J. K. Long, and R. R. Smith
        Trans. Am. Nucl. Soc. 10(2), 648 (Nov 1967)   Abstract

A Magnetic-Signaled Automatic Fuel-Surveillance System
    H. Lawroski, J. E. Hutton, and R. N. Curran
        Trans. Am. Nucl. Soc. 10(2), 639 (Nov 1967)   Abstract

Fabrication of V-Ti-Cr Alloy Fuel Cladding for LMFBR Applications
    R. M. Mayfield and F. J. Karasek
        Trans. Am. Nucl. Soc. 10(2), 475 (Nov 1967)   Abstract

Fast-Neutron Scattering from Tantalum, Rhenium, and Platinum
    A. B. Smith, P. T. Guenther, R. Hayes, and J. F. Whalen
        ANL-7363

The Application of Cover-Gas Monitoring in the Recent EBR-II Fission-
Product Release
    R. R. Smith, C. B. Doe, and F. S. Kirn
        Trans. Am. Nucl. Soc. 10(2), 634 (Nov 1967)   Abstract

Effect of Sodium Exposure on the Mechanical Properties of Potential
Fuel Jacket Alloys at 550-700°C
    F. L. Yaggee and E. R. Gilbert
        Alkali Metal Coolants, Proc. IAEA Symp., Vienna, November 28-
        December 2, 1966. Intern. Atomic Energy Agency, Vienna, 1967,
        pp. 215-229

II. GENERAL REACTOR TECHNOLOGY

A. Applied and Reactor Physics Development--
Research and Development

1. Theoretical Reactor Physics

    a. Cross-section Data Evaluation (C. N. Kelber)

       Last Reported: ANL-7391, p. 119 (Oct 1967).

       Tapes containing most of the revised ENDF/B data have been received from Brookhaven, and the data are being processed in order to yield library tapes for the MC^2 code. This involves checking the tapes for "bookkeeping" type errors with CHECKER, changing from BCD to binary ENDF/B tapes using DAMMET, and producing MC^2 library tapes using ET∅E. In some cases changes were made in the original ENDF/B data, using CRECT in order to obtain compatibility with MC^2 formats. Most of these changes involved inelastic and (n,2n) secondary energy distributions.

       The DAMMET program has been run successfully on the system 360, and test problems are being attempted with the recently compiled 360 version of ET∅E.

    b. Reactor Computations and Code Development (B. J. Toppel)

       Last Reported: ANL-7391, pp. 119-120 (Oct 1967).

       Test problems are now being run on the Phase-1* version of the fuel-cycle package within the current ARC system. The following outline includes all features of the model currently under development. A general calculation system of this type must, of course, be built up by stages. Status of the computer algorithms is highly fluid at the present time so that a precise statement of calculation capability or solution techniques is not possible. When some reasonable stage of development is reached a production code package will be frozen and made available for use. The following represents the current best guess as to the final form of the system.

       The enrichment ratio of freshly charged fuel may be adjusted to obtain a specified static criticality factor in the system without control rods at a given time during the at-power phase of the cycle. Criticality of the system may be maintained by means of space-dependent control adjustment (fuel or poisons) at a given number of time points. Burn time may be adjusted to satisfy burnup conditions in selected discharge batches. The search procedures necessary to achieve these conditions depend on the type of problem defined by the user.

---

*See Progress Reports for May 1966, ANL-7219, pp. 34-35; for December 1966, ANL-7286, p. 43.

The isotope-chain matrix may contain β^-, β^+, and α-decay terms as well as (n,γ), (n,p), (n,α), $(n,2n)$, and (n,f) reactions. Fractional yields of fission products may be dependent upon the fissioning isotope. Isomeric states also may be considered. Isotope decay chains may be computed throughout the external cycle, within the limitations of the real-time accounting scheme. Core fluxes are normalized to a specified total power after each flux recalculation.

The fuel-management scheme permits all the flexibility possible in a real reactor with solid fuel elements. All common movement patterns, such as out-in shuffling and fractional batch or scatter refueling, are included as special cases. The limitations are those imposed by the particular spatial model of the core in zero, one, or two space dimensions. Fractions of a discharged fuel batch may be assigned to any of the multiple reprocessing plants, each of which may have three outputs. For the purpose of simplifying refabrication specifications, one output from each plant is designated as Class 1 (normally high fissile content) and the other as Class 2 (low fissile content). The only requirement of this separation is that the system reactivity be reasonably sensitive to changes in the relative fractions of the two classes in the fresh charge. The third output represents waste and losses.

Each class of output from the several plants may be used for fabrication of one or more fuel charges, or sold, according to a user-defined priority ordering scheme. Makeup fuel may be taken from any number of predefined external feed lines, also according to the given priority ordering. The volume of Class 1 material required for a charge is defined by the enrichment fraction times the total volume; the remainder will be obtained from the Class 2 grouping. Any number of charge batches may be fabricated with different compositions and enrichments.

Two main types of problems are considered. The object of the first type is to find the equilibrium (infinite-time) operating conditions of a recycle system under fixed conditions. Current plans call for only single-step equilibrium problems, i.e., those in which the same fuel-management procedures are carried out after each burn step. The second type of problem, nonequilibrium, is a direct mockup of reactor operation, with the exception that fuel-charge enrichment may be adjusted to meet burnup and reactivity requirements during the at-power phase.

Two capabilities originally scheduled for Phase 1 are not included. The first, the zero-dimensional survey program, will be added when the package is brought to full production status. The interrupt facility cannot be implemented until the general question of storage of data generations in the ARC environment is settled.

The main activity in recent months has been in the area of interaction with the IBM 360/75 software systems, both in learning the systems and in debugging. These problems have been overcome and the debugging of the fuel-cycle system is now proceeding satisfactorily.

Two major portions of the output edit have been defined. The core-performance edit, taken for initial conditions and at the end of each burnup substep, includes the following: region-averaged group fluxes, k_{eff}, atom densities and volume fractions, breeding ratio at the current time and for the last time interval, power-density distributions, and neutron-balance summary. The fuels and economics edit, taken after each burnup substep, includes: burnup as fraction of initial actinides and as megawatt-days per metric ton, mass of each isotope present, and change in mass of each isotope over the substep. The final edit, given at the end of the burn-refuel step, includes summations of the items in the fuels and economics edit over all substeps. Two further edits, namely, input conditions and external cycle edit, are not yet fully defined. Monitor lines concerning problem progress also are not in final form.

2. Nuclear Data--Cross-section Measurements

   a. Burnup Analysis and Fission Yields for Fast Reactors
       (R. P. Larsen)

       (i) Determination of the Absolute Fast-fission Yields of Burnup
            Monitors and Nonfission Nuclear Transformations in a
            Fast Reactor

       Last Reported: ANL-7302, pp. 37-38 (Jan 1966).

       An irradiation is being carried out in EBR-II to provide material for the determination of fast-fission yields of burnup monitors and for the study of nonfission nuclear transformations. The following materials are being irradiated: ^{233}U, ^{235}U, ^{238}U, ^{239}Pu, ^{240}Pu, ^{241}Pu, ^{232}Th, and ^{237}Np. The irradiation began in December 1966 and will terminate when the ^{239}Pu has reached a burnup of 20-25%; at present, the burnup is between 1 and 2%.

       (ii) Absolute Determinations of Fast-fission Yield of Monitors
             for the Calculations of Relative Burnup in Fuels Containing
             Two Fissile Nuclides

       Last Reported: ANL-7302, pp. 37-38 (Jan 1966).

       The irradiation described in Sect. II.A.2.a.(i) above will also provide material for calculations of relative burnup in fuels containing two fissile nuclides.

(iii) Development of Analytical Procedures for Fission-product Burnup Monitors

Last Reported: ANL-7382, pp. 96-98 (Sept 1967).

In the determination of burnup of fast reactor fuels by fission-product analysis, not only must accurate analytical methods be developed, but these methods must be evaluated using actual reactor fuel. In such an evaluation of burnup methods, two questions must be answered:

(1) Is the fission product(s) quantitatively retained in the sample submitted for burnup analysis?

(2) Is there any interference from constituents of the fuel and/or cladding?

A 13% enriched uranium dioxide fuel pin that was irradiated to approximately 6 a/o burnup in MTR is being used to evaluate various burnup methods for applicability to oxide fuels. This fuel pin has also been examined in a separate program on the chemistry of irradiated fuels. The studies* which were performed on a microscale showed drastic migration of cesium, evidence of migration of molybdenum, technetium, ruthenium, and rhodium, and no evidence of migration of the rare earths. These data will be valuable in chosing monitors, e.g., if a nuclide does not migrate it is an excellent candidate for a burnup monitor. However, evidence of migration on a microscale does not preclude the use of a nuclide as a burnup monitor, that is, a cross-sectional cut of a fuel pin could still provide a representative sample even though a considerable amount of radial migration had occurred.

Current studies on the evaluation of molybdenum and total rare earths as burnup monitors is described below; future plans include the evaluation of technetium.

(a) Applicability of Molybdenum as a Burnup Monitor for Uranium Oxide Fuels. An evaluation of molybdenum as a burnup monitor was performed on three sections of the stainless steel-clad, 13% enriched uranium dioxide fuel pin discussed in Sect. II.A.2.a.(iii) above. These sections were 1/8 in. thick and were cut from the top, middle, and bottom portions of the pin.

Molybdenum was determined spectrophotometrically as the thiocyanate complex after separation from other interfering ions by ion exchange and solvent extraction. The uranium content of the samples

---

*Reactor Development Program Progress Reports for May 1967, ANL-7342, pp. 88-91; for June 1967, ANL-7349, pp. 94-95; for August 1967, ANL-7371, pp. 87-88.

was determined by mass-spectrometric isotope-dilution analysis. Burnup
was determined by pre- and postirradiation uranium isotopic analysis.
From the uranium analysis and mass-spectrometric burnup determination,
the number of fissions that took place in each section of fuel was calculated.

The number of fissions that occurred in each section of
fuel was compared with the molybdenum content. These data are presented
in Table II.A.1. The theoretical molybdenum-to-fission ratio (fractional
fission yield) is 0.244. The ratios in the middle and bottom section are in
good agreement with this value; however, the ratio in the top section is
about 20% lower. On the basis of these data, it appears that molybdenum
has migrated out of the top section of the fuel pin.

TABLE II.A.1. Comparison of Total Fissions and
Molybdenum Content of UO_2 Fuel

Sample	Uranium Fissioned (μmole/ml)	Molybdenum (μmole/ml)	Molybdenum-to-Fission Ratio
Top	2.35	0.492	0.209
Middle	1.94	0.470	0.242
Bottom	1.68	0.418	0.249

The validity of this conclusion was further checked in
another experiment. This was done because of the possibility of an error in
the mass-spectrometric burnup analysis. (Mass-spectrometric and autora-
diographic data had shown the starting material to be isotopically inhomo-
geneous.) In this experiment the cerium-144 count rate of each section was
compared with the number of fissions. (Cerium-144 was chosen for this
comparison because no evidence of migration of the rare earths was found
on a microscale.) The cerium-144 count rate was determined using a Ge(Li)
detector system and integrating under the 134-keV photopeak. These results
are shown in Table II.A.2.

TABLE II.A.2. Comparison of Total Fissions and
Cerium-144 Count Rate of UO_2 Fuel

Sample	Uranium Fissioned (μmole/ml)	^{144}Ce Count Rate (counts/min/ml x 10^{-4})	Cerium-to-Fission Ratio (x 10^{-4})
Top	2.35	3.91	1.66
Middle	1.94	3.21	1.66
Bottom	1.68	2.81	1.67

The agreement of the cerium-to-fission ratios, coupled with the molybdenum results, indicates that some of the molybdenum formed in fission has left the top section. This variability in molybdenum content eliminates molybdenum as a monitor for oxide fuels.

(b) <u>Photometric Titration of Total Rare Earths</u>. A method of determining burnup by photometric titration of total rare earths is being developed. The 13% enriched uranium oxide fuel described in Sect. II.A.2.a.(iii) above is being used to pinpoint any difficulties that might be encountered in the application of this method to oxide fuels. Preliminary results have been reported (see Progress Report for Sept 1967, ANL-7382, pp. 96-97), when the possibility of interference by the constituents of stainless steel was discussed. (The stainless steel cladding was dissolved with the fuel.) To determine the extent of interference of stainless steel, an experiment was performed in which solutions containing appropriate amounts of rare earths, iron, chromium, and manganese were put through the separation and titration procedure. Analytical results for the rare earths amounting to 102.2 and 103.3% indicate that the constituents of stainless steel interfere slightly. However, this interference can probably be eliminated in future samples either by dissolving the fuel in nitric acid to minimize the dissolution of the stainless steel cladding or by the removal of the stainless steel constituents by electrolysis at some point in the procedure.

The advantages of using a total rare earth analysis for determining burnup have been discussed.* In order to realize these advantages, yttrium must be separated before the rare earth titration. In the proposed procedure, the separation of yttrium from the rare earths is accomplished by ion exchange in 90% methanol-10% 5$\underline{N}$ nitric acid. In this step, the rare earths are retained on the column and yttrium is eluted. Since early experiments** left no doubt that under the proper conditions this separation was possible, it was decided that relatively little effort should be expended to determine the conditions for optimum separation until the feasibility of the total rare earth analysis had been demonstrated on an irradiated fuel sample. Optimization of the rare earth-yttrium separation is now being undertaken. In optimizing the separation, the criterion that was arbitrarily established was a maximum error of 0.1%.

The separation of yttrium from the heavier rare earths is difficult because the differences in the distribution coefficients are small. (Yttrium and ytterbium have approximately the same distribution coefficient.) Fortunately, europium is the heaviest rare earth with a fission yield large enough so that its loss would be significant in determination of a total rare earth fission product. For uranium fuel, the separation procedure must

---

*Chemical Engineering Division Semiannual Report July-December 1965, ANL-7125, p. 241.
**Chemical Engineering Division Semiannual Report January-June 1966, ANL-7225, p. 229.

remove all but 1% of the yttrium present and not lose more than 30% of the europium. For plutonium fuel, the separation procedure must remove all but 2% of the yttrium and not lose more than 8% of the europium.

Experiments to test this ion-exchange separation showed the following factors to be important: (1) close control of the amount and height of resin in the column, (2) close control of the methanol and nitric acid concentrations in the step where the column is converted to this medium from a dilute nitric acid medium, and (3) reslurrying of the resin after this conversion to insure homogeneity of the column packing.

Using these closely controlled conditions, an experiment was performed to determine the amount of wash solution necessary for optimum separation of yttrium from europium. Known amounts of yttrium and europium were each passed through columns and various fractions of the wash solutions were collected. The yttrium and europium in each fraction were determined by a photometric EDTA titration.

The data indicate that yttrium can be separated from europium well enough so that the criterion of $<0.1\%$ error is met in a total rare earth determination of either uranium or plutonium fuel samples. This separation can be accomplished within the range of 140 to 180 ml of wash solution. In the future the separation of yttrium from the rare earths will be performed using 150 ml of wash solution.

b. Fast-neutron Cross Sections (A. B. Smith)

Last Reported: ANL-7391, pp. 121-125 (Oct 1967).

(i) Fast-neutron Cross Sections

(a) (n, n', γ) Cross Sections of Germanium. The study of the gamma-ray spectrum resulting from the inelastic excitation of states in natural germanium has been completed. The results are correlated with the direct measurement of the inelastically scattered neutrons to obtain a definitive understanding of inelastic neutron scattering from germanium at incident neutron energies of less than 1.5 MeV. These results formed the substance of a paper presented at the November meeting of the American Physical Society and are being formally documented in a journal manuscript now in preparation.

(b) Fast-neutron Scattering from Tantalum, Rhenium, and Platinum. This work has been formally completed with submission of a manuscript to Physical Review for publication. The results well define both elastic and inelastic neutron scattering from these elements in the incident neutron energy range from 0.3 to 1.5 MeV.

(c) <u>Fast-neutron Elastic Scattering from Palladium</u>. In previous work with this element the energy interval from 1.0 to 1.3 MeV for incident neutrons was uncertain due to an unexplained instrumental uncertainty. Remeasurements in this energy region are being processed. When finished the measurements will extend from 0.3 to 1.5 MeV at incident-neutron-energy intervals of 10 keV or less. The measurements have also resulted in a good knowledge of the inelastic excitation of low-lying states in palladium, but more work will be required to determine the contribution from the excitation of high-lying levels.

(d) <u>Measurements of Fission Cross Section in the keV Energy Range</u>. The production of proper ^{235}U fission foils is under way as is the checking of the gas scintillation counter. A program for the calculation of the efficiency of the neutron counter used in the experiment was written for the CDC-3600, and values for the actual size and material of the detector were calculated. Several corrections for the detection efficiency were considered, including corrections due to scattering events in the fission counter and in air.

In addition to the relative fission counter discussed above, work has started on the construction of a precision 4π gas scintillation fission counter. It is the intent to use this device to normalize absolutely the above relative measurements at one or more selected energies of the incident neutrons.

c. <u>Determination of Other Nuclear Constants</u> (A. B. Smith)

(i) <u>The $^{7}Li(p,n)^{7}Be$ Reaction</u>. The $^{7}Li(p,n)^{7}Be$ reaction is a widely used source of fast neutrons in this and other laboratories. Two series of measurements of the angular distribution for the $^{7}Li(p,n)^{7}Be$ reaction have been made for incident proton energies between 1.9 and 2.7 MeV at approximately 20-keV intervals. It is hoped that the results of these measurements will permit more precise determinations of the input capture and fission cross sections at incident energies of less than 100 keV. In the first series a collimator defined the beam of neutrons reaching the detector. An open geometry was used in the second series. Neutrons were detected by means of proton recoils in a hydrogen-filled proportional counter. Most of these data have been processed.

(ii) <u>Cross Sections of $^{7}Li(p,p'\gamma)^{7}Li$ and $^{7}Li(p,n'\gamma)^{7}Be$</u>. Excitation functions for the $^{7}Li(p,p')^{7*}Li$ and $^{7}Li(p,n')^{7*}Be$ reactions leading to the first-excited states of the residual nuclei have been measured from below threshold for the $^{7}Li(p,n')^{7*}Be$ reaction to about 3.2 MeV. The experimental method utilizes a Ge(Li) detector to observe the de-excitation gamma rays. The data have been reduced to absolute cross sections. The results will be particularly useful in the interpretation of inelastic scattering of neutrons.

d.   Nuclear Instrumentation and Digital Techniques (A. B. Smith)

(i) Digital Interfacing. The on-line computer system employed with the fast-neutron laboratory and accelerator is the oldest such operating system in the country. After 6-7 yr of steady operation the failure rate had increased to a point requiring a general overhaul and updating of components. This is at present nearly completed. The downtime in the program was appreciable, but lost time will rapidly be gained back with the increased reliability of the system.

One of the main problems has been the change in available components, particularly transistors, since the initial design and construction; replacements simply were unavailable. With the modification and service all components are of current manufacture, and all modules will be either redundant or have a tested spare available.

(ii) Accelerator Operation. Despite the above downtime, accelerator operation was maintained at a good level by scheduling fission studies in coordination with the Chemistry Division. This work did not demand the digital system. Operational records for the month are:

Manned Time	552 hr
Chemistry Division Time	120 hr
Downtime	43 hr
Percent of Manned Time in Operation	92%

B. Reactor Fuels and Materials Development

1. Behavior of Reactor Materials

a.   Irradiation Behavior of Advanced Ceramic Materials
     (L. C. Michels)

Last Reported: ANL-7391, p. 126 (Oct 1967).

A series of irradiations are in progress on ceramic fuels of interest for FBR's and other high-temperature reactor applications, including UC-20 w/o PuC and US. All materials are jacketed in Nb-1 w/o Zr. They are being irradiated in instrumented, temperature-controlled capsules in MTR. A summary of the irradiations is shown in Table II.B.1.

The ANL-56-12 capsule that was removed from MTR after one cycle on January 31, 1966, was opened in the Alpha-Gamma Hot Cell Facility. This capsule had been irradiated to an estimated burnup of 0.3 a/o (1.0 x 10^{20} fiss/cc). Fuel pins C-73, Z-1, and Z-2 containing UC-20 w/o PuC in

capsule positions 4, 5, and 6, respectively, were found to be intact. In PuC
fuel pin C-42 (capsule position 1), six small circular areas of apparent
reaction were observed. These are believed related to thermocouple weld-
ments made on the jacket before irradiation. Further analysis will be
performed by metallographic examination.

TABLE II.B.1. Status of Ceramic-fuel[a] Irradiations in Progress in MTR

| Capsule No. | Specimen No. | Design Parameters | | Operating Conditions | | |
| | | Fuel Composition (w/o) | Effective Density (%) | Max Cladding Temp (°C) | Estimated Burnup to Date | |
					a/o (U+Pu)	fiss/cc x 10^{-20}[b]
56-11	MV-2	UC-20 PuC	79	470	8.8	23
56-8	MV-3	UC-20 PuC	81	715	9.2	25
56-8	MV-5	UC-20 PuC	80	705	8.9	24
56-11	MV-6	UC-20 PuC	80	480	9.3	24
56-8	S-7	US	80	535	7.5	15
56-8	S-8	US	89	725	9.5	19
56-8	S-9	US	76	750	9.5	18
56-8	S-10	US	91	690	9.5	21
56-11	S-15	US	82	380	6.4	13
56-11	S-16	US	90	510	8.6	19
56-11	S-17	US	88	500	7.2	16
56-11	S-18	US	77	610	9.1	17

[a]All cladding of fuel is Nb-1 w/o Zr alloy of 0.281-in. OD and 0.012-in. thickness.
[b]Based on effective density.

The ANL-56-13 capsule, which was removed from MTR on
September 11, 1967, was opened in the hot cell facility. Fuel pins Z-4,
Z-5, and Z-7, consisting of UC-20 w/o PuC (in capsule positions 4, 5, and
6, respectively) were intact. Fuel pin C-45 consisting of PuC (in capsule
position 1) had failed. This pin also had thermocouple weldments on the
cladding before irradiation. Further analysis awaits metallographic
examination.

b. Structures and Properties of Advanced Fuel Materials

(i) Thermodynamic Studies: Preparation of $(U, Pu)O_2$
Specimens (D. R. Messier)

Last Reported: ANL-7382, p. 110 (Sept 1967).

Work was continued on the fabrication of solid-solution
$(U,Pu)O_2$ specimens of good homogeneity and accurately known composition
for use in equilibration experiments. The results of this work also will
apply to the fabrication of oxide specimens for measurements of mechanical
properties.

Sintering experiments are being made on specimens cold pressed from physically mixed oxide powders. The specimens are sintered for 4 hr at 1500°C under identical heating conditions in hydrogen containing various concentrations of water vapor. The weight loss that accompanies sintering is continuously monitored by thermogravimetric analysis.

The results of a series of experiments on the sintering of uranium, plutonium, and mixed-oxide specimens are summarized in Table II.B.2. The theoretical density used in calculating the percentage densities listed in the table is that for the stoichiometric composition. Although the sintering of either uranium or plutonium oxide alone is unaffected by the sintering atmosphere, the sintering of mixtures appears to be enhanced by the use of an atmosphere that maintains the composition at the stoichiometric value.

TABLE II.B.2. Results of Experiments on the Sintering of
Oxide Specimens at 1540°C in Various Atmospheres

Specimen Type	Number of Runs	Sintering Atmosphere	Oxygen Pressure (atm)	Average Sintered Density (% of theoretical)	Final Oxygen-to-Metal Ratio
$(U_{80\%}Pu_{20\%})O_2$	2	He-6% H_2-H_2O	1.73×10^{-12}	91.8	2.00
	2	H_2-H_2O	6.30×10^{-15}	91.9	1.99
	2	Dry He-6% H_2	$<10^{-15}$	90.4	1.94
	2	Dry H_2	$<10^{-15}$	89.4	1.91
UO_2	1	He-6% H_2-H_2O	1.73×10^{-12}	93.3	2.00[a]
	1	Dry H_2	$<10^{-15}$	93.4	2.00[a]
PuO_2	1	He-6% H_2-H_2O	1.73×10^{-12}	88.3	2.00[a]
	1	Dry H_2	$<10^{-15}$	88.9	1.69[a]

[a]Estimated from weight loss.

Sintered specimens are being examined metallographically to determine the effect of stoichiometry on the degree of solid solution that is obtained. In the near future, electron-microprobe analysis will be used to determine the homogeneity of the distribution of plutonium in specimens sintered in various atmospheres.

(ii) **Properties of Prospective Fuels:** Measurement of Out-of-pile Thermal Conductivity of Nuclear Reactor Fuel (J. B. Moser and O. L. Kruger)

Last Reported: ANL-7382, pp. 101-102 (Sept 1967).

The thermal conductivity of a fuel material must be determined because: (1) its value is needed for calculating the stress developed in an operating fuel rod as a function of thermal resistance and energy

output; (2) a knowledge of the thermal conductivity as a function of temperature permits estimation of the fission-gas release of the fuel and prediction of the temperature coefficient of the reactor core; and (3) a study of heat transfer in a fuel material, with purity, stoichiometry, and density as variables, is required in establishing fabrication standards. In the uranium-plutonium carbide program, preliminary studies have already shown that changes in the content of oxygen and nitrogen as well as variations in metal-to-carbon ratio, affect transport properties. Pore configuration is another fabrication variable that affects transport properties.

The thermal conductivity of well-characterized uranium-plutonium carbides of controlled stoichiometry--UC to pure $PuC_{0.87}$--will be obtained first. Then the effects of the presence of higher carbides and of added oxygen and nitrogen will be assessed. How the concentration, morphology, and distribution of porosity affect the thermal conductivities of a number of selected compositions also will be investigated. The effective heat-transfer characteristics of mixed U-Pu carbide fuel-element mockups, fabricated by standard techniques, will be simulated for study outside the reactor. Temperatures from slightly above room temperature to 2000°C will be covered.
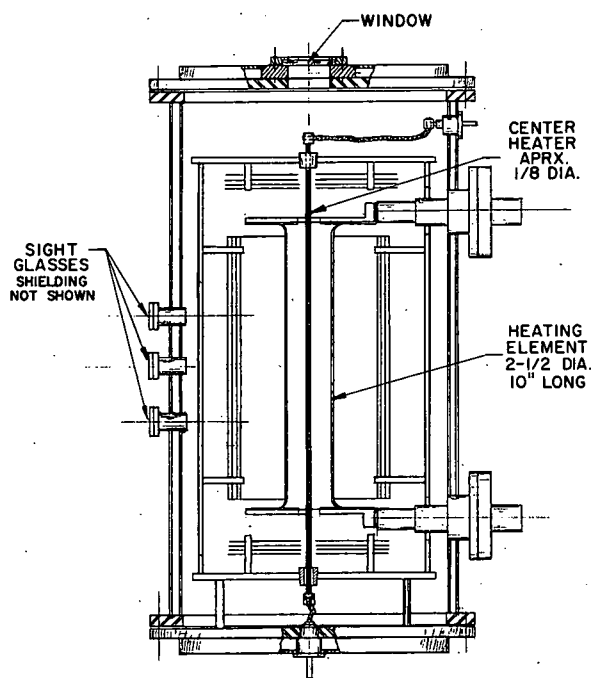
Fig. II.B.1. Radial Heat-flow Thermal-conductivity Apparatus

Both sintered specimens and vibrationally compacted specimens will be studied over a wide range of temperature by means of a radial heat-flow method. Bids on an apparatus for the study have been received. The unit will consist of a modified high-temperature furnace equipped with a tungsten-mesh heating element plus a central heater, as shown in Fig. II.B.1. The portion of the heater inside the cylindrical specimen is tapped to permit the determination of power dissipation in that zone. When the furnace is at the desired temperature, in a vacuum or gaseous atmosphere, a radial temperature gradient is induced in the specimen by the heater. The temperature is monitored near the center and near the surface of the specimen, either optically or by means of thermocouples. The thermal conductivity is calculated from the physical dimensions of the specimen, the power dissipated through it in a radial direction, and the localized temperature. A wide range of temperature gradients can be applied to the specimen. This method lends itself well to the duplication of in-pile conditions.

(iii) Fundamentals of Corrosion in Liquid Metals
(C. A. Youngdahl, S. Greenberg, J. Y. N. Wang,
W. F. McFall, and K. G. Figlik)

Last Reported: ANL-7391, pp. 132-134 (Oct 1967).

(a) Corrosion Inhibition by Dissolved Getters in Liquid-sodium Environment. Oxygen and hydrogen analyses of loop-input sodium indicate an oxygen concentration of 30 ppm by weight (by amalgamation) and a hydrogen content of 3.4 ppm by weight (by deuterium exchange and mass spectrometry).

Analyses of sodium samples withdrawn from the isothermal nickel loop after dissolution of magnesium metal into the loop sodium were made. Dissolution and homogenization had been carried out at 650°C, and sampling was done at 275°C. Wet-chemical analysis for magnesium indicated only about 100 ppm by weight, although an amount intended to produce 1000 ppm by weight had been dissolved. The disparity is being investigated. Possibilities considered are (1) that the sampling temperature was too low, (2) that there is interaction of magnesium with nickel impurity, and (3) that the analysis did not reveal all of the magnesium that was present. An unintended solidification of the melt before sampling, although followed by a homogenization effort, may have contributed to the result. The analysis for nickel indicated less than 12 ppm by weight. Thus, the magnesium does not appear to be strongly associated with nickel in the sodium solution.

A 180-hr exposure of vanadium-alloy coupons to the flowing sodium solution at 650°C has been completed. Visually, the samples appeared little affected by the exposure. However, weight gains of 306 ± 6 $\mu g/cm^2$ were observed for three coupons of V-20 w/o Ti and of 313 ± 5 $\mu g/cm^2$ for three coupons of V-15 w/o Cr-5 w/o Ti. The weight gain of all samples combined was 25.3 mg, an amount comparable with the total weight of 23 mg of oxygen originally found in the sodium. Thus, the samples may have taken up all of the available oxygen in the loop, in spite of the presence of magnesium. Hardened surface layers were revealed by microhardness traverses, the layer thickness being greater for V-15 w/o Cr-5 w/o Ti. Internal-friction analysis of a vanadium wire sample will help to determine whether the weight gains and hardening were due to oxygen.

Further exposure of samples is being postponed until the magnesium interactions discussed above are better understood.

(b) Studies of Corrosion in Lithium at Elevated Temperature. The study of tantalum-silicon interaction in the presence of lithium at temperatures equal to or greater than 1000°C has continued.

Tantalum specimens were embedded in a Li-1.6 a/o Si mixture in a tantalum capsule. Each capsule was then electron-beam sealed in vacuum. Capsules were heated at 1000 ± 25°C. Duration of tests were 96, 384, and 864 hr.

During the course of these tests, a thin tantalum silicide layer was formed on each of the tantalum specimens. The thickness of the layer was determined microscopically. Weight changes were measured with a microbalance. The results are summarized in Table II.B.3.

TABLE II.B.3. Measured and Calculated Data of a Protective Layer Formed in a Li-1.6 a/o Si Solution at 1000°C

| Tantalum Specimen | Test Time (hr) | Weight Increase (mg/cm^2) | Silicide Layer (μ) | | Corresponding Crystal Structure |
			Observed	Calculated	
Ta-37	96	0.177	2.03	1.80	Ta_2Si
Ta-38	384	0.206	1.94	1.85 (2.09)	Ta_5Si_3 (or Ta_2Si)
Ta-39	864	0.195	1.74	1.75 (1.98)	Ta_5Si_3 (or Ta_2Si)

There are four known tantalum silicides reported in the literature:* Ta_2Si, $TaSi_2$, Ta_5Si_3, and $Ta_{4.5}Si$. Theoretical densities were calculated from available X-ray data. The measured weight changes and surface areas of the test samples were successively combined with the value of the X-ray density of each compound to derive the layer thickness that might be expected of a crystalline layer composed entirely of that compound. The actual thicknesses were measured microscopically and compared with the test set of calculated values to identify tentatively the compound present on the specimens. The results are included in Table II.B.3.

Results indicate that Ta_2Si was formed during the first experimental period. The compound Ta_5Si_3 (or possibly Ta_2Si) was formed within the second and third experimental periods. X-ray powder patterns will be examined to verify these results. The calculated and observed curves for layer thickness as a function of time agreed within the limits of experimental error.

The silicon reaction was apparently completed within the first experimental period, but the data were not sufficient to determine

---

*Bartlett, R. W., Trans. AIME 236, 1230-1231 (1966).

the kinetics of layer growth. A higher concentration of silicon will be employed to study the layer-growth effect at 1000°C. Pending procurement of a high-temperature, high-vacuum furnace, plans for experimentation at higher temperatures are postponed.

2. Chemistry of Irradiated Fuel Materials

a. Development of Analytical Facilities, Microstructure-sampling Techniques, and Analytical Procedures for Analysis of Irradiated Fuels (C. E. Crouthamel)

Last Reported: ANL-7391, p. 134 (Oct 1967).

Construction of an analytical facility for the study of irradiated fuels is proceeding approximately on schedule. Concrete block walls have been completed, and pipe fitting is about 75% complete. Painting and electrical work has been started.

A Leitz metallograph (Model MM5 RT), which will be installed in an inert-atmosphere cave facility, has been tested in a glovebox. The tests showed minor leaks in various fittings. The manufacturer has been contacted to obtain information on effectively sealing the leaks.

While the box was open, the drive motors for the stage were replaced with motors containing Stackpole 660 brushes.

Shipment of the MS-7 mass spectrometer, scheduled for the first of November, has been rescheduled for some time in December. A representative of the manufacturer visited Argonne recently to discuss the final testing of the instrument.

(i) Preparation of Fuel Specimens and Sampling. Preparation of irradiated fuel samples for metallographic examination, electron microprobe analysis, microdrilling, laser sampling, or cathodic etching requires that the sample be held in some type of mounting material. The most generally useful material for this purpose is a conductive copper-filled Bakelite. The sample can be molded directly in the Bakelite or it can be cemented with an epoxy resin into a previously prepared Bakelite mount. The latter process is more convenient for remote operation. However, in a dry helium atmosphere, epoxy resins set slowly, and complete hardening requires several weeks. When these resins are heated to 55°C in a helium atmosphere, the initial setting period is shortened, but the final hardening still requires a longer time than is desired. Many catalyzing materials are being investigated to determine if epoxy resins can be cured more rapidly in a helium atmosphere.

Polyester resins, e.g., Vibrin 136A, will harden in a helium atmosphere when heated to about 60°C. These resins shrink on hardening, and the possibility exists that a sample will fall out of the mount. Furthermore, when the resin is filled with copper powder (1:1), it does not become conductive (conduction is necessary if the sample is to be cathodically etched or examined by electron microprobe). Unless a conductive filler that eliminates shrinking can be found, it would appear that the polyester resins will not be suitable for this use.

(ii) <u>Cathodic Etching of Unirradiated Materials</u>. Failure to accomplish etching by ion bombardment of specimens mounted in Bakelite was discussed in the Progress Report for September 1967, ANL-7382, pp. 102-103. Difficulties were attributed to the release of organic vapors from the mounting material. Several types of metallic masks have been unsuccessful in overcoming these difficulties. However, when the mounted sample was covered with a Teflon cap containing a hole to expose the sample, etching took place rapidly. The Teflon cover appeared to have the effect of focusing the ion beam. The area etched could be increased by enlarging the hole or by increasing the argon pressure in the system.

(iii) <u>High-resolution Solid-state Detector System</u>. Frequent breakdowns have been experienced with the multichannel analyzer (Nuclear Data 3300 Series). The manufacturer has agreed to replace the present analyzer with a new unit. Estimated delivery date is January 1968.

The Ge(Li) detector purchased for use with this system does not meet specifications. However, this detector will be used for the present with the possibility of replacement in the future.

These difficulties will delay completion of the multichannel analyzer system for several months.

(iv) <u>Laser Sampling System</u>. Experiments have been performed to determine the depth of craters formed by laser-beam vaporization. Since the thicknesses of some of the fuel specimens analyzed are of the order of 100 μ or less, it is important to establish that the laser beam does not penetrate the specimen completely.

The depths of laser-produced craters have been measured by a calibrated microscope eyepiece; however, this operation is difficult, because of the small diameter of the craters (~30 μ). Another approach has also been tried. A specimen was prepared with two polished perpendicular faces. Craters were then made on one surface, and the surface perpendicular to it was cut away gradually on a polishing wheel; thus, a cross section of the crater was exposed. The depth was measured from a photomicrograph of known magnification.

Specimens of UO_2, cadmium, and manganese have been examined in this manner. The craters made in both cadmium and manganese metal were ~10 μ deep and were approximately segments of a sphere, the predicted shape. Multiple laser shots on the same spot increased the depth but not the diameter of the crater. In the case of UO_2, the shape of the crater was quite different. The upper portions near the surface were similar to those made in cadmium and manganese, that is, more or less spherical. However, from the bottom a narrow hole extended 100 to 120 μ deeper into the body of the specimen. Multiple laser shots on the same spot seemed to increase the size of the opening of the narrow hole slightly although the depth did not seem to be affected.

No explanation can be offered at this time as to why the depth of craters in UO_2 should be ten times the depth of craters made with the same laser output in cadmium and manganese. To date, only a few craters have been examined in this manner.

b. <u>Postirradiation Studies of Reactor Fuels</u> (M. D. Adams)

Last Reported: ANL-7391, pp. 134-135 (Oct 1967).

(i) <u>Electron Microprobe Analysis of Irradiated UO_2-PuO_2 Fuel Pin</u>. A complete transverse cross section of a vibratorily compacted UO_2-20 w/o PuO_2 fuel pin (0.296 in. in diameter) that was irradiated in EBR-II to 2.9 a/o burnup was prepared for analysis in an unshielded electron probe microanalyzer. The cross section was reduced in thickness to 0.001 to 0.003 in. by grinding and polishing. The activity of the sample was 1 R/(hr)(12 in.) gamma and 10 R/(hr)(12 in.) beta-gamma.

Examination of the optical image of the unetched specimen indicated a possible intergranular attack of the 0.021-in. Type 304 stainless steel cladding to a depth of 0.003 in. Sixteen different areas of the fuel-cladding interface were analyzed with the electron probe microanalyzer. Intergranular attack of the cladding was verified, and the mechanism of attack was shown to be interaction with cesium in the fuel. All the analyses showed a depletion of iron and chromium, and an enhancement of nickel in the cladding grain boundaries. Cesium was found in the grain boundaries, associated with chromium on the fuel side of the cladding-fuel interface and unassociated with uranium, plutonium or fission products in voids and fissures near the cladding. Electron microprobe scanning images of one of these areas is shown in Fig. II.B.2. The iron, nickel and chromium X-ray images are biased to show the enhancement of nickel and the depletion of chromium and iron at the grain boundaries. The depletion of iron and chromium in the grain boundaries can be seen in Figs. II.B.2(b) and (c). The enhanced concentration of chromium at the fuel side of the cladding was found in each of the areas analyzed and was always associated with cesium (Fig. II.B.2).
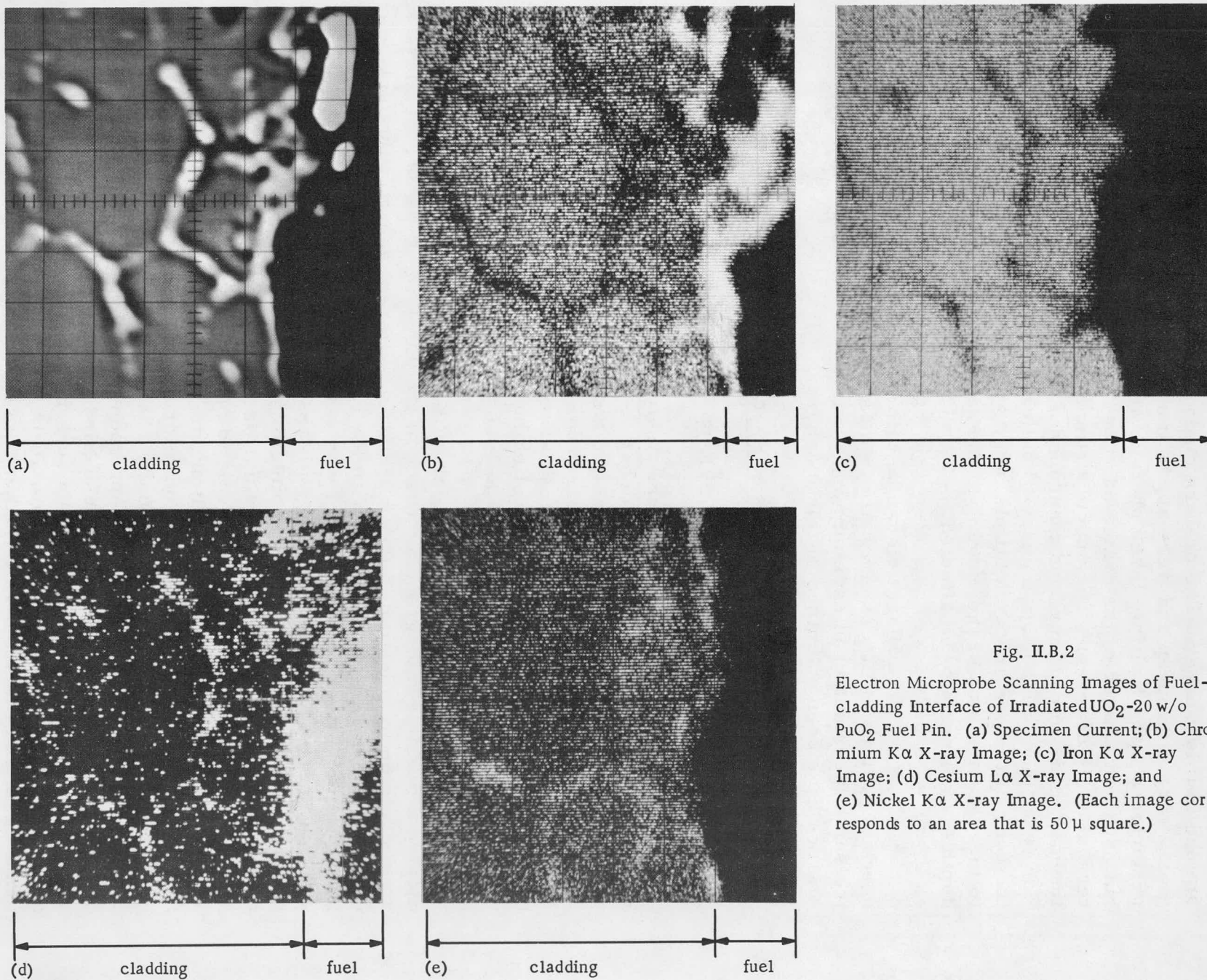
Fig. II.B.2

Electron Microprobe Scanning Images of Fuel-cladding Interface of Irradiated UO$_2$-20 w/o PuO$_2$ Fuel Pin. (a) Specimen Current; (b) Chromium Kα X-ray Image; (c) Iron Kα X-ray Image; (d) Cesium Lα X-ray Image; and (e) Nickel Kα X-ray Image. (Each image corresponds to an area that is 50 μ square.)

Samples of the cladding-fuel interface of 13% enriched UO_2 fuel pins irradiated from 0.7 to 7 a/o burnup in MTR were also analyzed. A description of these pins and results of previous microprobe analyses were given in the Progress Reports for March 1967, ANL-7317, p. 73; May 1967, ANL-7342, pp. 88-91; and June 1967, ANL-7349, pp. 94-95. No interaction between cesium and the Type 304 stainless steel cladding was detectable in any of these samples.

The reason for this difference is not known; however, it should be noted that there was a significant difference in cladding temperatures in the two types of fuel. The inner cladding temperature of the EBR-II fuel was ~580°C, whereas that of the MTR fuel was ~180°C.

3. Techniques of Fabrication and Testing--Basic Fabricability--Research and Development

    a. Development of Nondestructive Testing Techniques (H. Berger)

    Last Reported: ANL-7391, pp. 135-137 (Oct 1967).

    (i) Ultrasonic Measurement of Elastic Moduli. Data are being compiled to determine the elastic moduli of Type 316 stainless steel. The moduli will then be computed and the results compared with the data obtained from the tests on Type 304 stainless steel. Temperatures up to 1300°C are involved in tests of both steels.

    (ii) Transducer Technique Development. The optimum angle for the conical rear face of backing members in ultrasonic transducer probes was determined. Copper and polystyrene specimens were evaluated. The rear-face cone angles for successive probes increased from 0 through 80° in 10° steps. Polaroid photographs of the cathode-ray-tube presentations were taken.

For the copper specimen, a 30° cone angle provided optimum results, i.e., ultrasonic reflections from the rear face were the lowest in amplitude at this angle. Such a condition is desirable in ultrasonic probes when minimum pulse lengths are the main objective. In the polystyrene specimen, a 20° cone angle produced the best results, although good results were also obtained with a 30° angle.

Longitudinal wave velocities in porous metal backings (nickel, Type 304 stainless steel, and tungsten), investigated earlier in this program, are generally between the values for polystyrene and copper. Therefore, in most cases a cone angle of 30° on the rear face of porous metal backings, no matter what density is required for matching purposes, should provide optimum probe performance. A 20° cone angle in low-density tungsten backings with sound velocities near those of polystyrene would provide better probe performance than a 30° angle.

(iii) <u>Neutron Studies</u>. The conical neutron beam obtained from a water moderator surrounding the Am-Cm-Be neutron source has been studied further. A 200-mR/hr gamma intensity at the output end of the 50-cm-long collimator can be improved by the use of lead filters in the beam. A value of 45 mR/hr is obtainable with a lead-filter thickness of 0.63 cm. The gamma radiation is of relatively high energy since the intensity does not change appreciably for lead-filter thicknesses between the previously stated value and 0.1 cm.

Work continues on the track-etch neutron-image detector. Some improvement in contrast capability for this detection method has been observed recently. It is not clear whether this improvement is due to a change in cellulose nitrate material or merely to a greater thickness uniformity of the plastic detecting layer. Further studies are in progress.

The capability of separated gadolinium isotopes for neutron-image detection has been under study. The investigation has involved the oxides of natural gadolinium, ^{155}Gd, and ^{157}Gd. As expected, some differences in speed and resolution have been observed. The ^{157}Gd, the isotope of higher cross section has yielded improvement, both in speed and apparent resolution, over the normal oxide and the ^{155}Gd oxide. Both of the latter materials produce about the same results. The ^{157}Gd doubles the speed. Detailed measurements of resolution are still in progress. An unexpected result is that there appears to be some improvement in contrast capability with radiographs produced with ^{157}Gd. This improvement may result from less gamma-ray interference because of the shorter required exposure time.

(iv) <u>Passive Ultrasonic Techniques</u>. Lithium niobate and tourmaline piezoelectric elements have been received. A system is being assembled for measuring the mechanical Q (a frequence-dependent quality factor) of these elements before probe manufacture.

Type 304 stainless steel housings are being fabricated for the piezoelectric elements. Tubing and face discs for the housings are complete. The face discs will be welded to one end of each tube.

4. <u>Engineering Properties of Reactor Materials--Research and Development</u>

   a. <u>High-temperature Mechanical Properties of Fuel Oxides (G. D. White)</u>

Last Reported: ANL-7391, pp. 138-139 (Oct 1967).

In the evaluation of pellets and particles of $U_{0.8}Pu_{0.2}O_2$, oxygen-to-metal ratios were determined by the oxidation-reduction technique and

the inert-gas-fusion method. All of the particle fractions were heated in vacuum for 4 hr at 1600°C. The pellets were reaction sintered at 1650°C for 4 hr in vacuum, helium, and helium-6% H_2. Table II.B.4 lists the two stoichiometries for each of the specimens.

TABLE II.B.4. Comparison of Stoichiometries for $U_{0.8}Pu_{0.2}O_2$ Specimens

| | Oxygen-to-Metal Ratios | | |
Designation	Oxidation-Reduction	Gas Fusion	Difference
-10 +18 (as received)	1.998	2.018	0.020
1600°C (4 hr in vacuum)			
-10 +18	1.981	2.002	0.021
-20 +30	1.982	2.012	0.030
-35 +50	1.988	2.024	0.036
-50 +325	1.976	2.025	0.049
Pellets			
Vacuum	1.977	1.987	0.010
Helium	1.985	1.997	0.012
Helium-6% H_2	1.972	1.981	0.009

The increasing difference in the two values with decreasing particle size probably reflects a neglect of undetermined adsorbed gas on those powders analyzed by the oxidation-reduction procedure. The results for the pellets agree within a more acceptable margin.

C. Engineering Development

1. Development of Master-Slave Manipulator Systems (R. C. Goertz)

Last Reported: ANL-7391, pp. 140-141 (Oct 1967).

a. Development of Manipulator Systems

(i) Electric Master-Slave Manipulator, Mark E4A. A conceptual design of a filtered-gas-cooling system for the slave arm has been completed. Detail design of test parts is presently underway. This will enable testing of the complete slave arm for various atmospheres.

The concept is based on enclosing the entire upper portion of the manipulator slave body with a sheet metal cover to act as a plenum for the gas and facilitate decontamination procedures. This cover will also enclose the necessary fan and support the filter. Investigation showed little difference in a fan's physical size for cooling with prefiltered (90% efficiency) air or absolute filtered (99.97% efficiency) argon. The cover adds approximately 10 in. to the height of the manipulator body, and the filter will either add 4 in. for absolute filters or be the same as the present body depth with prefiltering. The first tests will be conducted with the prefilter and no fins on the servomotors, with both air and argon as the cooling medium. If results are satisfactory then 95 and 99.97% efficiency filters will be tried. In an argon atmosphere the latter will probably require fins on the motor.

In the past it was assumed for the Model-3 manipulator that fan cooling was a constant source of contamination to the servo drive units. Recently one of the slave units and its bridge were removed from the Chemical Engineering Senior Cave. Background readings of 1.8 R at 2 in. were obtained from the servo drive units, and 9 R at 2 in. from the bridge. This indicates that the fan blows contamination off the servo drive units. However, the reading of 1.8 R still shows the need for filtered cooling to enable servicing servo drives in hoods.

Cyclic testing of the brake system continued. After reaching 800,000 cycles, the test was suspended pending installation of a new and harder pawl; the initial pawl had worn excessively. At 500,000 cycles, the solenoid plunger was modified to accept a pin of larger diameter, since three pins had previously failed. There have been no pin failures since this increase in diameter. Target life is still two million cycles.

(ii) Low-inertia AC Servomotors for Manipulators. More studies have been carried out on alternative cooling methods for the ac motors. The promising methods require a different rotor and stator design.

The same laminations can be used in the new stator configuration. These new designs are about ready for detail design so that the motor can be made and tested.

(iii) <u>Low-inertia DC Motors for Manipulators</u>. Design studies now indicate that the first test motors should have a shell armature of 0.7-in. diameter and be 3-in. long, or of 1-in. diameter and 2-in. long. Each shell armature would require a magnetic air gap of 0.050 in.

The calculations indicate that a manipulator of 100-lb capacity could be built having less than 4 lb reflected rotor mass with the motor losses not exceeding 50 W. In an ac constant-frequency induction motor it is absolutely necessary to have the rotor loss at 407 W (when stalled) and also have $I^2 R$ losses in the stator. The total losses in the ac motor are about 600 W when stalled compared to the 50 W for the dc motor.

2. <u>Instrumentation and Control</u>

 a. <u>Boiling Detector</u> (T. T. Anderson)

Last Reported: ANL-7382, pp. 111-112 (Sept 1967).

To establish specifications for commercial units, acoustic sensors are being designed and fabricated; the first set of acoustic sensors is nearly ready for assembly. For quick tests to determine room-temperature sensitivity, portions of one sensor are being constructed of easily fabricated, rapidly assembled standard materials; the others will be built to perform in a high-temperature environment.

Three types of piezoelectric crystals to be used as sensing elements have been received: (1) X-cut quartz-mounting development, (2) Z-cut lithium niobate for evaluation of its properties as a higher-sensitivity material, and (3) Z-cut tourmaline for investigation of its characteristics at high temperatures. The measured electrical resonance frequencies and capacitances of the crystals agree with published properties, verifying that the crystals are of the correct composition and orientation. Instrumentation is being assembled to measure the resonating characteristics of the crystals. Containers and crystal-backing cylinders are on hand for assembly of the first sensors. After assembly, the sensors will be tested to determine performance of the mounted crystals.

Information has been received about a commercially available hydrophone calibrator; however, the equipment does not include a secondary standard for determining sound-pressure levels.

Measurement of sounds within a reactor is complicated by spatial effects: cavity resonances, dispersion, attenuation, and diffraction. To resolve these effects, measurements are being made of the sound produced by boiling from a heated wire in a water-filled container. A notable recent achievement was the use of a heterodyne frequency analzer to obtain spatial maps of boiling sounds in a 3-ft-dia tank. Two types of measurements were made: (1) the sound spectrum in the frequency range from 0 to 10 kHz as a function of position and (2) for individual resonant frequencies, a continuous scan along a major axis to obtain pressure nodes and antinodes. An unexpected result of these measurements was that, depending on the frequency selected, both nodes and antinodes were found at the boundaries. From the node information, the measured resonance frequencies could be predicted within 10%. The tests will be expanded with a mechanical scanner, presently being installed, to speed data acquisition and improve accuracy. After verification of predictions for different tanks and water levels within the tanks, portions of the internals of the EBR-II reactor vessel will be simulated.

3. Heat Transfer, Fluid Flow, and Mechanics of Materials

   a. High-temperature Boiling Sodium Experiments (J. V. Tokar)

   Last Reported: ANL-7391, p. 141 (Oct 1967).

   (i) Niobium-1% Zirconium Loop. Seven additional runs have been completed in the range from 1595 to 1670°F. The data have not been analyzed, but the superheat required to initiate boiling appears to be increasing with time at constant heat flux, flow rate, and boiler outlet pressure. This indicates that boiling agitation is decreasing the number of gas-filled cavities available to promote nucleation.* The increased superheat is accompanied by increased pressure and flow oscillations during short-term boiling runs (<3 min).

   b. Liquid-metal Heat Exchangers (R. P. Stein)

   Last Reported: ANL-7391, pp. 141-142 (Oct 1967).

   (i) Nonsymmetrical-duct Heat Exchangers. The sodium heat-exchanger loop with the first test section installed has been successfully leaktested with helium. The final electrical connections to the main sodium heaters, loop preheaters, instruments, and electromagnetic pump are nearly complete. Tests of the heating and air-cooling systems, instrumentation calibration, and final checkout of the sodium-filled loop are planned.

---

*Holtz, R. E , The Effect of the Pressure-Temperature History upon Incipient Boiling Superheats in Liquid Metals, ANL-7184 (June 1966).

(ii) <u>Liquid-metal-heated Steam Generators</u>. The loop to be used for experiments on simple simulations of liquid-metal-heated steam generators is being constructed.

c. <u>Liquid-metal-cooled Reactor Channels</u> (R. P. Stein)

Last Reported: ANL-7391, p. 142 (Oct 1967).

An application of the WKBJ method for obtaining asymptotic solutions for eigenvalues and eigenfunctions, as used by Lundberg* for laminar forced-convection heat transfer in annular ducts, has been extended to the case of turbulent flow. This extension is necessary for the evaluation of certain coefficients for use of a new "engineering-type" relationship for predicting convection heat transfer during flux transients (see Progress Report for July 1967, ANL-7357, pp. 116-117).

4. <u>Engineering Mechanics</u>

a. <u>Core Structural Dynamics</u> (M. W. Wambsganss)

Last Reported: ANL-7391, p. 144 (Oct 1967).

Spectral plots of the response and forcing function have been made for a considerable amount of the real-time data. The plots indicate considerable structural-vibration amplitude, which, when included in the rms values, indicate no significant trends. Because the brass rod produced only one-third the motion of the previously used plastic rod, the undesirable structural vibration of the test equipment tended to mask the motion of the rod due to the pressure variation of turbulent flow. As expected, this problem was worse at the low flow rates for which the flow-induced vibration is at lower levels. Efforts are being made to identify the sources of the structural vibrations.

The piping from the pump to the test section exhibits a bending-mode vibration which is a major source of noise on the recorded data. The present data are being re-evaluated with rms levels calculated from only those portions of the power-spectral density plots which can not be shown to be due to structural vibration. When plotted versus flow rate, these data have the same trends and slope as were reported for the plastic rod. When the vibration survey has been completed and all the structural-vibration portions of the data have been eliminated, the magnitudes of the data associated with flow-induced vibration will be reported.

---

*Lundberg, R. E., McCuen, P. A., and Reynolds, W.C., <u>Heat Transfer in Annular Passages. Hydrodynamically Developed Laminar Flow with Arbitrarily Prescribed Wall Temperatures or Heat Fluxes</u>, Int. J. Heat Mass Transfer <u>6</u>, 495 (1963).

The experimental apparatus is being modified to reduce the structural vibration. Although this loop was constructed only for developing instrumentation to record vibration, it has provided useful data with very flexible test items (plastic rods).

D. Chemistry and Chemical Separations

1. Fluoride Volatility Process

At the request of the AEC, the fluoride volatility development program on the reprocessing of light water reactor fuels is being discontinued, and the program is being reoriented toward an evaluation of the potential of the process for application to fast breeder reactor fuels. The work reported below represents, in some instances, work which was done prior to reorientation of the program. Much of this work, however, is applicable to both fast breeder reactor and light water reactor fuels.

a. PuF_6 Chemistry and Purification Procedures (M. J. Steindler)

Last Reported: ANL-7329, pp. 72-73 (April 1967).

Plutonium can be separated from spent nuclear fuel by reaction of PuF_4 with fluorine to form PuF_6, which could be transported from the reaction zone in a gas stream containing fission products (e.g., Sb, Nb, and Ru) that form volatile fluorides. A procedure is needed whereby plutonium can be recovered in the form of a suitable end product (e.g., PuF_4) that is nearly free of fission product elements.

Since previous experimental work has shown that the removal of ruthenium may be the most difficult separation problem (see Progress Report for April 1967, ANL-7329, pp. 72-73), experimental work has continued on testing of procedures to separate mixtures of plutonium fluoride and ruthenium fluorides. This report describes the results of two experiments in which gaseous mixtures of fluorine, PuF_6, and ruthenium fluorides (containing ^{106}Ru tracer) were passed through a bed of granulated LiF in a trap. Lithium fluoride was chosen for these tests because (1) workers at ORNL have reported[*] that PuF_6 reacts with LiF to form a complex from which PuF_6 can be conveniently recovered by treatment of the complex with fluorine, and (2) workers in the USSR have reported[**] that RuF_5 forms a complex with LiF. Conceivably, the stabilities of the two complexes may differ sufficiently at some optimum set of conditions that exposure of a mixture of the fluorides of plutonium and ruthenium to LiF at those conditions

[*] Ferguson, D. E., et al., Chemical Technology Division Annual Progress Report for Period Ending May 1, 1967, ORNL-4145, pp. 78-81.

[**] Prusakov, J. N., et al., Compt. Rend. Congr. Intern. Chim. Ind., Brussels, 1966, 1, 787 (1967).

would result in fixation of a large fraction of the ruthenium component of
the mixture as the solid complex, leaving a large fraction of the plutonium
component in the vapor phase.

In two experiments, similar experimental conditions were used
except for the temperature of the LiF bed and the total volume of fluorine
gas passed through the bed. In the first experiment, a charge of carrier
ruthenium metal, ^{106}Ru tracer, and 92 mg PuF_4 was fluorinated with fluorine,
forming a gas mixture that flowed through a LiF-containing trap; this trap
was kept at 300°C for 9 hr and at 400°C for 1 hr. The results of this experi-
ment were a ruthenium decontamination factor of 2.6 x 10^2 and retention of
1% of the plutonium by the bed. The charge for the second run contained
185 mg PuF_4 along with ^{106}Ru and carrier ruthenium, and the gas mixture
formed by fluorination with fluorine passed through the LiF trap for 7 hr at
300°C. A decontamination factor of 9 x 10^2 and retention of 26% of the plu-
tonium on the bed were observed. The decontamination factors were higher
than any obtained in tests of other procedures, but plutonium holdup on the
bed was also high in the second experiment. Additional experiments are
planned to define better the effects of temperature and total gas flow on the
decontamination factor and plutonium retention.

b. Fission Product Fluoride Chemistry (R. L. Jarry)

Last Reported: ANL-7391, p. 147 (Oct 1967).

(i) Chemistry of Ruthenium. There is evidence that volatile
fluorides of ruthenium other than RuF_5 are present in the gas phase dur-
ing the fluorination steps of the fluid-bed fluoride volatility process. These
compounds may include $RuOF_4$. Therefore, the preparation and further
characterization of $RuOF_4$ are being studied to suggest methods of removing
the compound from the process gas stream.

The reaction of ruthenium metal with a fluorine-oxygen
mixture produces a mixture that appears to consist of ruthenium fluorides
and ruthenium oxyfluoride. Dissolution of the mixture in BrF_3 followed by
distillation of the BrF_3 caused the formation of large crystals that were
separated from the remaining liquid by filtration. A sample of crystals is
being examined by X-ray diffraction techniques; other samples of the
crystals are being analyzed chemically for ruthenium, bromide, and oxygen
content.

c. Neptunium Fluoride Chemistry (L. E. Trevorrow)

Last Reported: ANL-7391, pp. 147-148 (Oct 1967).

The removal of NpF_6 from a gas stream by reaction with par-
ticulate NaF contained in a fixed bed is a potentially attractive method for

separating neptunium from uranium and plutonium. The behavior of NpF_6 in this operation is being studied.

In an earlier experiment (see Progress Report for October 1967, ANL-7391, p. 147) the NpF_6-NaF reaction to form a complex was carried out by circulating 10 v/o NpF_6-90 v/o F_2 over a sample of NaF heated to 250°C. Removal of 99.8% of the neptunium in the complex was accomplished by fluorinating with 100% F_2 at 400°C for 5.6 hr. To determine whether the presence of fluorine during the formation of the complex is a necessary condition for the subsequent removal of neptunium from the complex, samples of the complex were prepared in the presence and absence of fluorine. A gaseous mixture of NpF_6 with either fluorine or nitrogen was circulated over a powdered NaF sample at 250°C. Removal of the neptunium from the NaF by a stream of pure fluorine at 250-500°C was then attempted. The results indicate that neptunium is almost quantitatively removed at 400°C for both procedures: 98.4% was removed when a NpF_6-90 v/o F_2 mixture was used for preparation of the complex, and 99.9% when a mixture of NpF_6-nitrogen was used. Thus, the presence of fluorine during formation of the complex is not a necessary condition for the subsequent recovery of neptunium from the complex. The application of the information obtained in this work to tests of the separation of UF_6-NpF_6 mixtures by reaction with NaF is planned.

d. Engineering Development of Fluid-bed Fluorination Procedures (J. T. Holmes)

Last Reported: ANL-7391, pp. 148-149 (Oct 1967).

A topical report: Engineering Development of Fluid-bed Fluoride Volatility Processes. Part 13, Pilot-plant Studies on Fluorinating Uranium Oxide with Bromine Pentafluoride, John T. Holmes, Lowell B. Koppel, N. Saratchandran, James B. Strand, and D. Ramaswami, ANL-7370, is being prepared that describes work to determine the effects of process variables on the fluorination of U_3O_8 with BrF_5 in an engineering-scale fluid-bed facility.

e. Engineering-scale Development for UO_2-PuO_2 Fuel (N. M. Levitz)

Last Reported: ANL-7391, pp. 149-150 (Oct 1967).

(i) Engineering-scale Alpha Facility. A series of campaign-type fluorination experiments intended to verify the feasibility of producing, transporting, and recovering PuF_6 on an engineering scale is in progress. Data on plutonium fluorination rates, useful for scale-up work, will be provided by these experiments.

The campaigns (see Progress Report for October 1967, ANL-7391, pp. 149-150) consist of twelve fluorination-runs in which a total of 2300 g of PuF_4 are fluorinated.

The equipment used comprises a 3-in.-dia fluorinator, primary and backup filters, and two in-series cold traps where the PuF_6 produced during fluorination is collected. The bulk of the gas stream is recycled by a diaphragm pump, and a bleed stream is exhausted through NaF and activated alumina towers. All of the PuF_6 produced during the campaign is eventually transferred from the cold traps and sorbed on NaF. Analysis of the NaF serves as the chief basis for evaluating the experiments.

Most of the analytical data have now been obtained from the first campaign. The following are the significant results:

      1.   A preliminary material balance shows that more than 97% of the plutonium has been accounted for, a value considered to be within the range we expect (96 to 104%) based on our analysis of the sampling and analytical errors of the experiment.

      2.   The collection efficiency of the cold traps for PuF_6 was about 97%, as determined by measurement of the quantity of plutonium that passed through the cold traps and collected in a backup NaF trap. More complete collection of PuF_6 (>99%) in the cold traps would be desirable on a commercial scale. Lower cold-trap temperatures should give higher recovery; this will require verification at a future time.

      3.   Interim holdup of plutonium on the fluorinator filters and in other major equipment items (cold traps, secondary filter, lines, and valves) was low (as discussed below), and the residues were readily recovered by treatment with fluorine at 300°C.

      a.   Holdup on the filters amounted to only 2% of the plutonium charged. By comparison, the plutonium holdup was proportionately much higher in experiments in which relatively small amounts of plutonium were charged; e.g., in two experiments (Pu-14 and -15) in each of which about 20 g of plutonium were employed, about 15% holdup showed on the filters. Thus, percentage holdup appears to be an inverse function of the amount of plutonium processed. In extrapolation to even larger amounts of plutonium, the problem of interim plutonium holdup on filters is likely to become negligible.

      b.   Plutonium holdup in other equipment components, mainly due to alpha-radiation decomposition of the PuF_6 in the cold traps, represented only 1.5% of the plutonium charged. Thus, recovery of this plutonium would be necessary only at infrequent intervals.

Additional data show that 491.2 g of plutonium transferred in an inert gas stream to a NaF-filled trap was sorbed completely on the first three sections of the six-section trap. Each section contained about 875 g of NaF. The superficial gas velocity through the traps was 4.3 ft/min and the superficial contact time was 56 sec.

2. Compact Pyrochemical Processes

a. Process Chemistry of Molten Salt Systems (I. Johnson)

Last Reported: ANL-7391, p. 151 (Oct 1967).

Studies are being made of the $CaCl_2$-20 m/o CaF_2/Cu-33 w/o Mg-5 w/o Ca system which has been proposed for use in the oxide-reduction step of the current pyrochemical process for fast oxide breeder reactor fuels. In a recent experiment, PuO_2 was added to a salt of this composition, which was then premelted and contacted with the liquid metal at 800°C with an agitation rate of 800 rpm. Analyses of metal samples taken during the experiment indicated that at least 97% of the PuO_2 charged was reduced within one hour.

To gain a fuller understanding of the effects of operating variables on the reduction of UO_2 and PuO_2, the chemical reactions that occur in the molten salt phase are being studied. In the initial experiment, U_3O_8 powder was added incrementally to a 47.5 m/o $CaCl_2$-47.5 m/o $MgCl_2$-5.0 m/o MgF_2 salt mixture contained in a Vycor tube under a helium atmosphere. Each addition of U_3O_8 resulted in an initially rapid reaction that quickly subsided. After the melt had been cooled to room temperature, sampled, and remelted, magnesium metal was added. A reaction was observed at the surface of the molten magnesium, but it also subsided quickly. A second experiment in which $MgUO_4$ was added to a salt mixture of the above composition showed that the reaction of $MgUO_4$ with the salt mixture is slower than that obtained with U_3O_8. The rapidly diminishing reaction rates of all three materials (U_3O_8, Mg, and $MgUO_4$) suggest the formation of a film or layer on these materials which inhibits further reaction. The reactions of U_3O_8 and $MgUO_4$ with $MgCl_2$ that were observed, and changes in the color of the salt that were associated with these reactions, indicate that one of the reaction products from the two reactions may be UO_2Cl_2. Further studies will be made to investigate the nature of the reactions involved in the reduction of UO_2 and PuO_2.

The reactions of U_3O_8, UO_2, and $MgUO_4$ with $MgCl_2$ were investigated briefly by differential thermal analysis. Thermal evidence was obtained for reactions of U_3O_8 with $MgCl_2$ at 568 and 726°C. At the latter temperature chlorine was evolved. There was no thermal evidence for reactions of UO_2 or $MgUO_4$ with $MgCl_2$ at temperatures below the melting point of $MgCl_2$ (~ 717°C).

b.   Process Chemistry of Liquid Metal Systems   (I. Johnson)

Last Reported: ANL-7371, p. 97 (Aug 1967).

The use of mercury as a vehicle for removing metallic uranium precipitates from process vessels has been proposed. Suspensions of finely dispersed uranium-mercury intermetallic compounds can be formed readily, thereby permitting the removal of precipitated uranium from a vessel in a relatively small volume of mercury. A retorting step would be employed to recover the mercury for reuse.

Laboratory studies have shown that solid uranium metal reacts satisfactorily with mercury at 300-350°C, and that the mercury containing dissolved uranium and suspended intermetallic material is readily poured from a processing vessel. A subsequent investigation has shown that this procedure is less satisfactory when it is applied to a bed of precipitated uranium that contains magnesium because of the formation of a solid mercury-magnesium phase. However, this procedure should still prove feasible if the quantity of magnesium is small, or if a larger amount of mercury is used.

c.   Engineering Development   (R. D. Pierce)

Last Reported: ANL-7371, pp. 98-99 (Aug 1967).

In the oxide-reduction step of the current pyrochemical process, large quantities of precipitated uranium accumulate and adhere to the refractory metal crucible. Previous experiments (see Progress Report for December 1966, ANL-7286, pp. 33-34) with precipitated uranium in a Zn-Mg matrix have indicated that a hydriding-dehydriding procedure could be used to disintegrate the precipitate so that it could be removed from the reduction crucible.

However, in the current pyrochemical process the final treatment of the precipitated uranium in the reduction crucible is a wash with magnesium to remove the residual Cu-33 w/o Mg reduction alloy and any soluble fission products that are present. Because the precipitated uranium is expected to be in a magnesium matrix, an experiment was performed in which a U-Mg cake was hydrided and dehydrided at 300°C in an attempt to disintegrate it into small particles. However, the cake remained essentially intact. It is believed that the ductile nature of the magnesium matrix prevented material from breaking up.

Because of the success of earlier experiments with uranium in a Zn-Mg matrix, another experiment was performed in which a residue containing uranium in a Mg-34 w/o Zn matrix was subjected to three hydriding-dehydriding cycles at ~320°C. Most of this material disintegrated into

relatively small particles which were easily poured out of the container, and the remaining material was easily broken apart. Apparently the Mg-Zn alloy is brittle enough that it is rather easily disintegrated by this technique. These results indicate that the addition of zinc to the Mg-U residue in the reduction crucible would facilitate the removal of the residue by the hydriding-dehydriding technique. The magnesium and zinc would be separated from the uranium product by distillation.

d. **Pilot-plant Operations** (R. D. Pierce)

Last Reported: ANL-7391, p. 153 (Oct 1967).

Although the development work on pyrochemical processes in the past has generally been oriented toward batch-processing methods, continuous or semicontinuous processes employing countercurrent extraction columns appear to offer the possibility of higher capacities and more efficient separations which may be advantageous in future processes. Therefore, a conceptual flowsheet incorporating countercurrent extraction columns has been prepared as an alternative to the previous batch-processing flowsheet (see Progress Report for September 1966, ANL-7255, pp. 30-31). The chemical separations in this flowsheet (see Fig. II.D.1) are similar to those used in the batch version of the process. The stream quantities presented on the flowsheet are illustrative only and have not yet been optimized for maximum performance.

The following is a summary of the steps in the new flowsheet. The stainless steel cladding is removed from the spent fuel by dissolution in molten zinc in the decladding step (1). The fuel is reduced by a Cu-33 w/o Mg/salt system at 800°C in the reduction step (2). In this step, the volatile fission products are released, the alkali and alkaline earth fission products distribute to the salt phase, and the reduced uranium precipitates from the Cu-Mg alloy. The uranium is subsequently charged to a salt-transport separation step (3) to remove residual fission products. A Zn-Mg acceptor alloy is shown, but if the plutonium content of the uranium is high, a magnesium-rich acceptor alloy with low uranium solubility and high plutonium solubility would be used for further plutonium recovery. The purified uranium is subsequently recovered by vacuum retorting (4). The decanted Cu-Mg-Pu metal phase from the reduction step is processed at 600°C in a multistage rare earth-extraction column (5), where the rare earths are extracted into a salt containing ~15 m/o $MgCl_2$. The salt is reused after the rare earths are removed through contact with a Bi-Mg alloy in a mixer-settler (6). The Cu-Mg-Pu alloy leaves the rare earth-extraction column and enters a noble metal-separation column (7), where the plutonium is extracted into a salt phase containing 50 or 60 m/o $MgCl_2$ at 600°C. A single-stage mixer-settler (8) is used to remove any copper that may be entrained in the plutonium-bearing salt. The plutonium is then extracted into a Cd-Mg metal phase at 600°C in a small extraction column (9). The solvent Cd-Mg alloy is then separated from the plutonium product by vacuum distillation (10).
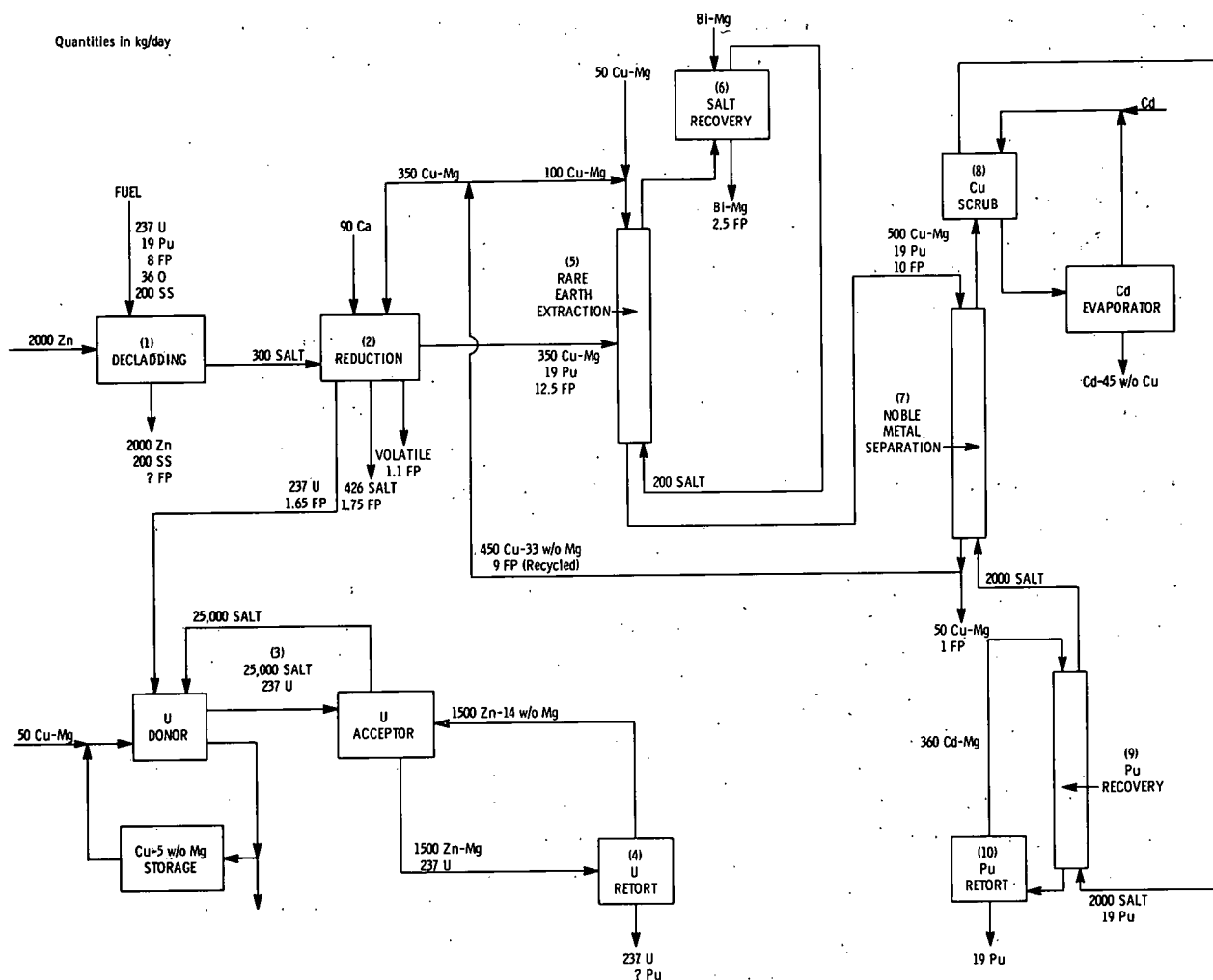
Quantities in kg/day

Fig. II.D.1. Conceptual Pyrochemical Flowsheet

Initial testing of the various steps in this flowsheet will be carried out in the equipment used for the plutonium salt-transport experiment (see Progress Report for May 1967, ANL-7342, pp. 81-82).

3. General Chemistry and Chemical Engineering

a. Characterization of Nitrogen-bearing Species in Sodium Systems (F. A. Cafasso)

Last Reported: ANL-7357, pp. 80-81 (July 1967).

(i) Solubility of Nitrogen in Liquid Sodium. The solubility of nitrogen in liquid sodium is being measured because its magnitude may be important to the understanding and control of nitridation, a corrosion phenomenon known to occur in sodium systems. In addition, there is a possibility that because sodium has no stable nitride, nitrogen will dissolve in it

diatomically rather than monatomically, in contrast to all other liquid metals previously examined. The measurements are being made with the aid of $^{15}N_2$-enriched nitrogen gas.*

To determine whether nitrogen dissolves in sodium atomically or molecularly, nitrogen of known isotopic composition (20.4 m/o $^{15}N_2$, 77.9 m/o $^{14}N_2$, 1.6 m/o $^{14}N^{15}N$, 0.1 m/o impurities) was circulated through 2 liters of sodium at 345°C. Samples of the equilibrated gas were taken intermittently over 96 hr. Mass-spectrometric analysis of these samples revealed that the isotopic composition of the gas after equilibration with sodium had not been altered significantly. If nitrogen had dissolved monatomically and the atoms had recombined randomly on exsolution, a significant change in the isotopic constitution of the starting mixture toward equilibrium (4.5 m/o $^{15}N_2$, 62.1 m/o $^{14}N_2$, 33.4 m/o $^{14}N^{15}N$) would have resulted. Because no such change was found, it was concluded that nitrogen dissolved diatomically and that, within experimental error, isotopic exchange did not occur. Future experiments on the pressure dependence of nitrogen solubility should confirm the manner in which nitrogen dissolves; a linear dependence of the solubility on pressure would indicate that nitrogen dissolves diatomically.

The reliability of the solubility apparatus with respect to the quantitative recovery of $^{15}N_2$-enriched nitrogen was demonstrated earlier. Accordingly, measurements of nitrogen solubility were started. From seven measurements at 500°C and 3-5 atm pressure of nitrogen, the solubility, expressed in terms of the Ostwald coefficient (volume of nitrogen dissolved per unit volume of sodium), was $2.5 \pm 1.5 \times 10^{-7}$.

b. Phase Diagram of the Ternary Oxide System U-Pu-O
(P. E. Blackburn and A. E. Martin)

The objective of this study is to define the phase boundaries of the ternary U-Pu-O system that are most relevant to fast reactor fuels. The compositional limits of the fluorite phase $(U,Pu)O_{2\pm x}$, i.e., the hyperstoichiometric and hypostoichiometric boundaries, extend from the uranium-oxygen side to the plutonium-oxygen side of the ternary phase diagram. However, a literature search has shown that these compositional limits have not been well-established. The establishment of these boundaries at a series of temperatures has been chosen as the initial goal of this study. Other aspects of the ternary diagram will be studied later.

Experimentation will be carried out in a three-module, $1\frac{1}{2}$-tier, stainless steel glovebox, which has been installed. Auxiliary equipment for the glovebox, such as the helium-atmosphere-purification system, is being

*The experimental technique was described in the Progress Report for July 1967, ANL-7357, pp. 80-81.

built. Three furnaces are being placed inside the glovebox. (1) The first and principal furnace is a front-opening, tungsten-mesh, resistance furnace. It is equipped with a quenching attachment, can be operated in vacuum or in an inert atmosphere to 3000°C, and will operate from an existing power supply. (2) The second is an arc furnace patterned after one developed by the Metallurgy Division at Argonne. It has a 4-in.-dia hearth and will be powered by an available transformer unit. (3) The third is a platinum-resistance furnace whose shroud has been lined with water-cooling coils to minimize the heat dissipated to the glovebox atmosphere. It will be equipped with an attachment for quenching samples. This furnace will be used for lengthy, moderate-temperature anneals, and for the preparation of samples for the study of the hyperstoichiometric boundary of the fluorite phase.

To a large degree, the phase-diagram study will depend upon the interpretation of sample structures observed metallographically. A metallographic facility for the preparation and examination of plutonium-bearing samples is available and will be upgraded by the installation of a low-speed, diamond cutoff wheel and two Syntron vibratory polishing machines. Improvements will also be made on the Leitz metallograph to simplify its operation.

c. Development of Some High-temperature Capabilities
(P. E. Blackburn)

Last Reported: ANL-7249, p. 43 (Aug. 1966).

(i) Congruently Vaporizing Composition of Plutonia. The effusion apparatus previously used to determine the congruently vaporizing composition of urania* as a function of temperature is being modified to enable similar studies with plutonia. The apparatus basically consists of an ultrahigh-vacuum furnace chamber and an induction heater. The furnace chamber will be coupled to a glovebox that has been designed and ordered.

The coupling arrangement requires that the flanges on the furnace chamber be opened and closed within the glovebox. In the past, these flanges were sealed with copper gaskets, which necessitated the use of numerous bolts and a high bolt torque to ensure a leak-tight seal. Since such manipulations would be difficult inside the glovebox, other gasket materials were sought. Tests with a small, ultrahigh-vacuum system have shown that both solid polyimide gaskets** (available up to $2\frac{3}{4}$-in. OD) and copper gaskets on which a polyimide coating† was applied (up to 6-in. OD) perfom satisfactorily. Leak-free seals were obtained with one-third as many bolts and with lower bolt torque than required for copper-gasketed

---

* See Progress Report for March 1966, ANL-7193, p. 61, and for August 1966, ANL-7249, p. 43.
** E. I. DuPont de Nemours and Co., Trademark "Vespel."
† E. I. DuPont de Nemours and Co., Trademark "Pyralin."

seals. The level of residual gases was about the same for polyimide and copper gaskets. A 12-in.-OD copper gasket, the largest on the furnace chamber, will be coated with polyimide and tested soon.

The performance of the sputter-ion vacuum pump associated with the effusion apparatus was examined with respect to its capability for pumping helium, the atmosphere planned for the glovebox. Although the pumping speed for helium with this type of pump is stated to be considerably less (~1/10) than for air, repeated evacuations of the helium-filled effusion apparatus easily brought the pressure of the system down to ~10^{-10} Torr. Thus, no difficulty due to pumping is anticipated when the effusion apparatus is coupled to the glovebox.

PUBLICATIONS

GENERAL REACTOR TECHNOLOGY

Solid-Solubility Relationships and Atomic Size in NaCl-Type Uranium Compounds
    Y. Baskin
        Trans. AIME 239, 1708-1712 (1967)

The EBWR Plutonium Demonstration Experiment
    F. G. Dawson,* P. H. Kier, S. Goldsmith,* and R. C. Liikala*
        Trans. Am. Nucl. Soc. 10(2), 500 (Nov 1967)   Abstract

Stress and Strain Considerations for Composite Rod Drawing
    J. E. Flinn and J. J. Rechtien
        Nucl. Eng. Design 6(3), 217-222 (Oct 1967)

Fast Neutron Scattering from Germanium
    D. B. Lister and A. B. Smith
        Bull. Am. Phys. Soc. 12, 1042 (Nov 1967)   Abstract

Sum Rule for Resonance Reactions
    P. A. Moldauer
        Phys. Rev. Letters 19, 1047-1048 (Oct. 30, 1967)

Programs for Analysis of Scattering Angular Distributions
    E. M. Pennington, J. C. Gajniak, and R. A. Mewaldt
        ANL-7306

A New Method for Measuring Strain Distribution
    E. M. Philofsky** and J. E. Flinn
        Proc. 2nd Intern. Congr. for Stereology, Chicago, April 8-13, 1967,
        Ed. Hans Elias, Springer-Verlag, New York, 1967, pp. 110-111

---

* Battelle-Northwest Laboratory.
** Northwestern University.

III. ADVANCED SYSTEMS RESEARCH AND DEVELOPMENT

A. Argonne Advanced Research Reactor-- Research and Development

1. Fuel and Core Development

a. Core Structure Development (W. J. Kann)

Last Reported: ANL-7391, p. 162 (Oct 1967).

(i) Permanent Reflector. The reflector block was pressed and sintered by Brush Beryllium Co. Preliminary checks indicated an average density of 1.85 gm/cm^3. After the block was machined and inspected ultrasonically, it was prepared for machining to a $52\frac{1}{4}$-in. diameter.

An estimate was received and approved for three revisions: (1) the boring of the vertical facility holes, (2) the leaving of excess stock on the outside diameter of the block until the final machining stages, and (3) the purchase of one of the cores from the large vertical facility holes.

The secondary machining has been delayed for resolution of questions concerning coolant-hole size and changes in the beam-tube sizes. After study of the effects on heat transfer, physics, and safety, it was decided to bore 3/16-in. coolant holes, rather than 1/8-in. holes. The larger holes improve cooling, and thus safety, and also cost less to bore than 1/8-in. holes through the 24-in.-thick beryllium.

(ii) Beam-tube-liner Seal Test. Component fabrication for the test fixture was completed and the liner was shrunk-fit to the test-chamber tube. The approximate differential of 0.027 in. was obtained on the liner at about -280°F and on the tube at room temperature. The liner remained loose for ~3 min, which allowed adequate time for adjustment. The final room-temperature interference fit is about 0.003 in. A test procedure has been written.

(iii) Vertical-experiment-facilities Liner Seal Test. Drawings of the test fixture were completed, checked, and approved. Fabrication of the test unit can proceed.

(iv) Stress Analysis. Three drawings from Franklin Institute Research Laboratories indicate the desired temperature-location points for the thermal-stress analysis of the beam-tube adapters. These drawings and dimensions are being reviewed.

b.   Heat-transfer Analysis (R. R. Rohde)

Last Reported: ANL-7382, pp. 126-129 (Sept 1967).

(i)   Analysis of Hydraulic Rabbits. Development of the computer code TRANTEMP, which will be used for heat-transfer analysis of the AARR hydraulic rabbit system (see Sect. III.A.2), has been completed except for overall debugging operations and minor additions and modifications. Code debugging and preliminary analysis of hydraulic rabbits will be done concurrently.

(ii)   Analysis of Core Structures. A heat-transfer and fluid-flow analysis of the beryllium reflector has been under study (see Progress Report for September 1967, ANL-7382, pp. 127-128) to show that the reflector meets design and safety criteria. The results of the analysis reflect corrections in the calculational models used; thus they more realistically estimate beryllium temperatures and heat fluxes. The amount of protection against burnout during normal operation has been determined.

The revision of the calculational models combines the removable beryllium into one model, and the semipermanent and permanent beryllium into another. This separation of the models was chosen because of the complete 0.065-in. annular gap separating the removable beryllium from the other two beryllium regions. Each model assumes a 0.005-in. water gap between the interfaces of the various pieces. Because the various beryllium pieces are carefully machined and tightly clamped, the assumption of 0.005 in. for the gap is conservative.

The steady-state results presented here are based on the AARR heating rates (see Progress Report for May 1967, ANL-7342, p. 105, Fig. 31). For the 115-MW design-overpower condition, the approximate temperatures were calculated at the center of each node for the case in which there is 0.005 in. of water between the beryllium pieces and also between the beryllium and the aluminum liner. These calculated temperature distributions are adequate for determining the thermal stresses in all the beryllium. However, the temperature levels are considered low because a reference fluid temperature of 120°F was used and the axial heat flux distribution was not specified.

Table III.A.I shows the average heat fluxes at 100 MW. The coolant slots located at the interface of the inner and center removable beryllium receive an axial average heat flux of 2.32 x 10^5 Btu/hr-ft^2 at 100 MW. The highest heat flux is 2.97 x 10^5 Btu/hr-ft^2 in the 1/8-in.-dia hole located at a 14.104-in. radius. In general, the heat fluxes are fairly uniform across most of the semipermanent and permanent beryllium.

TABLE III.A.I. Summary of Heat-transfer Conditions in Beryllium
Reflector at 100-MW Reactor Power[a]

Node	Location	Average Axial Heat Flux (Btu/hr-ft^2)	Water Temp Rise (°F)	Outlet Water Temp (°F)	Flow Instability Heat Flux / Operating Heat Flux
5-1	Aluminum liner	8.9×10^4	38.5	160	5.8
25-29 30-29 33-29	Inner-center removable beryllium	2.32×10^5	61.7	183	3.6
52-56 55-56 60-56	Center-outer removable beryllium	1.53×10^5	40.7	162	5.5
69-73 74-73	Outer removable beryllium	9.4×10^4	25.0	146	9.0
76 11-1	Outer removable beryllium Semipermanent beryllium	9.4×10^4	28.3 (56.6)[b]	149 (178)[b]	7.9 (4.1)[b]
51	Semipermanent beryllium	2.41×10^5	55.5	177	4.0
90	Permanent beryllium	2.97×10^5	68.4	189	3.3
111	Permanent beryllium	2.78×10^5	64.0	185	3.5
150	Permanent beryllium	2.66×10^5	61.2	182	3.6
171	Permanent beryllium	2.51×10^5	57.7	179	3.9
210	Permanent beryllium	2.38×10^5	54.8	176	4.1
231	Permanent beryllium	2.23×10^5	51.4	172	4.4
270	Permanent beryllium	2.18×10^5	50.2	171	4.5
291	Permanent beryllium	5.6×10^3	-	121	-

[a]Core power = 100 MW; water inlet temperature = 121°F; core inlet pressure = 600 psia;
core outlet pressure = 490 psia; uncertainty factor = 1.31.
[b]Parentheses denote effect of eccentric location of removable beryllium which reduces the
coolant gap from 0.065 to 0.020 in.

The average heat-flux value in Table III.A.1 is multiplied
by the heat-transfer area to determine the total heat delivered to the cool-
ant channel. This has a direct bearing on the estimation of burnout con-
ditions.* Burnout due to flow instability is estimated by comparing the

---

*Forgan, R., and Whittle, R. H., Pressure-drop Characteristics for the Flow of Subcooled Water at
Atmospheric Pressure in Narrow Heated Channels, Parts I and II, AERE—M-1379 (1966).

total heat added to the coolant to the heat necessary to reach saturated steam conditions at the channel exit. For practical sizes of reflector channels, diameters of approximately 1/8 to 3/16 in., burnout is estimated to occur when the ratio of the temperature rise of the coolant, ΔT_c, to the temperature rise required to reach saturated steam at the channel exit, $T_{sat} - T_{inlet}$, equals a certain value; for the AARR reflector this is $\Delta T_c/(T_{sat} - T_{inlet}) = 0.856$. Table III.A.1 shows that the ratio of burnout heat flux to operating heat flux (or burnout power to operating power) is very high, ranging from 3.3 to 9, at normal full-power operating conditions.

The steady-state analysis for 115 MW with 1/8-in.-dia holes shows that the design is adequate provided all system parameters are normal.

(iii) <u>Transient Heat-transfer Tests</u>. Shakedown and steady-state testing of the third test section were completed. When the transient power runs were started, unforeseen problems occurred which were caused by a recent thunderstorm during which lightning damaged the system.

During the storm, water leaked into the switchgear cabinet. Although the cabinet was allowed to dry out before the first power-pulse tests, when power was supplied to the test section, a power surge ruptured the tube. The location and appearance of the rupture indicated that there was insufficient cooling for the power being generated. It was tentatively hypothesized that a tube shift during the initial power transient had caused a flow reduction.

The fourth test section was assembled, tested, and installed. When power was supplied, this test section also was destroyed. This time, however, a high-speed recording of power, flow, pressure, and temperature had been made before and during tube destruction. Data analysis indicated only slight flow reduction, but input power was ~300 kW, four times the normal 75 kW. The trouble was traced to the line side of the switchgear, where a blown fuse had caused a loss of power control. It was concluded that lightning had blown the fuse. The fuse was replaced and low-voltage relays were installed to prevent recurrence of this problem.

The fifth test section was assembled, tested, and installed. After adiabatic tests, a series of steady-state tests was made to measure heat loss and flow characteristics with net power input. The voltage error due to the impressed voltage was evaluated by reversing the terminals (and thus the impressed voltage gradient) while operating the loop at similar flow and power conditions. This method was used because of the unsatisfactory results obtained with the third section (which used symmetrically located wall thermocouples, one insulated from the test section and one attached to the section, to evaluate the error).

The resulting corrected outer-wall temperatures were determined to be unaccountably high. This fact and the anomalous behavior of the adiabatic pressure drop indicated a deposit of some material inside the test section. When the test section was removed, a black crystalline cupric oxide deposit was found on the test-section walls. Methods are being sought for removing the cupric oxide and preventing its formation in future tests.

2. Component Development

    a. Sample-irradiation Devices (J. J. Dickson)

Last Reported: ANL-7382, p. 131 (Sept 1967).

(i) Rabbit Facilities. The preconstruction safety review has been completed. Components required for testing the prototype hydraulic rabbit are being fabricated. Design of the prototype rabbit-transport system is complete and ready for safety review.

Revisions to the vertical irradiation-facility mockup are about 75% complete. These revisions reflect the new thickness of the reactor vessel head and vessel-head to core-centerline dimensions. The existing designs for the hydraulic rabbit tube and handling tools for the static irradiation facility will be retested and modified if required.

Static leaktesting of the gas blowers for the rabbit and blower pressure vessel assembly has been completed. The blowers and vessel shaft seals are being fitted to the vessel assembly in preparation for operational tests.

Preliminary design of the reactor vessel instrument thimbles is 79% complete.

(ii) Rabbit and Sample. Reference designs have been completed for the sample carrier and a "typical" sample. Their characteristics and material properties will be used in all heat-transfer analyses of the hydraulic rabbit facilities (see Sect. III.A.1.b).

Seven sample carriers of the type shown in Fig. III.A.1 will be in each hydraulic rabbit facility during operation; the carriers will be made of Type-6061T6 aluminum. A carrier will accommodate one of three kinds of samples:

1. A target material interspersed in an aluminum matrix filler which will fill the core volume of the sample carrier and which will be compacted to approximately 80% of theoretical density.

2.   A sealed aluminum capsule containing a target-aluminum matrix compact; this capsule will be slipfitted into the sample carrier with a radial gap of 0.0005-0.002 in. and an axial gap of approximately 0.003 in.; these gaps will be filled with air or helium, or will be evacuated.

3.   A foil of target material, either bare or sealed in an aluminum envelope; this foil will be sandwiched between aluminum plugs within the sample carrier.
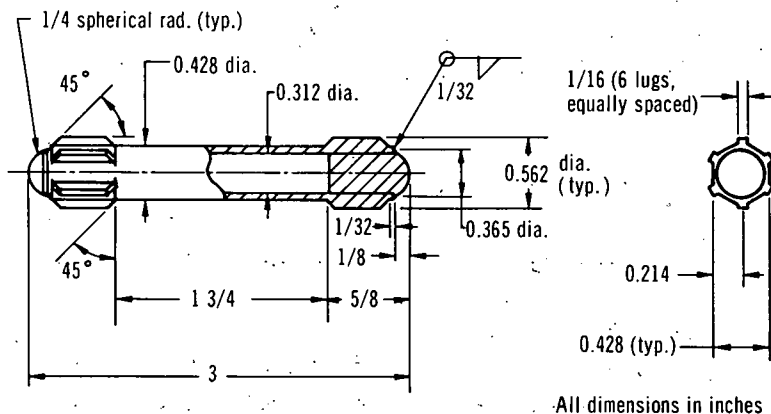

Fig. III.A.1

Hydraulic-rabbit Sample Carrier for AARR

All dimensions in inches

The sample carrier will be machined from aluminum stock rather than being extruded (in operations at HFIR, target rods have failed at the base of the extruded fins, which is a point of high stress concentration). After the sample carrier is filled, spherical end caps will be welded on.

_ This sample-carrier design was tested in the hydraulic-rabbit-facility test loop, where it exhibited dynamic stability in transfer, transport, and irradiation modes of facility operation. The carrier shows no signs of wear or abuse from repeated cycling of facility operations.

An evaluation of experimental samples for irradiation in hydraulic rabbit facilities produced the following information:

1.   Amounts of target material will be quite small, characteristically milligram or submilligram quantities.

2.   Although some heavy-element targets, e.g., fermium-254, have relatively large fission cross sections, the sample-carrier material will dominate the total heat generation because the quantity of the isotope will be very small.

3.   The use of AARR for irradiation of production-type targets similar to the ones in HFIR is very improbable and would, in any case, be accomplished in a static irradiation facility.

An estimate of the worst "typical" sample heat problem might be approximated by assuming a fissioning isotope interspersed in an aluminum matrix core which has a thermal conductivity of approximately 30 Btu/hr-ft-°F. In a flux of 5×10^{15} n/cm²/sec, heat generation in the target material can be conservatively assumed to be 150 W/cm³ of carrier core volume, or approximately 330 W. This does not include the heating due to the aluminum matrix in the core volume. For design evaluation, these values will be used in a computer program that will calculate temperature profiles in the facility. The program will be revised to evaluate: (1) the effects that positioning the sample eccentrically within the facility tube will have on facility temperature profiles and (2) the temperature profile of a sample carrier containing a sealed inner capsule with both radial and axial gaps.

b. Beam Tubes (A. R. Jamrog)

Last Reported: ANL-7391, p. 162 (Oct 1967).

(i) Beam-tube Test Facility. Assembly of the test facility is about 60% complete. Piping, fittings, and valves for connecting the facility to the general-purpose hydraulic loop have been received; about 40% of the piping lines have been fit and welded.

(ii) Handling Tool for Through-beam-tube Connector. To assemble the through beam tube within the AARR, its connector must be inserted, sealed, and locked well within the beam-tube adapter. This requires a long reach inward from the face of the biological shield. A handling tool has been designed and fabricated; tests will demonstrate its capabilities for inserting seating (seal), locking, and replacing the prototype through-beam-tube connector in the beam-tube test facility.

(iii) Metal-seal Test. Since the previously reported metal-seal tests (see Progress Report for September 1967, ANL-7382, p. 132) a Haskel "K" (Type-321 stainless steel, silver-plated) gasket has been received and tested. After the gasket and spacer were inserted in the test flanges, the flange bolts were torqued to 500 ft-lb, and the facility was pressurized with helium to 1100 psig and isolated. After 24 hr no leakage was detected. Then the facility was depressurized and disassembled, and the gaskets and flange-sealing faces were inspected.

The same gasket and spacer were reinstalled in the test flanges, and the flange bolts were tightened and torqued to 500 ft-lb. The facility was pressurized with helium to 1100 psig and isolated for 4 hr; no leakage was detected. The facility was then depressurized and repressurized to the same conditions three more times, with no leakage detected. Since then, the facility has been pressurized to 1100 psig and isolated with the same gasket; no appreciable pressure loss has been observed in 4 weeks.

c. Internal Thermal Column (J. J. Dickson)

Last Reported: ANL-7382, p. 137 (Sept 1967).

Detailed shop drawings for the ITC valve-head assembly have been completed and preconstruction safety review is underway. Detail work on the core-assembly drawings has started.

3. Instrumentation and Control (J. H. Tessier)

Last Reported: ANL-7391, pp. 162-165 (Oct. 1967).

a. Dynamics Analysis. The dynamics analysis includes studies of the loss-of-coolant accident and transient stress analysis.

(i) Loss-of-coolant Accident. A preliminary survey has been completed of the computer codes having possible use in loss-of-coolant accident analyses. The codes examined include: SATAN,[*] LOCO,[*] LOCTA-R,[*] FLASH,[**] FLASH-2,[†] RIP,[††] TACT-V,[††] BURST-I,[‡] RELAPSE-I,[‡‡] NURLOC-I,[§] and CHEMLOC-II.[§§] The tentative decision is to use either the FLASH or FLASH-2 code for coolant blowdown studies because of their availability and applicability to the AARR system. NURLOC-I and CHEMLOC-II could also be used in conjunction with the FLASH codes for detailed study of core heat-up and potential metal-water reactions.

The FLASH code was brought to operational status on the CDC-3600 computer by successfully running the sample problem supplied with the code. Attempts were made to calculate coolant blowdown for a system representative of the AARR, but difficulties were encountered; these are attributed to discrepancies in the tables of water properties stored in the FLASH code. The tables have been revised, and a series of new calculations is in progress.

---

[*]Indian Point Nuclear Generating Unit No. 2, Preliminary Safety Analysis Report, 1965, NP-16181, Exh. B, Vol. 1 and 2 (A and B).

[**]Margolis, S. G., and Redfield, J. A., FLASH, A Program for Digital Simulation of the Loss of Coolant Accident, WAPD-TM-534 (May 1966).

[†]Redfield, J. A. Murphy, J. H., and Davis, V. C., FLASH-2, A Fortran IV Digital Simulation of a Multinode Reactor Plant During Loss of Coolant, WAPD-TM-666 (April 1967).

[††]Dresden Nuclear Power Station, Unit 3, Plant Design and Analysis Report, USAEC Docket-50-249, Vol. I (1966).

[‡]Quarterly Technical Reports, Step Project, July--December 1965, IDO-17165 and -17167.

[††]Gruen, G. E., and Moore, K. V., Rod-ejection Analysis Using the RELAPSE IBM-7040 Code, Trans. Am. Nucl. Soc. $\underline{9}$(1), 307-308 (June 1966).

[§]Walters, C. T., and Genco, J. M., A Digital Computer Program for Thermal Analysis of a Nuclear Reactor Loss-of-coolant Accident, BMI-1807, July 1967.

[§§]Calculation of the Extent of Metal-Water Reaction, Core Heating, and Core Motion during a Loss-of-coolant Accident (CHEMLOC-I Program), Progress Report for May 1967, ANL-7342, pp. 117-126.

(ii) <u>Transient Stress Analysis</u>. A study of the AARR involute fuel plate under constant transverse pressure load was continued.* The analysis is based on the thin-shell small-deflection theory, which involves the Kirchhoff assumption that normals to the middle surface of the shell remain straight and normal after deformation. An additional assumption in the analysis is that the membrane force N_θ in the shell is small in comparison with its critical value (the value at which the shell may buckle laterally).

For a two-dimensional shell with the above assumptions, Timoshenko and Woinowski-Krieger* give the equations of equilibrium; reduced to one dimension, these become

$$Q_\theta = \frac{dN_\theta}{d\theta}; \tag{1}$$

$$\frac{dQ_\theta}{d\theta} + N_\theta = -pa\theta; \tag{2}$$

and

$$\frac{dM_\theta}{d\theta} = a\theta Q_\theta. \tag{3}$$

Figure III.A.2 shows the symbols used in these equations; "a" is the generating radius of the involute. Substitution of Eq. 1 into Eq. 2 yields an expression involving only N_θ:

$$\frac{d^2N_\theta}{d\theta^2} + N_\theta = -ap\theta. \tag{4}$$

Equation 4 has a standard solution resulting in an explicit expression for N_θ involving two constants of integration. Thus expressions for Q_θ and M_θ can be determined using Eqs. 1 and 3, respectively.
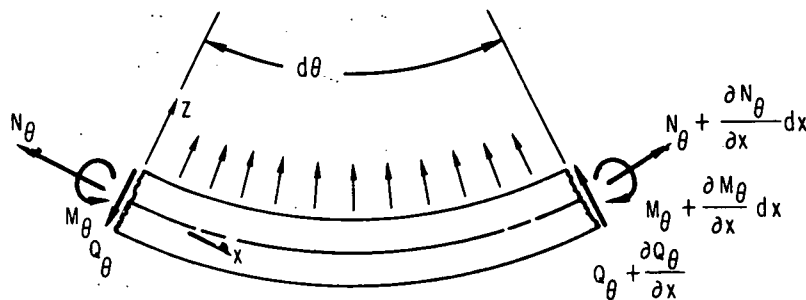

Fig. III.A.2
Differential Element of the Shell

---

*Timoshenko, S., and Woinowski-Krieger, S., <u>Theory of Plates and Shells</u>, Second Edition, McGraw-Hill Book Co., Inc., New York (1959).

Relationships are also available that express N_θ and M_θ in terms of displacements of u and w in the direction tangent and normal to the neutral surface, respectively. Adjusted for an involute shell, these are

$$N_\theta = \frac{12D}{ah^2\theta}\left[\frac{du}{d\theta} - w\right] \tag{5}$$

and

$$M_\theta = -\frac{D}{a^2\theta^2}\left[\frac{du}{d\theta} + \frac{d^2w}{d\theta^2}\right]. \tag{6}$$

Solution of Eq. 5 for $\frac{du}{d\theta}$ and substitution into Eq. 6 yields

$$\frac{d^2w}{d\theta^2} + w = -\frac{a^2\theta^2}{D}M_\theta - \frac{ah^2\theta}{12D}N_\theta, \tag{7}$$

which has the same form as Eq. 4 except for the right-hand side. Thus, w can be obtained in a manner similar to that used to obtain N_θ. This particular solution involves the previously incorporated constants of integration which appear in the expressions for N_θ and M_θ. When the solution for w is obtained, u can then be derived from either Eq. 5 or 6.

By the foregoing process, complete one-dimensional solutions for the involute plate are obtained that provide explicit expressions for N_θ, Q_θ, M_θ, w, and u in terms of six constants of integration. These constants are then evaluated by assigning boundary conditions appropriate for the particular problem to be investigated. Three boundary conditions must be prescribed for each end of the involute plate.

Three problems were solved using the above equations involving pinned, fixed, and what may be regarded as "rotated" supports. The corresponding conditions are represented mathematically as

$$w\bigg|_{\theta=0} = u\bigg|_{\theta=0} = M_\theta\bigg|_{\theta=0} = w\bigg|_{\theta=\theta_b} = u\bigg|_{\theta=\theta_b} = M_\theta\bigg|_{\theta=\theta_b} = 0, \tag{8}$$

$$w\bigg|_{\theta=0} = u\bigg|_{\theta=0} = \frac{dw}{d\theta}\bigg|_{\theta=0} = w\bigg|_{\theta=\theta_b} = u\bigg|_{\theta=\theta_b} = \frac{dw}{d\theta}\bigg|_{\theta=\theta_b} = 0, \tag{9}$$

and

$$w\bigg|_{\theta=0} = u\bigg|_{\theta=0} = \frac{dw}{d\theta}\bigg|_{\theta=0} = u\bigg|_{\theta=\theta_b} - \theta_b w\bigg|_{\theta=\theta_b} = \frac{dw}{d\theta}\bigg|_{\theta=\theta_b}$$

$$= Q_\theta\bigg|_{\theta=\theta_b} - \theta_b N_\theta\bigg|_{\theta=\theta_b} = 0, \tag{10}$$

where θ_b designates the outer boundary of the plate. The last boundary condition pertains to a physical situation for which the inner edge of the involute plate is assumed to be fixed, and the outer edge also fixed but allowed to move along a circular arc. This condition corresponds to a case in which the outside support cylinder of the fuel plates is permitted to rotate without restraint.

Corresponding qualitative deformation for the three above conditions are shown in Fig. III.A.3. Under a constant pressure, deflection may vary between positive and negative values with position along the plate.
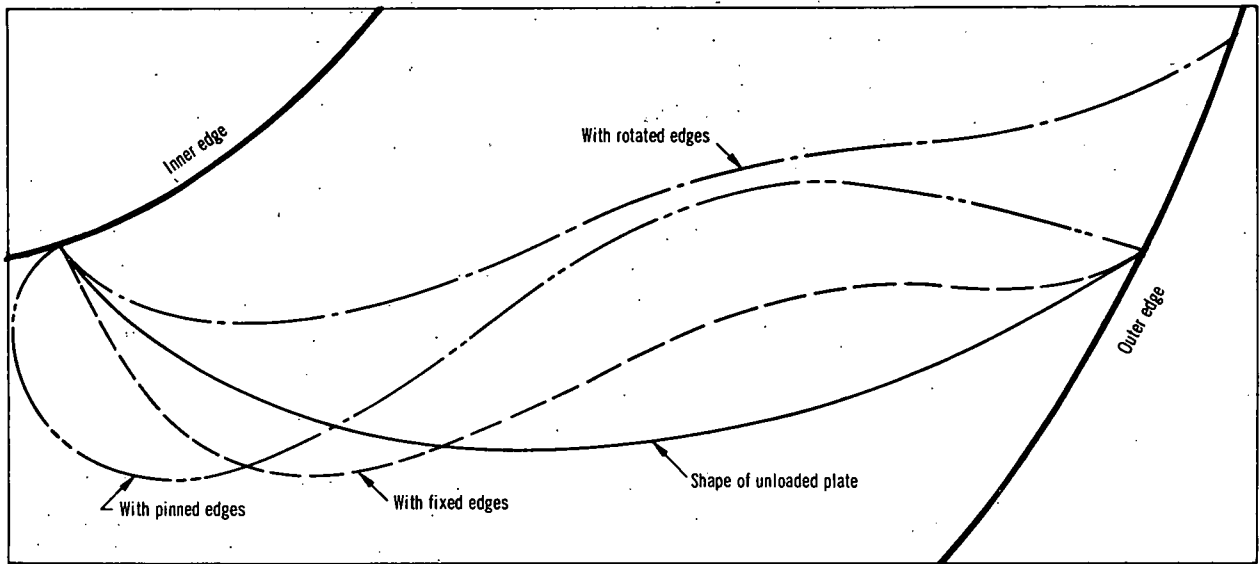

Fig. III.A.3. Deformation Tendency of AARR Involute Fuel Plate under Uniform Pressure on Convex Side

PUBLICATION

ADVANCED SYSTEMS RESEARCH AND DEVELOPMENT

Developments in the Elimination of Boron Loss during Fabrication of Stainless Steel-UO_2 Cermet Fuel
C. V. Pearson

IV. NUCLEAR SAFETY

A. Other Reactor Kinetics--Research and Development

1. Coolant Dynamics

a. Critical Flow (H. K. Fauske)

Last Reported: ANL-7391, p. 171 (Oct 1967).

(i) Sodium Tests. The first phase of the experiments using sodium as working fluid has been completed. Major conclusions have been presented;* a detailed description of the experiment facilities, data, and results will be reported.

The second phase of the sodium study, which involves detailed measurements and analyses of nonequilibrium effects in flashing liquid metals, has been initiated. The new test section is being installed in the sodium-loop facility.

(ii) Steam-Water Tests. Additional steam-water critical-flow data have been obtained using test sections described previously (see Progress Report for June 1967, ANL-7349, p. 120). The pressure range has been extended up to 350 psia. These data are in excellent agreement with an analysis based on previous data in the range 40 to 150 psia (see Progress Report for August 1967, ANL-7371, pp. 115-118).

b. Coolant Dynamics (R. M. Singer)

Last Reported: ANL-7391, pp. 171-172 (Oct 1967).

(i) Superheat. Operation of the sodium superheat experiment is yielding additional data, which are being analyzed.

(ii) Expulsion. Safety-interlock systems are being refined. One new interlock shuts off power to the electron-beam heater when test-section temperature exceeds a safe value. Another interlock requires that the electron-gun sweep circuit is operating before high voltage is applied; it will prevent localized melting of the test section. Difficulties have arisen with the high-vacuum pumping station; several relays have shorted out and some oil leakage has occurred. The station has been disassembled for repairs.

---

*Fauske, H. K., Two-phase Compressibility in Liquid Metal Systems, Proceedings International Conference on the Safety of Fast Reactors, in preparation, Aix-en-Provence, France, September 19-22, 1967; Fauske, H. K., et al., Sodium Flashing Experiment, ANS Transactions 10, No. 2 (Nov 1967).

c. <u>Convective Instability</u> (R. P. Heinisch)

Last Reported: ANL-7391, p. 172 (Oct 1967).

Runs with the current test section are almost completed. A second test section will be installed.

Data taken thus far compare favorably with analyses. The effect of convection on conduction in liquid-metal systems is not completely understood; however, the next test section is expected to contribute to our basic understanding of the heat-transfer mechanisms involved.

d. <u>Electron-bombardment-heater (EBH) Test Facility</u>
(R. D. Carlson)

Last Reported: ANL-7391, p. 172 (Oct 1967).

Tests with the present tube-flow-type EBH have yielded heat fluxes ranging up to 10^6 Btu/hr-ft^2 over a 22.5-in.-long, 0.430-in.-ID tube. and 2×10^6 Btu/hr-ft^2 over a 7.5-in.-long, 0.430-in.-ID tube. These steady-state heat fluxes are being supplied during continuous operation. Operation in both the emission-limited and space-charged-limited regions are being investigated.

The present limitation on the heat flux is the critical heat flux. In these initial tests, water is the coolant; the above heat fluxes approach the critical heat flux for the heated tube. Modifications to both the coolant system and the power supply are being planned so the heat-flux range can be extended.

e. <u>Core Component Dynamics</u> (M. W. Wambsganss)

Last Reported: ANL-7391, p. 172 (Oct 1967).

The details and results of three independent elastic analyses of fluid-structure coupling are being reviewed. The studies relate to (1) the system response of a coolant-filled (water) parallel-plate channel to a rapid insertion of energy, (2) a characteristic deformation length and the approximate elastic response of a shell, and (3) energy transmission by acoustic-impedance matching and frequency coincidence.

In the investigation of the plastic deformation of cylindrical shells under impulsive loads, some general conclusions have been inferred from existing solutions* for dynamic ring and uniform-band loads. Consider

---

*Eason, G., and Shield, R. T., <u>Dynamic Loading of Rigid-Plastic Cylindrical Shells,</u> J. of the Mechanics and Physics of Solids <u>4</u>, 53-71 (1956).

a circular cylindrical shell made of a rigid, perfectly plastic material, and let r, θ, z be the usual cylindrical coordinates with z = 0 being the location of the ring load or the center of the uniform band load. The plastic deformation is composed of four phases:

1. Hinge circles form at z = 0 and $|z| = z_1(t)$.

2. A hinge circle forms at z = 0, and a hinge band forms in the region $z_1(t) \le |z| \le z_2(t)$.

3. A hinge band forms in the region $0 \le |z| \le z_3(t)$ with a hinge circle at $|z| = z_1(t)$.

4. Hinge bands form in the regions $0 \le |z| \le z_3(t)$ and $z_1(t) \le |z| \le z_2(t)$.

The functions $z_1(t)$, $z_2(t)$, and $z_3(t)$ and the radial displacement $u(z,t)$ are connected by sets of coupled nonlinear differential equations, which may be solved in closed form for some loadings whereas a numerical solution must be resorted to in other cases.

Any or all of the four phases may occur, depending on the shape of the pulse and its time history. For example, consider a ring load of magnitude P_m with a triangular pulse shape (in time). The shell remains at rest until P reaches the static collapse load P_s:

$$P_s = 2\sigma_0 h \sqrt{h/R},$$

where σ_0 is the yield stress, h is the shell thickness, and R is its radius. The shell then deforms according to the first phase; if $P_m \le 2.39 P_s$ it will continue to deform until it comes to rest. However, if $P_m > 2.39 P_s$, the motion passes into the second phase at this value and later returns to the first phase before coming to rest.

An attempt will be made to find the plastic-deformation histories corresponding to a general loading, symmetric about z = 0 and monotonically decreasing with $|z|$, for an arbitrary pulse shape. Solutions for physically realistic impulsive loadings can then be obtained. An anticipated result of this investigation is the determination of what properties of an impulsive load's spatial and temporal shapes are important in determining the final shell deformation and amount of energy absorbed. This information is of great importance in the design and interpretation of experiments and the correlation of laboratory tests with actual reactor situations.

2. Fuel Meltdown Studies with TREAT

    a.   Meltdown Studies with Ceramic Fuels (C. E. Dickerman)

    (i) Examinations of Oxide-fuel Specimens Irradiated to 6 a/o Burnup Level. Transient experiments are being performed with irradiated oxide-fuel specimens to study fuel behavior under accident conditions. In order to obtain a complete description of the oxide-fuel behavior, it is necessary to evaluate the fuel condition after steady-state irradiation. A summary of the examinations on the specimens of highest burnup (6 a/o burnup) follows:

    Each of the pins in the 6-a/o-burnup group consisted of a stack of 13% enriched UO_2 cylinders,* 13.97 cm long and 0.381 cm in diameter, argon bonded and sealed in a Type 304 stainless steel jacket of 0.396-cm inner diameter and 0.442-cm outer diameter.

    Particle size of the enriched uranium oxide was equal to or greater than 2-3 μ after milling. The powder was mixed with 2-2.5% methyl cellulose to form a slurry and then dried, after which 10-15% H_2O was added and mixed thoroughly. The green density was 40% of theoretical density after extrusion under a 5- to 7-ton load. It was then cut into lengths and sintered in hydrogen at 1700 to 1750°C for 4 hr.

    The average density was 91.96% of theoretical density (theoretical density is 10.96, obtained by X-ray measurements**). The ratio of oxygen to uranium was calculated to be 2.019 from chemical analyses.

    (ii) Post-steady-state Irradiation. Inspection of the pins after irradiation consisted of checks on dimensional changes, axial gamma scanning, photography of the macroscopic condition of the pins, neutron radiographs (which were made utilizing a thermal-neutron beam from the Juggernaut reactor), X-ray radiographs, and burnup determination by radiochemical analysis of monitor wires and by the technique of laser-beam vaporization. One pin was set aside for destructive examination, which involved collection of released fission gases, burnup measurement by mass-spectrometric determination of uranium isotopic ratios, and ceramographic examinations with the aid of an electron probe microanalyzer.

    (iii) Conclusions. The results of the above-mentioned system of analyses have supplied data which may be summarized with reference to Fig. IV.A.1, as follows:

---

*Prepared by the Ceramics Group, Metallurgy Division, Argonne National Laboratory.
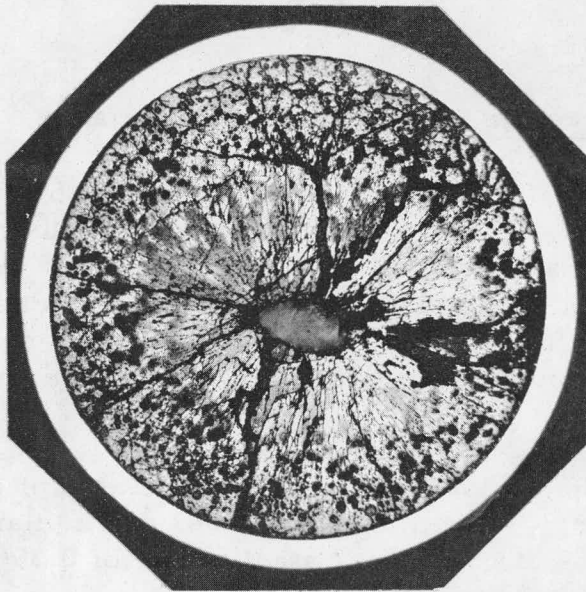**Reactor Handbook, Vol. I, Materials, p. 293.

Fig. IV.A.1. Cross Section of Irradiated UO_2
Fuel Pin of 6 a/o Burnup

1. Microscopic examination supported by an electron microprobe analysis showed the fuel to be non-homogeneous.

2. Moderate to severe cracking extended from the fuel central void to its outer surface.

3. Extensive fission-gas bubble formation occurred.

4. The pellets fused together as a result of irradiation (calculated maximum fuel center temperature was 2400°C).

5. Extensive bubbling occurred over the entire surface of the fuel, varying in intensity and degree.

6. Large round porous inclusions up to 100-μ diameter (these are viewed as dark spots in Fig. IV.A.1) were dispersed throughout the outer 1/4 of the radius, and contained uranium, cesium, barium, lanthanum, cerium, praseodymium, neodymium, promethium, samarium, europium, strontium, yttrium, and zirconium. These appear to be the source of the surface "bubbles."

7. Small, shiny metallic inclusions within the porous area were stainless steel particles with no detectable fission products and stainless steel particles containing transition metal fission products: molybdenum, ruthenium, technetium, rhodium, and palladium.

8. Stainless steel-impurity inclusions migrated during irradiation out of the center portion of the fuel matrix. No stainless steel inclusions were detected to remain in the columnar grain-growth region.

9. All inclusions analyzed in the columnar grain-growth regions of the samples contained metallic-appearing alloys of molybdenum, ruthenium, technetium, and rhodium, whose composition varied as a function of position. Further, these inclusions were free of uranium, indicating that no intermetallics or solid solutions of uranium-noble metal fission products were formed by reduction of the UO_2 matrix.

10. Inclusions in the peripheral areas of the fuel samples were either stainless steel or stainless steel containing the transition metal fission products molybdenum, ruthenium, technetium, rhodium, and palladium. There was no consistent ratio of fission product distribution in the steel-containing inclusions, although molybdenum and ruthenium were the major fission products.

11. The porous inclusions were formed in the region beyond the columnar grains to the periphery. At the periphery they appear

to project beyond the outer surface of the fuel, causing "bubbles" which in many cases appear to have burst. These porous inclusions are high-burnup regions and are associated with the fully enriched UO_2 particles of the original fuel material.

A report is in preparation.

b. **Meltdown Studies with Metallic Fuels** (C. E. Dickerman)

Last Reported: ANL-7391, p. 173 (Oct 1967).

(i) **Analysis of First Scale-up Sodium Loop Experiments** (7-pin Clusters). Two clusters of seven EBR-II Mark-I fuel pins were run to destruction inside Mark-I integral sodium loops in TREAT fast reactor safety experiments. Reactor Transient 1048 was performed with an initial flow rate of 3.25 m/sec,* and Tr 1050 was run with pump power off (although transient-induced flow was possible).** Since the initial reports, the samples have been examined and calculations performed; results were presented at the 1967 Winter Meeting of the American Nuclear Society.

Tantalum neutron absorbers shaped the power axially to a maximum to minimum ratio of 1.3. Each central pin was of 9% enrichment, and the six-pin rings surrounding the center consisted of 7% enriched pins, as approximate compensation for the radial neutron-flux depression across the cluster. The measured ratio of peripheral pin power to central pin power was 0.94, in good agreement with S_n transport-theory calculations.

Fuel-energy input during the reactor power peak of Tr 1048 was 928 J/g for the internal pin. Postexperiment examination showed large plugs of solidified fuel at the test-section inlet and outlet. Fuel was also frozen onto the inner wall of the test section, and a small amount was discovered in the remnants of the cladding tubes at the bottom of the section.

Power peak energy was 1043 J/g for the central pin in Tr 1050. When the loop body was removed from its sealed secondary container, it was found that the thin-walled, ac Faraday-type pump tube had been ruptured. The center region of the test section was lined with frozen fuel alloy and solidified fuel plugs were at inlet and outlet, but most of the fuel was found in the loop tubing below the test-section inlet.

The extensive failures of the EBR-II Mark-I pins in the two seven-pin cluster loop experiments are consistent with the failure thresholds determined previously for single pins in a sodium environment. The ratio of fuel volume inside the test cluster to the volume of coolant

---

*Reactor Development Program Progress Report for December 1966, ANL-7286, p. 70.
**Reactor Development Program Progress Report for February 1967, ANL-7308, p.87.

was approximately seven times that for the previous loop transients with single fuel pins surrounded by dummy pins; hence, coolant temperature rises were higher. Coolant thermocouples were in the channel between internal and peripheral pins. In the single-pin analyses reported previously, it was found that fuel heat losses up to approximately the time of peak power were determined principally by heat transfer only to the coolant between the central pin and the peripheral dummies.* The heat capacity of surrounding sodium and steel became significant after peak power. Thus, to first approximation, the central pin of the 7-pin clusters had only half the heat loss to coolant as the single pin for the earlier experiments. Heat loss from the six peripheral pins was intermediate between the two cases. Although the boundary conditions of the 7-pin clusters still were not identical with those of an actual fast reactor subassembly, the degree of simulation was increased markedly over that of the previous single-pin loop experiments.

After fuel failure occurred, the ratio of volume available for motion to the volumes of fuel and heated coolant was much closer to a real reactor than in the earlier loop tests. Fuel expelled from the two single-pin failures was frozen in situ on the test-section wall, and there was no evidence of appreciable secondary fuel movements.*,** Post-failure fuel behavior in the 7-pin cluster would more nearly be typical of that for a real subassembly.

These two scale-up experiments thus provide the first experimental check on application to cluster geometry of the fuel-pin-failure modeling developed in single-pin tests. In addition, the 7-pin-cluster tests provide the first data on post-failure secondary fuel and coolant movement from pin arrays.

Analyses of the experiment consisted first of correlation of data from the coolant thermocouples, test-section inlet flowmeter, and inlet pressure transducer, and, second, of transient heat-transfer calculations using reactor power data and ratio of sample power to reactor power. Models for heat transfer calculations were essentially the same as described by Stephany and Dickerman. Intact geometry is inherent in the calculations. The following is a summary of the information obtained on the transient behavior during the experiments:

(a) Tr 1048 (3.25-m/sec flow). At approximately peak power, a rapid coolant expulsion and the first pressure spike (of about 3.5 atm) occurred. Maximum expulsion rate measured was in excess of 5 m/sec. The onset of the abrupt expulsion coincided with a small pressure anomaly of about 0.5 atm, occurring approximately 75 m/sec before

---

* Stephany W., and Dickerman, C. E., Analyses of Behavior of EBR-II-type Pins under Transient Heating in Sodium Environment, Trans. Am. Nucl. Soc. 10, 343 (1967).

** Robinson, L. E., Purviance, R., and Willis, F. L., Results from High Specific Energy Input Single-pin, Sodium Loop Meltdown Experiments in TREAT, Trans. Am. Nucl. Soc. 10, 343 (1967).

the 3.5-atm spike. At the time of the small anomaly, the maximum calculated cladding surface temperature was below boiling, but maximum central fuel pin temperature was 1255°C. Thus, local boiling could occur at this time due to molten fuel moving from the center of the pin through a fuel-surface crack to contact the cladding. Such surface cracks have been found in pins carried to the threshold of failure. Outlet bulk-coolant temperature was calculated (assuming no vaporization) to be approximately 975°C at 2.00 sec and about 1110°C at 2.05 sec, so the first pressure spike was attributed to sodium vaporization. The rapid coolant expulsion indicated on the inlet flowmeter was also apparent on the record of the sodium thermocouple, showing rapid expulsion, both upward and downward, of high-temperature sodium. The second pressure spike (6 atm) corresponded to the calculated time of failure of the central (hottest) pin, due to vapor pressure of the sodium bond between fuel and cladding. Time at temperature was not sufficient for failure by penetration due to the formation of fuel-cladding eutectic. Out-of-pile and in-pile experiments have yielded a time of approximately one second for penetration of a 0.25-mm-thick steel EBR-II cladding tube by molten U-fissium alloy. Large amounts of eutectic could be formed before final solidification at the end of the experiment, however.

Voiding grew after inception of expulsion at about 2.00 sec, and by 2.15 sec the total expulsion recorded on the flowmeter corresponded to the distance between center of fuel and the inlet pressure transducer. This is in good agreement with the disappearance of the 120-cps pump-pressure signal at that time. Failure of the peripheral pins by internal sodium pressure was calculated to occur after the initial voiding, so that the pressure transducer would not necessarily detect a pressure pulse from release of bond sodium from a peripheral pin. Evidence of secondary fuel motion was seen at approximately 2.6 sec on the outlet thermocouple. The one spike of flow up into the test section (peaking at about 2 m/sec) correlated well with a small pressure spike of about 2 atm and short temporary recovery of flow past the inlet flowmeter. A second short period of no pressure modulation occurred before flow was finally re-established at a low rate.

It should be noted that relief of bond-sodium pressure without cladding failure produced by axial motion of molten fuel, such as found for single-pin loop experiments with flowing sodium, did not appear to occur. This difference can be explained qualitatively by the flatter radial temperature gradients in these cluster experiments because of the reduced amount of heat absorber around the pins.

(b) <u>Tr 1050</u> (no flow). The initial coolant expulsion from the test section, after 2 m/sec, was in qualitative agreement with the movement calculated from prefailure thermal expansion of sodium in the cluster. Cladding failure was indicated experimentally by a small (2-atm)

pressure spike associated with an increased expulsion peaking at 6 m/sec. Failure of the internal pin due to vapor pressure of the bond sodium was calculated to occur at the time of this pressure spike. A second 2-atm spike occurred at the time failure of the peripheral pins was calculated (also due to bond-sodium pressure). The second spike was coincident with another expulsion peak at 9 m/sec. Expulsion continued beyond this time, indicating coolant voiding extending beyond 40 cm below the test cluster inlet at the time a vigorous secondary pulse recorded as 16 atm occurred. Because of the voiding, the critical pulse may have been much higher at its point of origin. The extensive motion of molten fuel extending to ~45 cm below the test section inlet indicates that the final pressure pulse may actually have occurred in the inlet section where instrumentation and the pump are located, rather than in the test-section region.

Thus, these first loop cluster transient results show appreciably more movement of fuel and coolant than found previously for single fuel pins. They indicate the importance of secondary fuel movements and the possibility of "trapping" sodium between plugs of high-temperature fuel inside a reactor subassembly. Further scale-up loop transients and investigation of the effects of axial blanket sections will be necessary for evaluation of these post-failure effects.

c.   Development of Experimental Methods   (C. E. Dickerman)

Last Reported: ANL-7391, pp. 173-174 (Oct 1967).

(i)   Transparent Capsules for TREAT Experiments with Irradiated Fast Reactor Fuel Samples. This task supplies the basic technology for transient irradiations in TREAT of EBR-II-type fuel specimens. Seven capsules developed for remote hot-laboratory assembly of EBR-II Mark-I-size uranium specimens have been inspected and set aside for transient irradiations. Capsule components, including the cadmium-fiberglas "sandwich" thermal-neutron filters, have been used previously in TREAT experiments but were designed for reuse and were found to be acceptable. The capsules are to be used with the existing "slot liner" capsule containers which have been routinely reused in similar irradiated-pin experiments.

3. Materials Behavior, Equation of State, and Energy Transfer

a.   Interactions of Fuel, Cladding, and Coolant   (R. O. Ivins)

Last Reported: ANL-7230, pp. 69-70 (June 1966).

Studies relating to the possible physical or chemical interactions between reactor materials and the reactor coolant, sodium, have been continued. In initial studies, a survey was made of the interaction

of molten fuel and cladding materials with liquid sodium; in some cases extensive fragmentation of the samples occurred, resulting in violent expulsion of a portion of the fragmented material (see Progress Report for May 1965, ANL-7046, p. 81). In an attempt to determine the cause of the fragmentation phenomenon, later experiments (see Progress Report for January 1966, ANL-7152, p. 90) compared the effects of dropping molten metals into sodium and into water; molten silver, for example, when dropped into water did not fragment, but did fragment when dropped into liquid sodium.

It was hypothesized that the breakup results from violent formation and collapse of vapor bubbles in the nucleate and transition boiling regimes. Cladding metals are in a molten state in the violent boiling regime for sodium (900-2300°C) and thus fragment; however, they are not in a molten state in the violent boiling regime for water (100-373°C) and, therefore, do not fragment in that medium. This hypothesis is supported by the observation that low-melting metals such as tin, bismuth, and lead fragment when dropped into water, whereas aluminum and zinc, with boiling points above the critical temperatures of water, do not fragment when dropped into water.

The examination of thermal effects on the fragmentation of metals with low melting points has been extended in an attempt to clarify this phenomenon further. The dynamics of the fragmentation process have also been investigated by varying the distance (entrance velocity) of the drop into water. The initial experiments in this extended study consisted of a survey of the dynamics of fragmentation of six low-melting metals. In subsequent experiments that utilized only one of these metals in order to reduce the fragmentation parameters, the thermal effects on fragmentation were investigated more extensively.

(i) Survey Study of Low-melting Metals. The six metals used in this investigation were zinc, lead, bismuth, tin, gallium, and mercury. The samples were resistively heated to 600°C in a crucible, and dropped from heights of 1 and 4 ft into water maintained at about 30°C. In the experiments with mercury, both the sample and the water were kept at room temperature (~25°C). It was hoped that mercury would provide a purely dynamic effect in its fragmentation process, exclusive of any heat-transfer mechanism.

The method used to estimate the degree of fragmentation was to count the number of fragments of significant size resulting from a sample drop. The fragments were weighed. The diameter of the particle was calculated from this weight, assuming that the initial sample fell as a single drop, and that both this drop and the resulting fragments assumed a spherical shape. For mercury, the number of fragments was obtained from high-speed motion pictures.

From the diameter of the drop and an assumption that its velocity was equivalent to that of a freely falling body in a vacuum, the dimensionless Weber Number, $\rho Dv^2/\sigma$, was calculated at the instant of contact with the water (ρ is the density of the water; D, the initial drop diameter; v, the speed of the drop upon contact with the water; and σ, the molten metal-water interfacial tension). The value of D was calculated on the basis of a free fa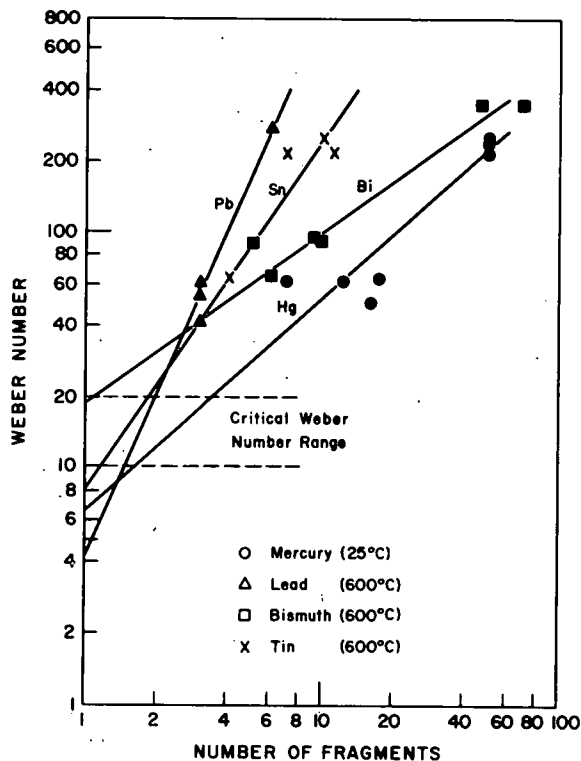ll in vacuum, and σ was assumed to be the difference between the metal-air and air-water interfacial tensions. The Weber Number can be used as an indication of the dynamic effects on the fragmentation process. Other investigations* have shown a critical Weber Number (in air) to be in the range from 10 to 20, with values above critical resulting in fragmentation.

The results of the study are shown in Fig. IV.A.2 as a plot of the number of fragments versus the entrance Weber Number for four of the low-melting metals. In general, the higher the Weber Number, the greater the fragmentation. (The zinc samples did not fragment under the conditions of the experiment, and the gallium results are given in more detail in the following.)

Fig. IV.A.2. Plot of Weber Number vs. Number of Fragments for Various Molten Metals Dropped into Room-temperature water

(ii) Thermal Effects on Gallium Fragmentation. In an effort to gain more insight about the thermal effects of fragmentation, the study was extended to include a more comprehensive examination of gallium. Gallium was chosen because of its low melting point (29.78°C), high boiling point (2403°C), low vapor pressure, absence of toxic properties, and resistance to oxidation; data could be collected over a wide range of liquid-state temperatures.

In the experiments described in Sect. IV.A.3.a.(i), a small stainless steel crucible was used to hold the sample while being heated. Because of the tendency of liquid gallium to wet the crucible, a modified drop technique was used. The furnace was fitted with a Vitreosil glass tube for sample expulsion. After heating to the desired temperature, the liquid metal was forced from the tube by increasing the pressure until a single drop was expelled.

*Hinze, J. O., "Forced Deformation of Viscous Liquid Globules," Applied Scientific Research, Vol. A1, Mechanics, Heat, The Hague (1949), p. 263; "Critical Speeds and Sizes of Liquid Globules," ibid., p. 273

Tests were made with a single drop size (of 0.37-cm diameter) at drop heights ranging from 2 to 32 in. (corresponding to Weber Numbers between 5 and 100). Drops were made at five initial gallium temperatures: 50, 100, 300, 400, and 600°C, and fall was into 30°C water. The maximum estimated temperature decrease (40°C) during the fall through air occurred at an initial gallium temperature of 400°C and a drop height of 32 in.

The results are presented in Table IV.A.1. Because the amount of scatter of the data was considerable, the number of fragments given in the table is the average for five separate drop tests run under identical conditions. If the sample does not fragment, the number of fragments is taken to be one.

TABLE IV.A.1. Fragmentation of Liquid Gallium Dropped into 30°C Water (Average of five drops of 0.37-cm diameter)

Drop Height (in.)	Weber Number	Number of Fragments at Indicated Initial Gallium Temperature				
		50°C	100°C	300°C	400°C	600°C
2	5.3	-	-	-	20.4	10.2
4	11.5	-	-	-	1.8	9.2
8	23	1.0	1.1	1.0	9.3	1.6
16	46	3.4	3.5	2.8	6.7	2.5
32	92	10.5	6.5	6.6	7.4	-

Two fragmentation mechanisms are evident from the data. One mechanism, a dynamic breakup at the lower temperatures, causes fragmentation proportional to the Weber Number of the falling drop when the Weber Number is greater than its critical value for fragmentation. The other mechanism occurs between 300 and 400°C, where a striking change in the extent of fragmentation is evident. The drop tests made at 400°C exhibit by far the greatest fragmentation, especially at low Weber Numbers, presumably because the drop passes through a violent (transition) boiling regime that exists over a temperature range between 300 and 400°C. At 600°C, the extent of fragmentation is less than at 400°C, particularly when the Weber Number is low, because the drop is in a film boiling regime during most of its fall through the water.

(iii) Fragmentation in Liquid Sodium. An experimental apparatus for dropping molten UO_2 into liquid sodium is being constructed. A tungsten crucible, fitted at the bottom with a ball valve, will be used to contain and drop the UO_2. The crucible will be heated inductively in an inert atmosphere glovebox.

b. <u>Pressure Generation due to Violent Meltdown</u> (R. O. Ivins)

Last Reported: ANL-7357, pp. 133-137 (July 1967).

A series of experiments using a sodium-filled piston-autoclave is planned in TREAT; these experiments should provide information on pressures generated in a sodium environment during fuel meltdown at high energy inputs. This information will be useful in the evaluation of problems of potential fuel failure that may be encountered in the operation of sodium-cooled fast reactors and experimental test loops.
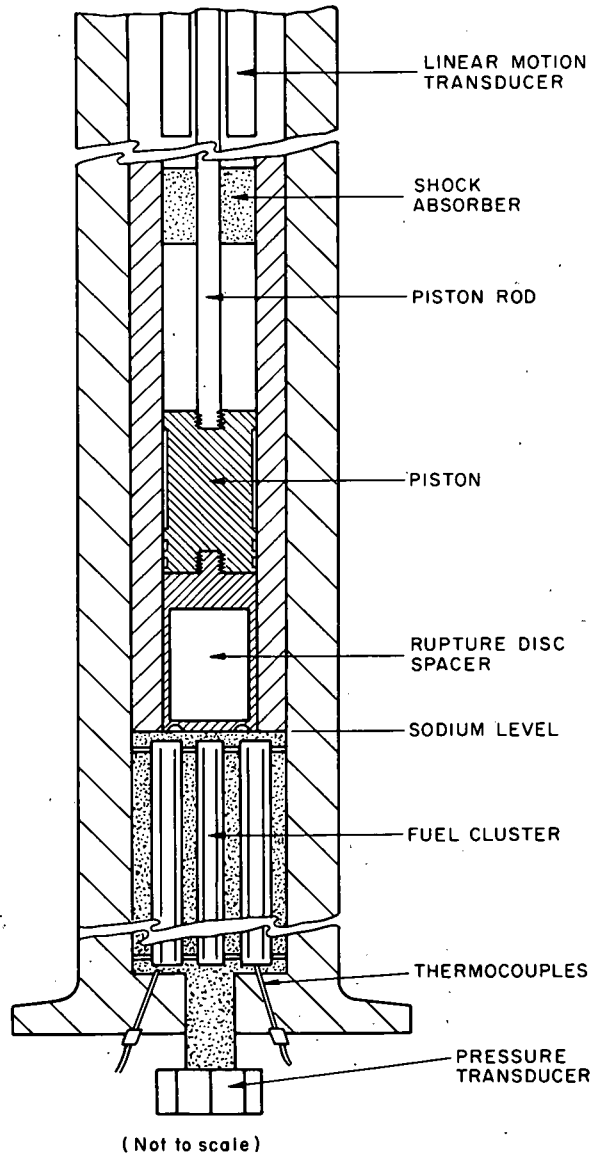
The autoclave assembly to be used in these studies is shown schematically in Fig. IV.A.3. Initial experiments will be carried out using clusters of fuel rods of sintered UO_2 pellets, 10% enriched, clad with Type 304 stainless steel. The fuel cluster, immersed in sodium in the autoclave, will be located beneath a piston coupled to a linear-motion transducer which measures the rate of expulsion of sodium. Variable-impedance transducers will measure the pressures generated during the transient.

A calibration run was made on this system in TREAT without sodium in the autoclave to correlate reactor integrated power with the fission energy generated in the fuel rod. The calibration factors (based on a ^{99}Mo fission product analysis) were 0.716 cal/(g UO_2)(MW-sec) for the center rod and 0.767 cal/(g UO_2) (MW-sec) for the four circumferential rods (see Fig. IV.A.4).

LINEAR MOTION TRANSDUCER

SHOCK ABSORBER

PISTON ROD

PISTON

RUPTURE DISC SPACER

SODIUM LEVEL

FUEL CLUSTER

THERMOCOUPLES

PRESSURE TRANSDUCER

(Not to scale)

Fig. IV.A.3. Autoclave Measuring System for High-energy Meltdown Experiments in TREAT in a Sodium Environment

Preliminary results of a safety analysis of the autoclave system indicated that several components must be redesigned, particularly in the shock-absorbing system. Space limitations in the primary autoclave require that additional shock-absorbing components be placed between the primary

and secondary autoclaves. With this addition, the assembly will then meet
the requirement that the external TREAT shock absorber should not move
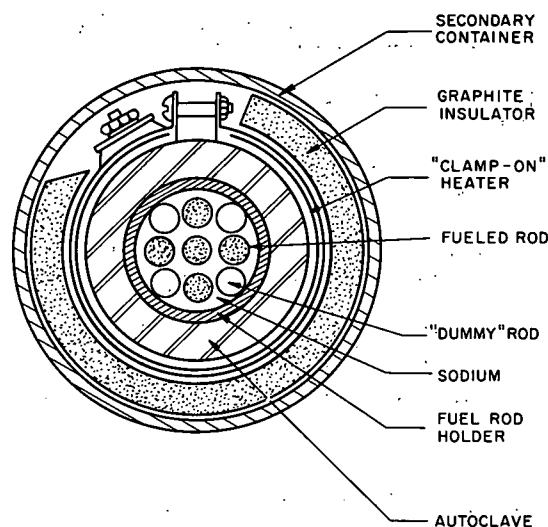during a normal transient.

SECONDARY
CONTAINER

GRAPHITE
INSULATOR

"CLAMP-ON"
HEATER

FUELED ROD

"DUMMY"ROD

SODIUM

FUEL ROD
HOLDER

AUTOCLAVE

Fig. IV.A.4
Top View of 9-rod Fuel Cluster for High-
energy Meltdown Experiments in TREAT
in a Sodium Environment

4. TREAT Operations

a. Reactor Operations (J. F. Boland)

Last Reported: ANL-7391, pp. 179-180 (Oct 1967).

Neutron radiographs of fuel materials of different enrichments
were made to obtain data on film density at various radiation doses. This
information will be used as a guide for setting exposure times for future
neutron radiographs. A neutron radiograph was also made of the fuel pin
from ANL experiment CEN-273-T.

The carbon steel studs originally installed in bolted flanges of
the large TREAT sodium loop were replaced with A-286 stainless steel
studs to reduce stresses produced by the difference in the thermal-expansion
coefficient of carbon steel compared to that of Type 304 stainless steel.
The flanges were satisfactorily helium leak tested following replacement
of the studs.

b. Development of Automatic System for Power-level Control
(J. F. Boland)

Last Reported: ANL-7391, p. 180 (Oct 1967).

A survey of digital-computer codes was made to determine if
one suitable for simulating the reactor and an automatic control system
was available for the computers at the NRTS. Since a suitable code was
not found for any of these machines, arrangements have been made to use

the "Continuous System Modeling Program" developed by IBM on the IBM-1130 computer at Idaho State University. Development of a reactor kinetics subroutine for this program has been started.

B. Chemical and Associated Energy Problems (Thermal)

1. Analysis of Loss-of-coolant Accidents (J. Hesson)

Last Reported: ANL-7329, pp. 94-98 (April 1967).

Experimental simulations of the environment of Zircaloy-clad, UO_2-core fuel rods following a loss-of-coolant accident in a water-cooled power reactor have continued. In such a situation, the fuel would be subjected to a slowly rising temperature (compared with that of a transient) because of fission product decay heating and the exothermic cladding-steam reaction.

The primary objectives of these out-of-pile simulations are to define, identify, and characterize fuel failure (in terms of fuel-rod geometry change) so that the behavior of a water-cooled reactor core following a loss-of-coolant accident may be predicted. The program will be useful in providing parameters for fuel failure for loss-of-coolant calculational studies such as the CHEMLOC Program.

The results of several experiments using induction heating of single rods and four-rod bundles have been reported previously (see Progress Report for April 1967, ANL-7329, p. 94). These experiments indicated that Zircaloy cladding will maintain its integrity (under the conditions of the experiment) at temperatures substantially higher than the melting point of zirconium (1850°C). Observed fuel-rod breakup (or movement) occurred only during cooldown, with or without the addition of an emergency coolant spray.

Since these scoping experiments did not reveal the conditions under which gross fragmentation would occur, the program has been extended to include a study of the behavior of a single fuel element over a much broader range of conditions. For example, cladding integrity will be investigated utilizing the following parameters:

1. Heating rates and maximum temperatures will be varied to determine the effect on fuel meltdown and oxide penetration.

2. Steam flow rates will be varied from steam-limited to excess-steam conditions for determination of oxidation rate.

3. A hydrogen atmosphere will be provided for the fuel rods to simulate the environment of the top of a reactor core (hydrogen is produced from the $Zr-H_2O$ reaction).

4. A bottom-flood method, as well as a top-spray method, will be used to simulate emergency cooling.

Construction of an apparatus for conducting these experiments is in progress. A second radio frequency transformer (with associated equipment and instrumentation) has been installed which will allow use of the induction generator by more than one experimenter. A reaction cell is being built to permit hydrogen collection (from the $Zr-H_2O$ reaction) during an experiment simulating spray cooling. Experimentation is scheduled to begin upon completion of the apparatus.

2. Analysis of Excursion Accidents (R. O. Ivins)

Last Reported: ANL-7349, pp. 126-132 (June 1967).

The general objective of the in-pile studies of excursion accidents is to contribute to the development of experimental and theoretical information needed for the analysis of accidents in water-cooled thermal reactors.

Ten photographic experiments to study the high-temperature behavior of Zircaloy-2-clad, UO_2-core (both sintered-pellet and vibrationally compacted) fuel rods during a reactor transient have been completed. In these experiments, which were conducted in TREAT, fuel rods were submerged in water within a transparent capsule and high-speed motion pictures of the meltdown were taken.

a. **Experiments with Pelletized UO_2-core Fuel.** Three of the photographic experiments with sintered-pellet UO_2-core fuel rods have been reported earlier (see Progress Report for June 1967, ANL-7349, p. 126).

The first of two recent experiments (CEN-230T) using similar pellet-core fuel rods was run at an energy level of 290 cal/g UO_2. Motion pictures of the transient show a relatively mild event with no visible evidence of a cladding breach. The fuel rod was intact although the cladding may have been breached at the completion of the transient; the uncertainty arises from the fact that the rod was broken during removal from the autoclave.

The film of the second recent pellet-core experiment (CEN-231T, 368 cal/g UO_2) showed considerably more activity. Two holes had been drilled in the bottom quarter of the fuel rod to simulate a cladding breach. At an energy input of 276 cal/g UO_2, a flash began at the bottom hole which grew rapidly, and finally completely obscured the fuel rod. After the flash, the apparently intact fuel rod could be seen for the remainder of the film. This run, the energy of which is bracketed nicely by two earlier pellet-type experiments (CEN-224T at 450 cal/g and CEN-225T at 330 cal/g),

exhibited much less destruction and less metal-water reaction than would be predicted on the basis of experiments with initially unbreached cladding. The residue consisted mainly of several broken segments of the original rod in contrast to nearly complete fragmentation of the rods in the two bracketing runs. The residue also indicated that most of the cladding melted, ran down the fuel rod, and formed a puddle at the bottom. This reduced destruction may have resulted from (1) a reduced pressure within the rod and (2) a relatively low-resistance exit point for molten UO_2 at failure due to the breached cladding.

The three experiments made with initially intact rods (CEN-224T, -225T, -230T) roughly define a threshold energy for fragmentation of pellet-type fuel rods that is consistent with the value of 290 cal/g UO_2 found in the opaque autoclave experiments (see Progress Report for April 1966, ANL-7204, p. 80). The films of these three experiments show one striking contrast; the flash that occurred when the energy of the transient was above this threshold energy was not observed in experiments below this energy. This flash is postulated as being due to the expulsion of molten UO_2 from the fuel rod at 2800°C while the cladding was at a much lower temperature. In the two higher-energy experiments (CEN-224T, -225T), the initial flashes occurred when 330 and 295 cal/g UO_2, respectively, had been delivered to the fuel.

b. Experiments with Vibrationally Compacted UO_2-core Fuel. Five TREAT photographic experiments using vibrationally compacted (vibra-packed) UO_2-core fuel rods have been completed. These fuel rods were supplied by Battelle Northwest Laboratory in two designs. Both of these have the same cladding structure, but have difference in the powder core. Type I contains 127 g 10%-enriched UO_2 in an active length of 4.2 in., whereas Type II has 168 g 5.0%-enriched UO_2 in an active length of 5.5 in.

Type-I fuel rods were used in three experiments. The film record of run CEN-227T (two transients, 235 and 241 cal/g UO_2) showed no incandescence or other evidence of extensive heating. The camera malfunctioned during CEN-228T (255 cal/g UO_2), so that no motion-picture information is available from that run.

The motion pictures of CEN-229T (357 cal/g UO_2) showed several interesting events. The first indication of heating during the transient was a flash on the rear side of the rod, approximately at the upper end of the powder column. The reaction from the fuel ejection accompanying this flash was sufficient to move the fuel rod to one side of the capsule. This event occurred at an energy input of 274 cal/g UO_2. At higher energies, three narrow bands of incandescence encircling the fuel rod became visible. After the transient, three breaks were found in the rod, which corresponded to the three incandescent bands seen on the film. An examination of the residues of the two other Type-I fuel-rod experiments revealed cladding deformation at similar locations on the fuel rods.

These observations suggested that densification or enhancement of heat-transfer properties of the powder was occurring at resonant nodes during vibratory compaction of the powder. Therefore, Battelle Northwest Laboratory provided a modified set of fuel rods (Type II).

The two experiments with Type II fuel (CEN-233T and -234T) were run at energies that bracketed that of run CEN-229T (357 cal/g UO_2), but both exhibited more violent reactions.

Run CEN-233T had a fission energy input of 335 cal/g UO_2. At an energy input of 277 cal/g UO_2, a bright flash started at the rear of the fuel rod, which rapidly grew in intensity and caused complete overexposure of the film. The flash, interpreted as ejection of molten core material through a cladding breach, started at a point corresponding to the upper end of the active core. The inner quartz window of the photographic capsule separated from the coolant container along one edge 20 msec after the start of the flash. About 1/3 of the fuel rod was above water for the remainder of the run as a result of this break.

The film of the second experiment (CEN-234T, 418 cal/g UO_2) showed a more violent reaction. The first indication of activity was the start of a flash at the rear of the fuel rod, corresponding to a position in the middle of the enriched fuel column. This occurred at an energy input of 235 cal/g UO_2. Three milliseconds after the start of the flash, the inner quartz window was blown to a position perpendicular to the face of the capsule (releasing along one vertical edge and pivoting around the other). The fuel-rod cladding appeared to split vertically at the same time the window was blown off.

c. Conclusions. A comparison of vibra-packed and pelletized fuels from the experiments thus far completed is difficult, due to the anomalous behavior of the Type-I vibra-packed fuel. However, the percent metal-water reaction observed in the two Type-II vibra-packed fuel runs is not markedly different from that observed in pelletized fuel runs at similar energies, although the vibra-packed fuel does undergo a somewhat more violent disruption as evidenced from the film records of the events. The extent of metal-water reaction observed for both the pellet-core and vibra-packed photographic experiments is, in general, in good agreement with the results from the opaque autoclave studies.

The photographic technique has proven to be a most effective method of demonstrating the violence of fuel meltdown. Detailed analysis of the above experiments is continuing, and further experiments of this type are planned for both vibrationally compacted and sintered-pellet fuel. In conjunction with pressure autoclave studies, these should provide a mechanistic explanation of excursion failure of fuel rods and subsequent pressure generation.

PUBLICATIONS

NUCLEAR SAFETY

Letter to the Editor--Fast Reactor Controversy
  I. Charak
      Nuclear News 10(11), 6 (Nov 1967)

Analyses and Significance of Initial EBR-II Mark I Cluster Fast-Reactor
Safety Integral Loop Experiments in TREAT
  C. E. Dickerman, R. T. Purviance, and A. B. Cohen
      Trans. Am. Nucl. Soc. 10(2), 698 (Nov 1967)   Abstract

Calculation of the Extent of Metal-Water Reaction and Core Heating during
a Loss-of-Coolant Accident (CHEMLOC Program)
  J. C. Hesson, R. O. Ivins, and L. Baker, Jr.
      Trans. Am. Nucl. Soc. 10(2), 705 (1967)   Abstract

Metastable Two-Phase Flow of a Saturated Fluid
  H. K. Fauske
      Proc. of the Japanese Society of Mechanical Engineers 1967 Semi-
      International Symposium, Tokyo, Japan, Sept. 4-8, 1967, p. 135.

Sodium Flashing Experiment
  H. K. Fauske, D. J. Quinn, and W. C. Jeans
      Trans. Am. Nucl. Soc. 10(2), 693 (Nov 1967)   Abstract

Thermal Gradient Apparatus for Use in a Glovebox
  D. F. Fischer and M. G. Chasanov
      Rev. Sci. Instr. 38(11), 1574 (1967)

One-Component Two-Phase Critical Flow at Low Qualities
  R. E. Henry, H. K. Fauske, and S. T. McComas*
      Trans. Am. Nucl. Soc. 10(2), 658 (Nov 1967)   Abstract

Theoretical Studies of the Response of Fast Reactors during Sodium Boiling
Accidents
  D. R. MacFarlane, N. A. McNeal, D. A. Meneley, and C. K. Sanathanan
      Trans. Am. Nucl. Soc. 10(2), 694 (Nov 1967)   Abstract

Initial (7-Pin) EBR-II Mark I Scale-Up Cluster Fast-Reactor Safety
Integral Loop Experiments in TREAT
  L. E. Robinson, C. E. Dickerman, and F. L. Willis
      Trans. Am. Nucl. Soc. 10(2), 697 (Nov 1967)   Abstract

On Coolant-Structure Coupling as Related to the Pressure Pulse and Coolant
Expulsion
  G. S. Rosenberg and M. W. Wambsganss, Jr.
      Trans. Am. Nucl. Soc. 10(2), 709 (Nov 1967)   Abstract

---

*University of Notre Dame.